**UNIVERSITY OF SOUTHAMPTON**

FACULTY OF ENGINEERING, SCIENCE AND MATHEMATICS

School of Ocean and Earth Science

# How Does Chinese Loess Become Magnetized?

by

Xiang Zhao

Thesis for the degree of Doctor of Philosophy

October 2010

UNIVERSITY OF SOUTHAMPTON

## <u>ABSTRACT</u>

FACULTY OF ENGINEERING, SCIENCE AND MATHEMATICS

SCHOOL OF OCEAN AND EARTH SCIENCE

<u>Doctor of Philosophy</u>

## HOW DOES CHINESE LOESS BECOME MAGNETIZED?

by Xiang Zhao

Thick loess deposits on the Chinese Loess Plateau provide an outstanding archive of paleoclimate, geomagnetic field and paleoenvironmental changes over at least the last 2.6 Ma. Much work on magnetic polarity reversals, pedogenic magnetic enhancement and climatic change has been carried out over the past 30 years. However, questions about how Chinese loess becomes magnetized remain unanswered. In this thesis, I have sought to address key questions concerning magnetization processes in the Chinese loess. To understand magnetization processes, it is important to understand which magnetic minerals are present and the processes that caused them to be present. Magnetic and other analyses of both loess and paleosol samples indicate that pedogenic superparamagnetic and single domain magnetite and hematite can be present. The mass concentration of hematite can exceed 90% of the magnetic particle assemblage. An eolian dust deposition simulator designed for laboratory redeposition experiments was then used to demonstrate that both a depositional remanent magnetization (DRM) and a post-depositional remanent magnetization (PDRM) can be acquired by Chinese loess. Water content significantly affects the efficiency of PDRM acquisition. No significant PDRM was observed when the water content was below a critical threshold of 40%. Published paleomagnetic data from the Chinese loess indicate the widespread occurrence of inclination error. Detailed paleomagnetic studies of U-channel samples from the last loess/paleosol sequence at Yuanbao were made to assess whether the Chinese loess can accurately record geomagnetic relative paleointensity variations. Three normalized remanence records were determined using conventional normalization as well as the pseudo-Thellier method. Strong coherence among the normalized remanence records indicate that the whole range of magnetic minerals has been affected by pedogenesis. Poor similarity among published normalized remanence records from the Chinese loess, as well as with marine relative paleointensity records indicate that the Chinese loess is not suitable for relative paleointensity determinations. The range of magnetic minerals present and their varying distribution within loess and paleosol sediments indicate that the magnetization is due to a mixture of remanence acquisition mechanisms including DRM, PDRM, chemical remanent magnetization (CRM) and viscous remanent magnetizations, which also indicates complexities in remanence acquisition that will complicate attempts to extract relative paleointensity information. This thesis has provided an improved understanding of the mechanisms of Chinese loess magnetization, and re-emphasizes the importance of pedogenic CRM acquisition.

*"The most incomprehensible thing about the world is that it is at all comprehensible."*

*Albert Einstein*

*"That is life. Deal with it!"*

*Andrew P. Roberts*

# Contents

# DECLARATION OF AUTHORSHIP

I, **Xiang Zhao**, declare that the thesis entitled "*How does Chinese loess become magnetized?*", and the work presented in the thesis are both my own, and have been generated by me as the result of my own original research. I confirm that:

1. this work was done wholly or mainly while in candidature for a research degree at this University;

2. where any part of this thesis has previously been submitted for a degree or any other qualification at this University or any other institution, this has been clearly stated;

3. where I have consulted the published work of others, this is always clearly attributed;

4. where I have quoted from the work of others, the source is always given. With the exception of such quotations, this thesis is entirely my own work;

5. I have acknowledged all main sources of help;

6. where the thesis is based on work done by myself jointly with others, I have made clear exactly what was done by others and what I have contributed myself;

7. parts of this work have been published as:

Zhao, X. and A. P. Roberts (2010). How does Chinese loess become magnetized? *Earth and Planetary Science Letters*, 292: 112-122.

**Signed:**

**Date:**

# Acknowledgements

I would first like to express my sincere appreciation to my supervisor, Professor Andrew P. Roberts. It is the best honour to be his PhD student. His rigorous scholarship, open-minded communication, friendly encouragement and great tolerance have helped me to grow through difficult times. Thanks to Linda for her great meals and to the whole family who have treated me as one of them, giving me the feeling of home and bringing me happiness, both in the garden and the house.

I owe my deepest gratitude to Professor Qingsong Liu. He led me into the huge and exciting world of Chinese loess. I thank his family for delicious food, happiness and care during my first year in Southampton.

I appreciate my panel chair Professor Eelco Rohling for his efforts during my study. Thanks to Richard Pearce for help with the SEM and to Bob Jones and John Ford for their many helps. I appreciate Frances Bradbury for her smiling organization of many things for me. Thanks to Professor José Torrent for his cooperation.

I appreciate Professors Zhu Rixiang and Pan Yongxin, who led me into paleomagnetism, and who gave me many opportunities to learn. I also thank Professors Deng Chenglong, Huang Baochun, and Dr He Huaiyu, who helped me to work well when I was in Beijing.

I thank Professors Chen Fahu, Sun Donghuai and Mr Yang for their help during my fieldwork near Lanzhou. Thanks to Dr Shao Mingshen, Li Lili, and especially Dr Zhang Baojun for their assistance in my fieldwork. I also appreciate the people on the top of Jiuzhoutai and the families in the Village of Yuanbao.

Professor Sun Youbin kindly allowed me to use his laboratory for grain-size measurements for free. I also thank Associate Professor Qiang Xiaoke, technician Wang Hua and Li Min for their help during my stay in Xi'an.

Thanks to Professor Ted Evans for his useful communications and encouragement during his stay in Southampton. Thanks to Drs Adrian Muxworthy, Greig Paterson, Liao Chang, Yuji Yamamoto, Jenny Stanford, Zhang Rui, Qin Huafeng, Zhang

# Chapter 1

# Introduction

## 1.1  Loess and Chinese loess

Loess, or "huangtu" (yellow earth) in Chinese, is defined as a wind-derived, not secondarily disturbed, unstratified, calcareous and porous yellow silty earthy deposit (Liu, 1985). Loess and reworked loess-like deposits cover about 10% of the land surface of the Earth, and are distributed across former periglacial regions adjacent to glacial till areas and semiarid desert margins (Liu, 1985; Heller and Evans, 1995). Loess in China is widespread between the northern foothills of the Kunlun and Qinling Mountains and the southern foothills of the Altay, Alashan and DaHingan Mountains (Figure 1.1).



**Figure 1.1**        Sketch map of Chinese Loess distribution, modified after Liu (1985). Red stars represent the sections studied here. Red dots represent the classic sections studied on the

Chinese Loess Plateau.

These deposits form an elongated belt from the northwest to the southeast, and cover a total area of about 380,000 km$^2$ (Liu, 1985). The best-developed loess sequences occur along the middle reaches of the Yellow River, where their thickness extends up to 300 m, on the Chinese Loess Plateau. The Chinese Loess Plateau covers about 300,000 km$^2$ with the thickness and grain size of loess decreasing from the northwest to southeast. A typical loess/paleosol section is traditionally subdivided into four stratigraphic units from the surface downward: Black Loam, Malan Loess, Lishi Loess, and Wucheng Loess, which span the last 2.6 Ma and contain at least 56 cycles of yellow loess and dark paleosols that represent glacial and interglacial periods, respectively (Heller and Liu, 1982; Liu, 1985; Kukla et al., 1988; Guo et al., 1996). On the basis of grain size and geochemical analyses, Ding et al. (1998) concluded that the Red Clay, which underlies the Wucheng Loess, also has an eolian origin. Significant wind-blown deposits in China are therefore known to date back to 22 Ma (Guo et al., 2002).

## 1.2   A brief history of loess studies

Loess has been recorded in ancient Chinese literature for more than 2000 years, in which formation was related to dust storms by the historian Bangu (Liu, 1985, and references therein). Loess studies, as summarized by Smalley et al. (2001), have undergone several significant events over the past 175 years. The word "loess" was used for the first time by Karl Caesar von Leonhard in 1820 when he described the "snail-shell soil" that appeared near Heidelberg bank on the Rhine River. Charles Lyell visited the Rhine with von Leonhard in 1833, and introduced the term loess to the world in his classic text "*Principles of Geology*" in which he considered loess from different sites to have a common source (probably alluvium). The origin of loess has been hotly debated since then. Ferdinand von Richthofen investigated loess in China during 1866-1872, and listed 12 characters of loess that suggest an eolian theory of loess formation (Richthofen, 1882). John Hardcastle did important work on loess in New Zealand, but his work was not widely noticed because of his remote location and the limited circulation of the journal in which he published his observations in 1891. Smalley et al. (2001) emphasized that Hardcastle was the first

person who connected loess deposition to glacial periods. Nevertheless, Tutkovskii (1899) established the connection between loess and glacials, with the so-called "cold (glacial) loess" theory. Since 1911, Obruchev published a series of papers, in which he proposed that sand and dust are produced by weathering and wind erosion, and thus that the dust was transported to the loess deposition area by wind, i.e., the "hot (desert) loess" theory. The most important subsequent event in loess studies was a paper published by Liu Tungsheng and Chang Tsung-hu at the 6th INQUA Congress in Poland in 1961, in which they demonstrated for the first time that loess and paleosol units occur as cycles within Chinese loess sequences. George Kukla had been studying European loess sequences at the same time, in the context of Pleistocene climate change, which then became a focus for studies of Chinese loess/paleosol sequences. Liu Tungsheng and his colleagues systematically studied the distribution, deposition, composition and texture of the Chinese Loess, and reported the results in his books (e.g., Liu, 1985). Heller and Liu (1982) reported the magnetostratigraphy of a borehole at the Luochuan section, which was published in *Nature* and established the first convincing magnetic polarity zonation of the Chinese loess and demonstrated that the loess can contain important paleomagnetic signals as well as paleoclimatic information.

Since the 1980s, Chinese loess has been studied in detail from many aspects. It is now recognized that dust from the Gobi and other deserts in north and northeast China began to accumulate in response to increased uplift of the Tibetan Plateau, and the associated changes in Asian atmospheric circulation patterns that resulted from this uplift (Fang et al., 1999; An, 2000; Sun and An, 2002). Magnetostratigraphy (Heller and Liu, 1982, 1984, 1986; Sun et al., 1997; Ding et al., 2001; Evans and Heller, 2001; Qiang et al., 2001; Wang et al., 2006; Liu et al., 2010) and detailed rock magnetic studies (Maher and Thompson, 1991; Banerjee et al., 1993; Evans and Heller, 1994; Maher et al., 1994; van Velzen and Dekkers, 1999; Deng et al., 2001; Guo et al., 2001a; Spassov et al., 2003; Liu et al., 2004a; Bloemendal and Liu, 2005; Yang et al., 2005) have also been undertaken over the last 20 years or so. As a result of these efforts, records of paleomagnetic variations, which include the main geomagnetic chrons (Heller and Liu, 1982), geomagnetic excursions (Zheng et al., 1995; Zhu et al., 1996; Fang et al., 1997; Zhu et al., 1999; Pan et al., 2002; Yang et al., 2007), paleoclimate changes, including long-term climate variability (Heller and Liu,

1984, 1986; Kukla et al., 1988; Hovan et al., 1989; Ding et al., 2002) and short-term climate instability (Porter and An, 1995; Zhu et al., 2004; Liu et al., 2005a), have been obtained for the last 2.6 Ma from Chinese loess/paleosol sequences.

## 1.3 Magnetic enhancement and paleoclimatic implications

Heller and Liu (1984, 1986) first recognized that low-field magnetic susceptibility variations in Chinese loess/paleosol sequences correlate with marine oxygen isotope records. The usefulness of magnetic susceptibility as a sensitive index of climatic variations was further supported by Kukla et al. (1988) and Hovan et al. (1989). Millennial-scale climatic oscillations have been identified using grain size variation in Chinese loess since the last interglacial by Porter and An (1995). Short-term climatic changes, such as the Younger Dryas event, which was the largest environmental change in the circum-North Atlantic region since the Last Deglaciation, have been detected in Chinese loess (Fang et al., 1999). Chen et al. (1999) demonstrated that high-resolution magnetic susceptibility records can be correlated with temperature deduced from the Vostok ice core in Antarctica (Jouzel et al., 1987), with episodic occurrences of cold air over Greenland (the millennial-scale Dansgaard-Oeschger cycles recorded in the GRIP ice core) (Dansgaard et al., 1993), and with the so-called Heinrich events (massive iceberg release events) and Bond cycles (episodes of unusually cold surface waters) (Bond et al., 1993). By combining $^{10}$Be and susceptibility measurements, Heller et al. (1993) deduced that high rainfall occurred at around 25 and 55 ka and that reduced rainfall of ~530 mm/yr occurred in the interglacial period relative to the modern value of ~630 mm/yr for Luochuan section. Maher et al. (1994) developed a transfer function that directly links precipitation to the logarithm of magnetic susceptibility for modern soils and applied it to determine paleoprecipitation from Chinese loess/paleosols sequences. Their assumptions were supported by Han et al. (1996) who investigated 63 topsoil samples from across the Chinese Loess Plateau. However, several studies have questioned the simple positive correlation between magnetic susceptibility and paleoprecipitation (Sun and Liu, 2000; Guo et al., 2001b; Balsam et al., 2004).

The higher magnetic susceptibility of paleosols compared to loess results from the neoformation of fine-grained magnetite/maghemite during pedogenesis (Zhou et al., 1990; Maher and Thompson, 1991). The fine-grained magnetic particles produced by pedogenesis typically occur in the superparamagnetic (SP) or single domain (SD) grain size range. The magnetic susceptibility depends on the frequency of the alternating current used for measurements (Stephenson, 1971a, b; Mullins, 1977; Maher, 1986), therefore the frequency-dependent magnetic susceptibility has been widely used as a proxy for pedogenesis (Liu et al., 1990; Verosub et al., 1993; Eyre and Shaw, 1994; Chen et al., 1999; Florindo et al., 1999; Deng et al., 2004; Liu et al., 2004b). Based on Néel theory, Liu et al. (2004b, 2005b) constructed a quantitative model for grain size distributions for pedogenic particles, and argued that these distributions are consistent across the Chinese Loess Plateau.

In addition to magnetite and maghemite formation during pedogenesis, the presence of other magnetic iron oxides could be important. Since Heller and Liu (1984) confirmed the presence of hematite in Chinese loess by thermal demagnetization and microscope observations, the existence of hematite and goethite has been demonstrated by thermomagnetic techniques (Heller et al., 1991; Liu et al., 2004c), X-ray diffraction (Zhu et al., 1994a; Deng et al., 2000; Chen et al., 2005; Torrent et al., 2006), and Mössbauer spectroscopy (Vandenberghe et al., 1992). The abundance of hematite in Chinese loess has been estimated and considered to be similar for loess and paleosol samples (Maher and Thompson, 1992; Evans and Heller, 1994). However, mathematical unmixing studies of loess and paleosol samples (Eyre, 1996; Spassov et al., 2003a, b) suggest that pedogenic hematite occurs in the SP (0.01 to 0.1 μm) grain size range (Schwertmann, 1988) and does not contribute to stable magnetic remanences at ambient temperatures. The pedogenic formation of hematite has been accepted (e.g., Torrent et al., 2006), but it is difficult to explain the high "hard" isothermal remanent magnetization in paleosols (Liu et al., 2004c; Bloemendal and Liu, 2005). Balsam et al. (2004) suggested that hematite does not form under the same processes as magnetite during pedogenesis, whereas Barrón and Torrent (2002) proposed a hypothesis for hematite formation in which hematite is produced from ferrihydrite via maghemite.

The magnetic enhancement of magnetite/maghemite and the enrichment of hematite during pedogenesis provide information about paleoclimate and

paleoenvironment. Although much work on magnetic mineralogy has contributed to our understanding of pedogenesis, relatively little is known about the mechanisms of pedogenic hematite formation, which could be important for fingerprinting paleoclimate signals from Chinese loess sequences.

## 1.4  Magnetostratigraphy and geomagnetism of Chinese loess

Magnetostratigraphy is an important tool for dating sediments via correlation of observed polarity patterns with the well-established geomagnetic polarity timescale (Cande and Kent, 1995). After several early attempts (Li et al., 1974; An et al., 1977), the first convincing magnetic polarity zonation for the Chinese Loess Plateau was established by Heller and Liu (1982). The boundaries between the Matuyama and Brunhes chrons (M/B boundary), and the Jaramillo and Olduvai subchrons were identified from a borehole from Luochuan. The same poarity pattern was then documented at a site a few kilometres from the Luochuan section (Torii et al., 1984). Subsequently, Heller and Liu (1984) re-sampled a natural outcrop about 3 km from the borehole site, and correlated the loess susceptibility with 55 marine oxygen isotope stages, and obtained a much more detailed chronology than from the polarity reversals alone. Following these early reports, magnetostratigraphic investigations have been conducted across the Chinese Loess Plateau, such as for outcrops from Lanzhou (Burbank and Li, 1985; Rolph et al., 1989), Xifeng (Liu et al., 1988a, b), Baoji (Rutter et al., 1991a, b; Yang et al., 2007), Linxia (Thompson and Maher, 1995), Weinan (Zhu et al., 1999; Pan et al., 2002) and Sanmenxia (Wang et al., 2004). Red Clay sequences at Lingtai and Pingliang have also been studied (Ding et al., 1998a; Sun et al., 1998). The magnetostratigraphic polarity zonation of the Chinese Loess Plateau is therefore well established for the last 2.6 Ma for loess sequences and for Red Clay sequences back to 22 Ma (Guo et al., 2002).

In addition to identification of the major polarity chrons and subchrons, details of the morphology of the geomagnetic field have been studied. The high sedimentation rates of the loess should assist such studies compared to the generally lower rates for marine sediments. Sun et al. (1993) investigated the M/B transition from the Xifeng section, which spans a 3.8 m stratigraphic interval and corresponds to

a time interval of 20 kyr. Paleomagnetic directions from the transition have a complex pattern with five polarity switches between normal and reversed polarity. The termination of the Olduvai subchron was studied by Liu et al. (1993) from the Wangning section, and Rolph et al. (1993) first reported results from the upper Jaramillo transition at Lanzhou, which is noisy with many rapid fluctuations that are often represented by single samples. Zhu et al. (1994a) investigated the Weinan loess section and recognized the M/B and upper Jaramillo transitions across 50 cm stratigraphic intervals, which they suggested represent transitional periods of some 5000 years and 3200 years, respectively, which is consistent with estimates from marine sediments (Clement, 2004). Their results also indicate numerous back-and-forth oscillations.

The Blake geomagnetic event has been identified in the Xifeng section by Zhu et al. (1994b, 1998a), while Fang et al. (1997) reported a detailed record from Jiuzhoutai. A complex signature is observed with two reversed polarity intervals separated by a short normal-polarity interval. Based on correlation to the marine oxygen isotope record and on TL dating, the Blake excursion was estimated to have occured from 117.1 $\pm$ 1.2 to 111.8 $\pm$ 1.0 ka (Zhu et al., 1994b) and from 119.97 to 114.47 ka (Fang et al., 1997), which is broadly consistent with the widely accepted age of 110–125 ka for the Blake excursion (Guillou et al., 2004; Singer et al., 2009). Detailed paleomagnetic investigations of the Malan Loess at Weinan by Zhu et al. (1999) and Pan et al. (2002) revealed two distinct geomagnetic excursions that are accompanied by lower relative paleointensities. These two excursions were estimated to have occurred at about 27 and 42 ka based on $^{14}$C and thermoluminescence (TL) dating, which probably correspond to the Mono Lake and Laschamp excursions, respectively. Similar results were obtained from the Lingtai section (Zhu et al., 2000). Wang et al. (2005) reported two anomalous intervals between the M/B and upper Jaramillo boundaries at Sanmenxia, which they interpreted to be a remagnetization due to magnetic particle realignment in the coarsest loess L9. However, the remanence carrying magnetic particles (<2 μm) are usually far smaller than matrix particles (20-40 μm) in Chinese loess (Pye, 1987), so the interpretation in favour of remagnetization due to the coarse grain size requires more evidence. In addition to the Mono Lake, Laschamp, and Blake excursions, many other short-lived geomagnetic excursions and polarity intervals, such as the Santa Rosa and Punaruu events, have

been observed from different loess sections (Zhu et al., 1994b, 1998a, 1999, 2000; Zheng et al., 1995; Fang et al., 1997; Pan et al., 2002; Yang et al., 2007). Moreover, these excursions are well correlated with those discovered globally in both volcanic and/or sedimentary paleomagnetic records (e.g., Langereis et al., 1997; Lund et al., 2006; Singer et al., 2002; Oda, 2005). Furthermore, some paleomagnetic studies with dense sampling demonstrate that loess units are capable of recording geomagnetic paleosecular variation (PSV) (e.g., Zhu et al., 1998, 2000; Heslop et al., 1999; Liu et al., 2005a). These observations suggest that Chinese loess-paleosol deposits have the potential to record geomagnetic episodes as short as a few kyr or less in duration, as well as long term reversal patterns.

## 1.5 Doubts about geomagnetic recording by Chinese loess

Successful recording of magnetic polarity zonations indicates that the Chinese loess has faithfully recorded geomagnetic information. Closer inspection, however, reveals serious problems. Building on work by deMenocal et al. (1990), Tauxe et al. (1996) compiled 19 records of the M/B boundary from carbonate sediments cored from widely distributed marine sites. All but one of the sites locates the M/B boundary within marine oxygen isotope stage 19, which was an interglacial period. However, at most sites on the Chinese Loess Plateau, the M/B boundary is found within loess unit L8, which is a glacial interval (Liu et al., 1988a; Wang et al., 1990). Tauxe et al. (1996) explained that this conflict is due to "delayed remanence acquisition" in loess. Zhou and Shackleton (1999) further addressed this problem by paying particular attention to the occurrence at Luochuan of 16 glassy particles 65-220 μm in size, which are attributed to the Australian microtektite layer, which occurs below the M/B boundary. On the Chinese Loess Plateau, however, the glassy particles are found above the measured position of the M/B boundary. To resolve this conflict, Zhou and Shackleton (1999) proposed that the "lock-in" depth for magnetic remanence at Luochuan is about 2 m with a corresponding time delay of about 15~20 kyr. In contrast to the thick lock-in explanation, Zhu et al. (1998) demonstrated that loess L8 is capable of recording PSV and that the lock-in depth in Chinese loess is no more than that of marine sediments based on detailed studies from six loess sections. Zhu et

al. (1998) suggested that a paleoclimatic recording phase lag between the ocean and the continent is responsible for the M/B boundary discrepancy. Recently, Wang et al. (2006) proposed that paleosol S8, rather than paleosol S7, should be correlated with interglacial MIS 19, and attributed the M/B boundary discrepancy to incorrect correlation of paleoclimatic records between Chinese loess and marine sediments. Liu et al. (2008) used quartz grain size instead of magnetic susceptibility to correlate Chinese loess sequences to marine sediments, and argued from the revised position of boundaries between loess and paleosol units that there is no obvious lock-in depth in Chinese loess and that the M/B boundary should be located at the transition from S8 to L8. Liu et al. (2008) concluded that there is no mismatch between Chinese loess and marine sediments if marine sediments have a <20 cm lock-in depth, which is similar to the thickness of the bioturbated surface mixed layer in many types of sediment. In addition, some studies indicate no apparent lock-in delay for loess L1 and paleosol S1 based on the timing of the Mono Lake and Laschamp excursions (Pan et al., 2002).

In addition to the problem of the location of the M/B boundary, the complex paleomagnetic behaviour observed during polarity transitions and excursions has caused concern. Oscillations of both declination and inclination are observed during polarity transitions and excursions, and sometimes the same transition produces different behaviour at nearby sites, which would not be expected for genuine geomagnetic field behaviour. The failure of alternating field demagnetization in the study of Heller and Liu (1984) made them suggest that the original remanence in the Chinese loess is a chemical remanent magnetization (CRM) that resides in hematite and that if hematite growth is sufficiently slow, short-lived excursions such as the Blake event may be easily obscured. This has been demonstrated to be incorrect by later studies (e.g., Zhu et al., 1994b). A modified view has developed whereby the remanence of Chinese loess is considered to have two parts; one is a detrital remanence (primary) and the other is a pedogenic remanence (secondary). An implication of the potential complexity of paleomagnetic recording in Chinese loess is that it is difficult to trust detailed paleomagnetic records without a better understanding of the processes by which the loess records paleomagnetic information.

# 1.6 Major unresolved problems in paleomagnetic studies of the Chinese loess

Zhu et al. (1994b) concluded "more research is needed to understand the exact processes of remanence acquisition of loess deposits". Laboratory redeposition experiments provide a means of understanding the magnetic remanence of sediments, and to test whether a detrital remanence is prominent. However, only one such study has been done over the past 30 years. McIntosh (1993) undertook limited laboratory re-deposition experiments under wet conditions and found that, in addition to a viscous remanence, a stable depositional remanent magnetization (DRM) was produced as soon as the sediment dried. McIntosh (1993) did not simulate the formation process of loess (e.g., dust deposition) and acknowledged that his experiments were an initial simulation that needed further work.

As summarized above, the magnetic enhancement that occurs during pedogenesis gives rise to a paleoclimatic signal in Chinese loess. Neoformation of magnetic minerals will definitely produce a chemical remanent magnetization (CRM), which will complicate detrital paleomagnetic signals. Removal of secondary signals and separation of detrital information, therefore, is an important aim for paleomagnetic studies of Chinese loess sequences. While the pedogenic neoformation of magnetite and maghemite are relatively well understand, the role of pedogenic hematite is relatively poorly studied.

The mismatch of the position of the M/B boundary, complex paleomagnetic behaviour observed during polarity transitions and geomagnetic excursions, pedogenic effects, and poor understanding of magnetic remanence mechanisms are four of the most important problems for paleomagnetic studies of the Chinese loess. Clarification of the magnetic remanence acquisition mechanism(s) will help to resolve the other problems, and will help to evaluate whether it is possible to use other paleomagnetic techniques, such as relative geomagnetic paleointensity, for developing detailed age models between successive geomagnetic reversals for loess profiles.

# 1.7 Aims and objectives of this study

Due to the importance of magnetic remanence acquisition mechanisms of Chinese loess for paleomagnetic studies, this PhD project is aimed at understanding magnetization processes in Chinese loess. To study the effects of pedogenesis, we sampled the Baicaoyuan section that spans loess unit L1 (almost pristine loess) and most of paleosol unit S1 (strongly pedogenically soil). Hematite formation is investigated with several methods, which helps to establish the previously poorly studied effects of pedogenic hematite formation on paleoclimatic signals. Laboratory simulation of DRM and post-depositional remanent magnetization (PDRM) processes in Chinese loess has also been performed to understand the role of these processes that give rise to paleomagnetic signals in the Chinese loess. An additional Chinese loess section at Yuanbao has been sampled from the western Chinese Loess Plateau. Detailed paleomagnetic and rock magnetic measurements, which aim to assess whether relative paleointensity signals have been faithfully recorded, have been made on samples from these two sections.

Given that paleomagnetic studies have been made on Chinese loess for more than three decades, concerted efforts to understand the mechanism(s) by which Chinese loess becomes magnetized are long overdue. The overarching aim of this study is to make significant contributions to our understanding of magnetization processes in Chinese loess.

# Chapter 2

# Paleomagnetic Theory and Methods

## 2.1 Physics of magnetism

### 2.1.1 Introduction to magnetism

The term "magnetic field" simply describes a volume within which there is a change in magnetic energy. This change in energy can be detected and measured. The location where a magnetic field can be detected exiting or entering a material is called a magnetic pole. Magnetic poles have never been detected in isolation but always occur in pairs, which are referred to as dipoles. A dipole has a magnetic pole on one end and a second, equal but opposite, magnetic pole on the other. A bar magnet can be considered a dipole with a north pole at one end and south pole at the other (Figure 2.1a). A magnetic field can be measured leaving the dipole at the north pole and returning to the magnet at the south pole.
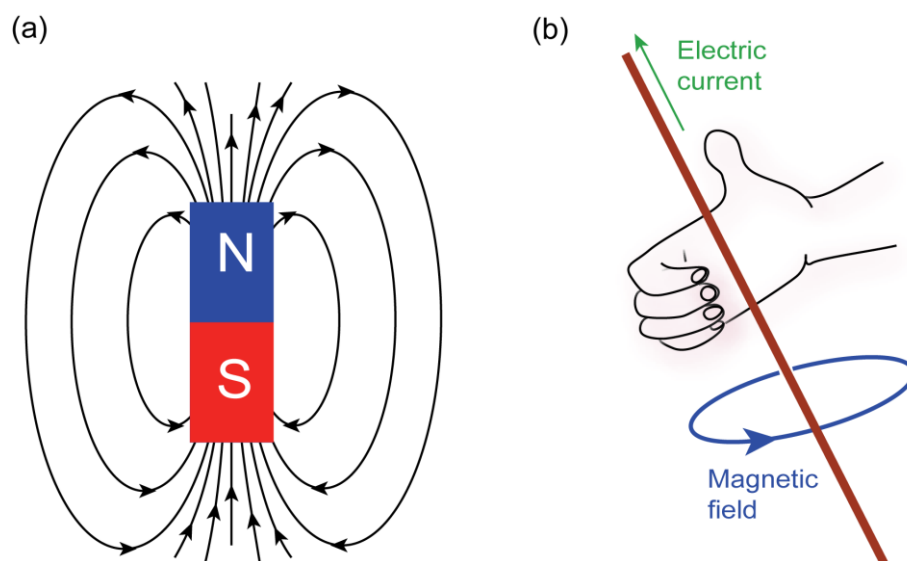


**Figure 2.1**     (a) Magnetic field produced by a bar magnet. The lines represent the lines of magnetic force. (b) Relationship of magnetic field to current for a straight wire (Ampère's Law).

All matter is composed of atoms, and atoms are composed of protons, neutrons and electrons. Protons and neutrons are located in an atom's nucleus and electrons are in constant motion around the nucleus. Electrons carry a negative charge, based on Ampère's Law, and produce a magnetic field as they move through space. A magnetic field is produced whenever an electrical charge is in motion. The strength of this field is called the magnetic moment, which is the sum of individual magnetic moments from multiple atoms. Ampère's Law (Figure 2.1b) is a simple approximation to the modern physical interpretation of magnetism and is applicable to diamagnetic materials. However, our understanding of paramagnetism and ferromagnetism is based on the quantum spin of atomic electrons. These types of magnetic behaviour are described below.

## 2.1.2 Types of magnetic behaviour

When a material is placed into a magnetic field $\boldsymbol{H}$, the field will induce a magnetization $\boldsymbol{M} = \chi\boldsymbol{H}$, where $\chi$ is the *bulk magnetic susceptibility* of the material. The total measurable magnetic flux, which has contributions from the applied field and the induced magnetization, is the magnetic induction $\boldsymbol{B} = \mu_0 (\boldsymbol{M} + \boldsymbol{H})$, where $\mu_0$ is the magnetic constant. Most materials produce their own magnetization in response to the applied external field. Typically, the response is weak and exists only when the magnetic field is applied. The term "magnetism" is used to describe how these materials respond on the microscopic level and is used to categorize the type of magnetic behaviour of a material. There are several types of magnetic behaviour.

**Diamagnetism** is the property of an object that causes it to create a magnetic field in opposition to the externally applied field, thus causing a repulsive effect. Specifically, the external magnetic field alters the orbital velocity of electrons around their nuclei, thus changing the magnetic dipole moment in the direction opposing the external field. Diamagnetism is a property of many materials, but it is a weak effect: for a purely diamagnetic material, $\chi$ is typically $< -10^{-7}$ SI.

**Paramagnetism** is due to incomplete electron shells. Paramagnetic materials contain permanent magnetic moments, which align with an applied field to produce a positive induced magnetization. The magnitude of the induced magnetization is dependent on temperature and on applied field strength. In pure paramagnetism, the dipoles do not interact with one another and are randomly oriented in the absence of

the external field due to thermal agitation, which results in zero net magnetic moment. Paramagnetic behaviour is also observed in ferromagnetic materials above their Curie temperature ($T_C$), and in antiferromagnets above their Néel temperature ($T_N$).

Unlike diamagnetism and paramagnetism, ferromagnetism (*sensu lato*) has the potential to provide long-term remanent magnetizations that record paleomagnetic information. Ferromagnetism can be divided into three sub-types.

**Ferromagnetism** (*sensu stricto*) results when the arrangement of atoms causes electron orbitals containing unpaired spins to overlap. Strong exchange forces between these interacting spins cause them to align with each other in order to minimize exchange energy. These interactions cause strong induced magnetizations in the presence of magnetic fields, which also lead to magnetic hysteresis: the alignment of atomic moments is preserved even in the absence of an applied field, thereby producing a spontaneous magnetization (Figure 2.2a). At $T_C$, the effects of thermal fluctuations become sufficiently large to break the magnetic coupling of the electrons and a ferromagnet becomes paramagnetic.
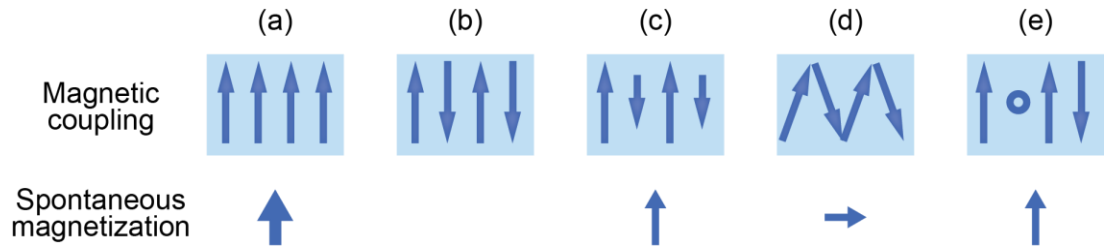


**Figure 2.2**      Schematic illustration of different magnetic coupling mechanisms and their spontaneous magnetizations. (a) Ferromagnetism (*sensu stricto*), (b) antiferromagnetism, (c) ferrimagnetism, (d) spin-canted antiferromagnetism, and (e) defect antiferromagnetism.

**Antiferromagnetism** results when the atomic moments within each magnetic sublattice align in a perfectly antiparallel manner (Figure 2.2b). The magnitudes of the sublattice magnetizations are equal, which results in zero net spontaneous magnetization. Antiferromagnetic materials do not have a $T_C$ but a $T_N$ at which magnetic ordering breaks down and the material becomes paramagnetic. Occasionally, the sublattices are not perfectly aligned in an antiparallel orientation, but are canted by a few degrees which give rise to a weak net moment in so-called canted antiferromagnets (Figure 2.2d). Also, antiferromagnetic materials can have a net moment if spins are not perfectly compensated owing to defects in the crystal structure (Figure 2.2e), as occurs in fine-grained hematite.

**Ferrimagnetism** also occurs when the two magnetic sublattices have antiparallel alignment, but in this case the magnitudes of the moments in each direction are unequal (Figure 2.2c), which results in a spontaneous magnetization. Ferrimagnets are not limited to two sublattices, and the magnetizations of the sublattices need not be perfectly antiparallel but can be inclined at some intermediate angle. Magnetite is an example of a ferrimagnetic material.

## 2.1.3 Magnetic anisotropy

The magnetic energy of a ferromagnetic grain is minimized by aligning its magnetic moment in the direction of the ambient magnetic field. In the absence of other controls on the orientation of their magnetization, ferromagnetic grains would always align with the ambient geomagnetic field and no older remanence would be preserved. However, the energy required to magnetize a grain is usually not constant in all orientations; there are 'easy' directions of magnetization in which the associated energy is lower. Alignment of magnetization along the easy axis of magnetization in a ferromagnetic grain enables recording of long-term remanent magnetizations. There are three principal sources of magnetic anisotropy.

**Magnetocrystalline anisotropy** occurs when the exchange energy between coupled spins is minimized when spins are aligned along particular crystallographic axes.

**Shape anisotropy** can be considered as follows. If atomic magnetic moments are modelled as pairs of magnetic charges, a magnetized grain will have a surface distribution of charges, which not only produces an external field but also an internal demagnetizing field that opposes the overall magnetization. The strength of this field depends on the surface charge distribution. Therefore an elongated grain has a smaller demagnetizing field along its long axis. The long axis of the grain then becomes the easy axis of magnetization because a smaller percentage of the surface is covered by magnetic charges.

**Magnetostrictive anisotropy** occurs because spin realignment exerts stresses on the magnetic crystal, which changes its shape. Conversely, therefore, applied stresses, which further alter the shape of the crystal, can affect the spin alignment and give rise to magnetostrictive anisotropy.

## 2.1.4 Domain theory

A magnetic domain describes a region within a magnetic material that has uniform magnetization. Magnetic domains result from energy minimization. Landau and Lifshitz (1935) proposed theoretical domain structures based on the minimum energy concept, which forms the basis for modern domain theory. Domain formation provides a magnetic configuration for a magnetic particle that will maintain a minimum total energy at any equilibrium state. In the simplest case, for such a magnetic particle, the total energy, $E_{total}$, is the sum of several free energy terms:

$$E_{total} = E_{ex} + E_{\kappa} + E_{\lambda} + E_{D} + E_{H},$$

where $E_{ex}$ is the exchange energy, $E_{\kappa}$ is the magnetocrystalline anisotropy energy, $E_{\lambda}$ is the magnetoelastic energy, $E_D$ is the magnetostatic energy, and $E_H$ is the external field energy. Increasing grain size also increases $E_D$ associated with the surface distribution of magnetic charges. Above a certain size, it becomes energetically favourable for the grain to split into a number of uniformly magnetized domains, oriented along different easy directions of magnetization, which reduces the overall magnetization. The number of domains that form is determined by the balance between the resulting reduction in magnetostatic energy, and the energy required to form domain walls. Domain walls are narrow regions between adjacent domains across which spins must rotate from one easy direction to another.
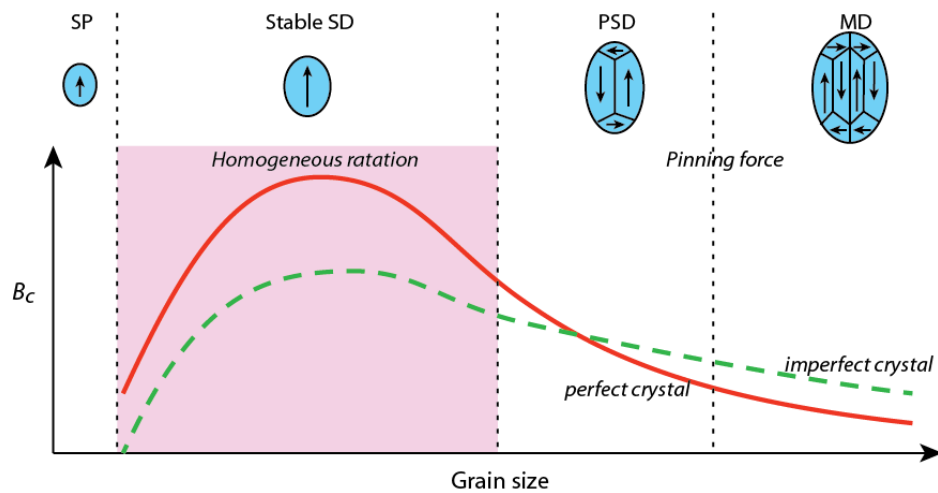


**Figure 2.3**      Schematic representation of the variation in domain state and coercivity with increasing grain size. After Moskowitz (1991).

**The single domain (SD) state**: Below a critical grain size, the energy required to create a domain wall exceeds the reduction in magnetostatic energy achieved in

forming one. An SD grain therefore has a uniform magnetization that can only be changed by rotation of its magnetic moment; when SD grains are relatively large and thermally stable, it is energetically difficult to change the direction of magnetization, resulting in high coercivities and magnetic stability. SD grains are the ideal carrier of magnetic signals. Theoretical understanding of the stability of SD particles is based on Néel's relaxation equation (Néel, 1949):

$$\tau = \tau_0 \exp\left(- K_{eff}V / 2kT\right),$$

where $\tau$ is the relaxation time, $\tau_0$ is the pre-exponential factor that corresponds to the resonance relaxation time of the spin system, $K_{eff}$ is the effective anisotropy energy, which has different expression depending on the type of anisotropy, $V$ is grain volume, $k$ is Boltzmann's constant, and $T$ is absolute temperature. $\tau$ is small for extremely small particles, whose remanence decays rapidly, but it increases as grain size increases. At a critical grain volume, $\tau$ is sufficiently long that a stable magnetic remanence is preserved. Below this volume, magnetic particles display superparamagnetic (SP) behaviour. This critical volume is called the SP/SD boundary, and is temperature dependent. For magnetite, this boundary occurs at about 20 nm at room temperature.

**Superparamagnetism**: Below the SP/SD boundary, the thermal energy is insufficient to overcome the exchange interaction between neighbouring spins, but it is sufficient to change the direction of magnetization within the entire grain. Thermal fluctuation randomizes the direction of magnetization of each grain, which therefore minimizes the total magnetization of a sample. SP particles can be magnetized in an external field, and the magnetization is described by the Langevin function:

$$M = N\left(\coth \gamma - (1 / \gamma)\right)M_s,$$

where $N$ is the number of particles, and $\gamma = M_sB_v / kT$, where $M_s$ is the magnetic moment of SP particles, and $B_v$ is the applied field.

**The multi-domain (MD) state**: For large particles, the demagnetizing energy becomes significant due to the large surface area. To reduce the demagnetizing energy, and therefore the total energy of the system, the magnetization of the particle will be divided by domain walls. Particles with domain walls are referred to as MD grains. Additionally, rather than causing realignment of magnetic moments, applying a field to a MD grain promotes preferential growth of domains with magnetization parallel to the field. Domain wall movement is a low energy process that can be accomplished in

relatively low fields; thus, MD grains have low coercivities and are magnetically unstable over geological timescales.

**The pseudo-single domain (PSD) state**: The transition from SD-like to MD-like behaviour is not abrupt. Small MD grains contain a small number of domains and can have a substantial magnetic moment. Micromagnetic modelling indicates that such particles have vortex structures (e.g., Williams and Dunlop, 1989). These particles are the so-called PSD grains, which can have large remanent magnetizations, high coercivities, and can be magnetically stable over geological timescales. The PSD size interval is approximately 1-20 μm for magnetite.

### 2.1.5 Natural remanent magnetization

The natural remanent magnetization (NRM) is the remanent magnetization recorded by a rock or sediment. NRM depends on the geomagnetic field during rock or sediment formation, the composition of the rock or sediment, and on geological processes during the subsequent history of the sample. An NRM can have thermal, chemical or depositional origins, and is usually composed of more than one component. The component acquired during rock formation is referred to as the primary NRM and is the component sought in most paleomagnetic investigations. However, secondary NRM components can be acquired subsequent to rock formation and can alter or obscure the primary NRM. The total NRM is the vector sum of different components in the same sample. In order to avoid over-interpretation that can be associated with use of the term "primary" remanence, the term characteristic remanent magnetization (ChRM) is often used to refer to the highest-stability NRM component isolated during progressive stepwise demagnetization experiments.

**Thermoremanent magnetism (TRM):** TRM is produced by cooling from above $T_C$ in the presence of a magnetic field. If a rock is cooled through various temperature intervals in the presence of a magnetic field, the TRM acquired in each interval is found to be independent of that acquired in each other interval, which is known as the principle of partial TRM (PTRM) superposition. The sum of all PTRMs is equal to the total TRM acquired during cooling through the total temperature interval. This is known as the law of PTRM additivity. The NRM of igneous rocks is mostly attributable to TRM.

**Chemical remanent magnetization (CRM):** CRM is the remanent magnetization produced when a magnetic mineral forms chemically or crystallizes in an external magnetic field. Examples of CRM acquisition include pedogenic magnetite growth in soils, and growth of the iron sulphide greigite during reductive diagenesis in rapidly deposited sediments. A CRM does not necessarily record a primary paleomagnetic signal, therefore it is important to be able to remove or separate a CRM from the NRM.

**Viscous remanent magnetization (VRM):** When magnetic minerals are exposed to a weak external magnetic field, they will gradually acquire a VRM. Due to thermal relaxation, this kind of remanent magnetization will gradually decrease in a zero field. The VRM acquisition (or decay) rate is temperature and grain size (i.e., volume, $v$) dependent $[\tau \propto \exp(v/T)]$. Rocks and sediments, which are exposed to the geomagnetic field over geological time scales, usually have this type of remanence to varying extents. VRM acquisition follows the same theory as TRM acquisition, but at relatively constant temperature. A magnetization acquired in a weak magnetic field over long periods of time, at temperatures above ambient, but below $T_C$, is referred to as a thermoviscous remanent magnetization.

**Depositional or detrital remanent magnetization (DRM):** DRM is the remanent magnetization acquired during deposition and lithification of sediments or sedimentary rocks. DRM is complicated because many processes can be involved in the formation of sedimentary rocks. A variety of magnetic minerals can be present, and minerals are often not in chemical equilibrium with each other or with the environment of deposition. For marine or lake sediments, deposition occurs under aqueous conditions. For wind-blown deposits such as Chinese loess, however, deposition normally occurs under dry conditions, but precipitation after deposition could be important for remanence acquisition. The efficiency of magnetization acquisition depends on the relative diameters of the magnetic and bulk matrix grains, and is most effective when the magnetic grains are smaller than matrix grains. The size of voids in the sediment progressively decreases with compaction; therefore the ability of magnetic grains to rotate is progressively impeded and decreases sharply at a critical porosity value. The processes that operate after deposition, particularly bioturbation for marine sediments or rain for loess, are probably more important, because they enable realignment of grains within the ambient field before sediment consolidation to form a post-depositional remanent magnetization (PDRM). Chemical

processes can also alter or remove original detrital ferrimagnetic minerals and/or cause precipitation of new ferrimagnetic minerals, with attendant effects on the paleomagnetic record. For example, how pedogenic magnetic minerals affect the paleomagnetic record of Chinese loess is an important unsolved problem. DRM also remains less well understood than TRM.

**Isothermal remanent magnetization (IRM):** An IRM is induced by applying a strong magnetic field for a short period of time at a constant temperature. The saturation IRM (SIRM) is the IRM when it is in a saturated state; it is acquired in a sufficiently strong field to saturate the remanence. SIRM is usually large and unstable because it is not in the most favourable energy state. IRM is usually induced in the laboratory, but it can also be induced in nature through lightning strikes.

**Anhysteretic remanent magnetization (ARM):** An ARM is a laboratory-induced remanence that is imparted by placing a sample in an applied alternating field (AF) with a small direct current (DC) bias field at the same time. As the AF decreases from a maximum value to zero, the magnetization preferentially aligns in the direction of the bias field. The ARM is acquired by decreasing the external field energy, and is widely used in rock magnetic studies.

## 2.2 The geomagnetic field and paleomagnetism

### 2.2.1 The Earth's magnetic field

If we could place a bar magnet inside the Earth, inclined approximately $11\,°$ to the rotational axis and offset about 550 km from the Earth's centre, we could account for 95% of the observed magnetic field, which refer as the diploe part of Earth's magnetic field. The other ~4% of the field is contributed by the Earth's crust, which refer as the non-diploe component. The magnetic field strength at the Earth's surface is 30-60 $\mu$T. The Earth's magnetic field is a vector quantity, with both strength and a direction at any point in space. To completely describe it we need to know three quantities (Figure 2.4a). These are usually described in one of three ways:

- three orthogonal strength components: $X$, $Y$, and $Z$; or
- the total field strength and two angles: $B$, $D$, and $I$; or
- two strength components and an angle: $H$, $Z$, and $D$.

In these representations, *X* is the north component, *Y* is the east component and *Z* is the vertical component of the magnetic field vector (by convention *Z* is positive downward); *B* is the total intensity of the magnetic field vector; *H* is the horizontal component of the magnetic field vector; *D* is the magnetic declination, which is defined as the angle between true north and the horizontal component of the field measured eastward from true north; *I* is the magnetic inclination, which is defined as the angle measured from the horizontal plane to the magnetic field vector (and is positive downward).
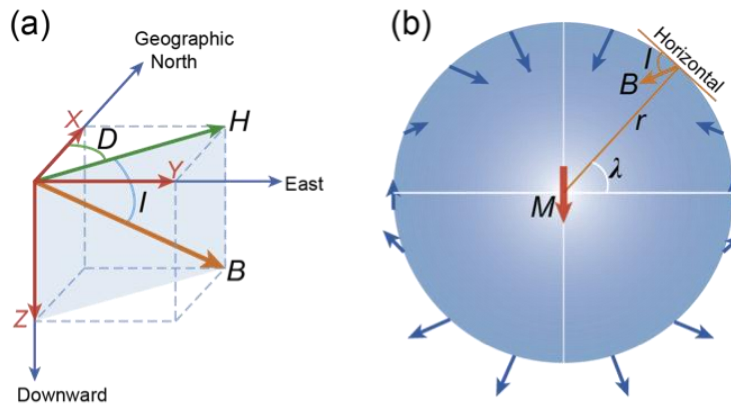


**Figure 2.4**          (a) Schematic illustration of the main elements of the geomagnetic field. (b) Geocentric axial dipole model. A magnetic dipole *M* is placed at the centre of the Earth and is aligned with the rotation axis. *λ* is the geographic latitude; *r* is the mean radius of the Earth; *I* represents the inclination at that point. After Butler (1992).

The Earth's magnetic field is slowly changing on timescales that range from years to millennia. Such changes are referred to as secular variation. Secular variation over the last few millennia has the following characteristics: 1) a decrease in the strength of the dipole part of the magnetic field; 2) westward drift of the non-dipole part of the magnetic field; and 3) changes in the non-drifting part of the non-dipole field (Constable, 1992; Cox et al., 1975; Thompson et al., 1985).

## 2.2.2 Geocentric axial dipole model

The geocentric axial dipole (GAD) model is a fundamental hypothesis in paleomagnetism (Figure 2.4b). In this model, the Earth's magnetic field, when its variation is averaged over a sufficiently long period of time, is represented by a single magnetic dipole at the centre of the Earth that is aligned with the rotation axis. A GAD field has the following properties:

$$H = M \cos \lambda / r^3,$$

$$Z = 2M \sin \lambda / r^3, \text{ and}$$

$$B = M \, (1 + 3\sin^2 \lambda)^{1/2} / r^3,$$

where $M$ is the dipole moment of the geocentric axial dipole; $\lambda$ is the geographic latitude, which ranges from -90° at the south geographic pole to +90° at the north geographic pole; and $r$ is the Earth's mean radius.

The lengths of the arrows in Figure 2.4b schematically illustrate the factor of 2 increase in magnetic field strength from equator to poles. The inclination of the field can be determined by:

$$\tan I = Z \, / \, H = 2\sin \lambda \, / \cos \lambda = 2\tan \lambda \, ,$$

where $I$ increases from -90° at the geographic south pole to +90° at the geographic north pole. The relationship between $I$ and $\lambda$ is essential to understanding many paleogeographic and tectonic applications of paleomagnetism. For a GAD, $D = 0°$ everywhere.

### 2.2.3 Demagnetization methods

The total NRM of a sample does not always only have a single magnetization component. Instead, it can comprise the vector sum of a number of different components. For sediments such as Chinese loess, the NRM may consist of a DRM and/or a PDRM from or shortly after the time of deposition, a CRM caused by pedogenic magnetite formation and a VRM that carries a present-day field overprint. It is necessary to separate these different components to extract useful paleomagnetic information. This is usually achieved through the use of stepwise demagnetization, which relies on the principle that different magnetic components are carried by distinct populations of grains, with different mineralogies and grain sizes, and therefore different stabilities. Stepwise demagnetization progressively removes low stability NRM components, and isolates the more stable components that are more likely to record an ancient magnetization. The most stable component is referred to as the ChRM. The two techniques commonly used to isolate the ChRM are thermal and AF demagnetization.

**Thermal demagnetization**: The characteristic relaxation time $\tau$ is inversely proportional to temperature. Therefore, grains that are stable at room temperature will become unstable when heated to their unblocking temperature $T_b$, which is higher for

more stable grains. Thermal demagnetization involves heating a sample to temperature $T$ then cooling it back to room temperature in zero magnetic field. All grains with blocking temperature $T_b < T$ have their directions randomized, thereby erasing the NRM carried by these grains and allowing more stable components to be isolated.

**AF demagnetization**: When a sample is exposed to a sinusoidally varying magnetic field, which is smoothly reduced to zero from a specified peak value to randomize the magnetization of the sample, it is being subjected to AF demagnetization. This process effectively randomizes the magnetization of grains with coercivities below the peak AF intensity, which allows the remanence of higher coercivity grains to be isolated. In this study, we used an in-line AF demagnetizer on a 2G-Enterprises cryogenic magnetometer (Roberts, 2006), with which an AF was applied along three mutually perpendicular sample axes at progressively increasing fields after each measurement step.

The relative effectiveness of the thermal and AF demagnetization methods can differ depending on the mineralogy of the remanence-carrying grains, and on the distribution of coercivities and unblocking temperatures for the different components. For example, AF treatment is less effective at removing the remanence carried by hematite compared to the thermal method. This is because hematite has high coercivities, but its remanence will be totally removed by heating above the Néel temperature of 680°C. An example is given in Figure 2.5 for a Chinese loess sample that has been subjected to combined AF and thermal treatment.
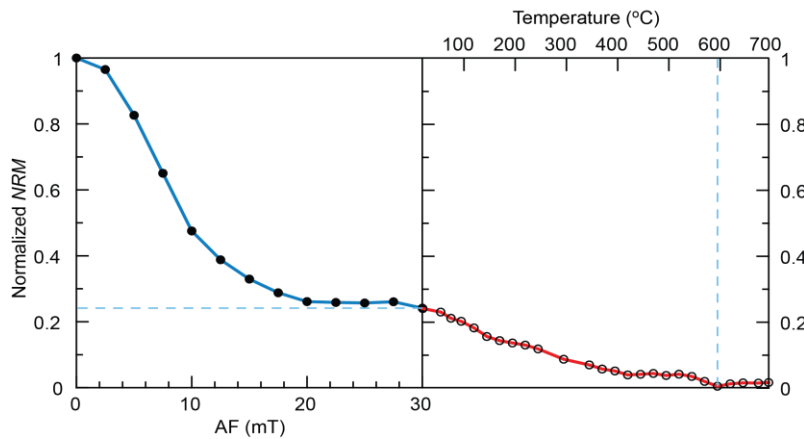


**Figure 2.5**        An example of combined AF and thermal demagnetization for a paleosol sample. The sample was first treated using AF demagnetization up to a 30 mT peak field, followed by stepwise heating up to 700°C. The blue dashed lines are auxiliary lines.

## 2.2.4 Polarity reversals and excursions

Although the origin of the geomagnetic field is not well understood in detail, it is generally accepted that the field is generated by a magnetohydrodynamic dynamo that is derived by fluid motion in Earth's outer core. The field has not always been in a normal polarity state such as at present. It has changed polarity many times as a result of polarity reversals. Rocks, such as basalts and marine sediments, record these polarity changes. Combined with other dating methods, the geomagnetic polarity pattern has been developed into a standard timescale. Magnetostratigraphic studies depend on identification of a polarity pattern that can be correlated with the geomagnetic polarity timescale.

During a polarity reversal, the magnetic pole diverged from its original position. If the reversal was short-lived, the pole would return to its original position; this process is called a geomagnetic excursion. Many excursions have been reported from around the world at different times. However, some may not have had global expression and need further investigation. Well-established excursions have the potential to serve as stratigraphic tie points. The Mono Lake and Laschamp excursions are the two excursions that have been confirmed to have a world-wide expression during the past 100 ka (Roberts, 2008); they have also been identified in Chinese loess profiles (for more information see Chapter 1).

## 2.2.5 Paleointensity

After thermal or AF demagnetization, the ChRM direction recorded by a sample can be obtained through principal component analysis (Kirschvink, 1980). The geomagnetic direction can then be identified for the time that the sample formed. The paleointensity of the paleo-geomagnetic field, however, is a much more difficult quantity to determine. Based on Néel's theory of SD remanence (Néel, 1949, 1955), and incorporating assumptions concerning the behaviour of magnetic particles within a sample, Thellier designed a method to detect the absolute geomagnetic paleointensity using volcanic rocks. This method makes use of Thellier's three laws of TRM: independence, additivity and reciprocity (Thellier, 1938, 1981; Thellier and Thellier, 1959). The limitation is that the NRM type must be a TRM, and the studied sample must be heated to simulate the NRM acquisition process. In order to reduce the effects of thermal alteration during heating, which frequently compromises results

of the Thellier and Thellier (1959) method, the Shaw method (Shaw, 1974) and microwave method (Hill and Shaw, 2000) have been developed.

The difficulty of finding long volcanic sequences with rapid eruption rates from which continuous absolute paleointensity records can be determined, means that sediments have been considered for paleointensity studies. However, the non-linear relationship between DRM and applied field based on laboratory re-deposition experiments indicates that this task is not simple. A DRM is a complicated function of applied field, and magnetic matrix mineralogy, magnetic mineral concentration, and grain size, chemistry of the water and post-depositional mineral re-alignment. In natural settings, the sediment might have undergone pedogenesis or diagenesis, and hence magnetic mineral enhancement or dissolution and/or overprinting by a CRM. Assuming that one is studying a simple sedimentary sequence, one can assume that only the magnetic mineral concentration has affected the NRM intensity. In such a case, we can normalize the NRM by a parameter that provides an indication of magnetic mineral concentration such as ARM, IRM, or $\chi$. Alternatively, one can use more complicated proxies that involve selective demagnetization of the NRM or of the respective normalizer to estimate the relative paleointensity. Tauxe (1993, 2006) summarized several criteria for relative paleointensity studies using sediments.

- The NRM must be carried by a detrital magnetic mineral with high magnetic stability. Furthermore, the portion of the NRM vector used for paleointensity should be a single, well-defined component of magnetization. The nature of the NRM can be checked with progressive demagnetization using AF and thermal techniques. Supplementary information from hysteresis and rock magnetic experiments can also be useful.

- The detrital remanence must be an excellent recorder of the geomagnetic field. It should exhibit no inclination error and if both polarities are present the two populations should have antipodal paleomagnetic directions. The associated directional data must therefore be plotted on equal area projections whenever they are available.

- Large changes in magnetic mineral concentration (more than about an order of magnitude) and any change in magnetic mineralogy or grain size will foil attempts at normalization because of the likelihood of magnetostatic interactions among the particles. These changes can be detected using bi-plots of, for example, IRM and $\chi$. Such bi-plots should be linear, with low scatter.

- Relative paleointensity estimates that are coherent with bulk rock magnetic parameters relating to paleointensity normalizers should be treated with caution. Coherence can be assessed using standard spectral analysis techniques.

- Records from a given region should be coherent within the limits of a common time scale. Whenever possible duplicate records should be obtained and compared.

- For a relative paleointensity record to have maximum utility, it should have an independent time scale.

- Changes in water chemistry and changes in clay mineralogy or concentration can significantly affect the tendency of magnetic minerals to flocculate with clays. Such changes are likely to have a profound effect on the DRM, yet their effects may be difficult to detect. Low salinity environments are particularly sensitive to this problem. It is therefore desirable to characterize changes in the clay fraction in relative paleointensity studies.

Chinese loess has a completely different depositional environment compared to marine sediments. The dust settles on a dry or semi-dry ground surface, and can be modified after deposition by precipitation or re-working. Evaporation rate, consolidation, and pedogenesis will also affect paleomagnetic recording by Chinese loess. More work needs to be done to adequately understand how Chinese loess records paleomagnetic information. It has been claimed that Chinese loess can record relative geomagnetic paleointensity variations (Liu et al., 2005a). This possibility needs testing in light of experimental work to determine the remanence acquisition mechanism(s) in Chinese loess.

## 2.3  Rock magnetism

Rock magnetism involves the study of the magnetic properties of rock-forming magnetic minerals. Analysis of the rock magnetic properties of paleomagnetic samples is recognized as being fundamentally important for understanding paleomagnetic signals. A wide range of parameters and properties are analyzed in rock magnetic studies, and are briefly summarized as follows.

## 2.3.1 Magnetic susceptibility

Magnetic susceptibility is the ratio of the induced magnetization to the applied field. At an atomic level, the magnetic susceptibility is the response of electron orbits and/or unpaired spins to an applied external field. The diamagnetic response is extremely weak and can be normally neglected in natural samples. Although the paramagnetic response is much higher, the response will be dominated by ferrimagnetic material if appreciable amounts of such minerals are present. SP particles have large magnetic susceptibility, which is why paleosols are magnetically enhanced. Magnetic susceptibility is also temperature and frequency dependent. These properties mean that magnetic susceptibility can provide additional information about magnetic minerals when it is measured at variable temperature and frequencies. Several definitions are widely used for magnetic susceptibility, which makes it important to be clear about which parameter is being used:
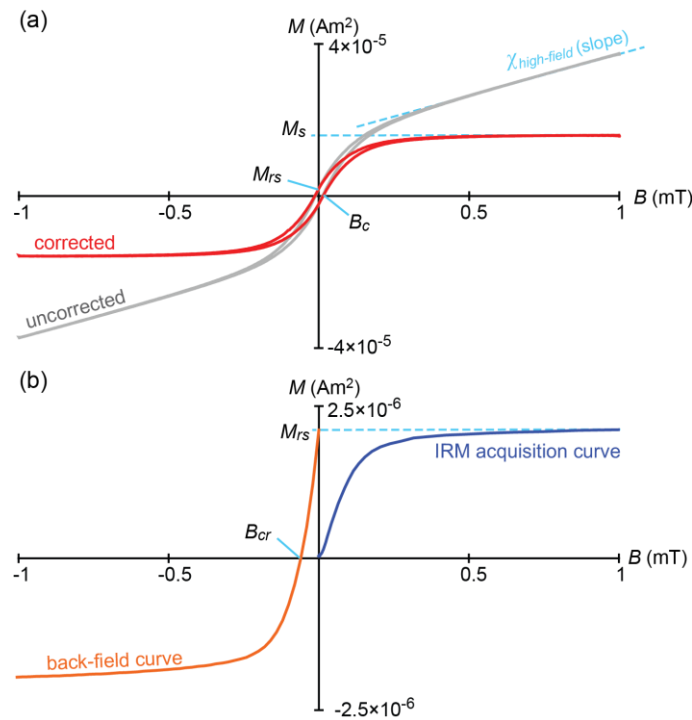


**Figure 2.6**      (a) Typical hysteresis loop for a Chinese loess sample (B125) that was acquired by measuring the magnetization $M$ in a varying magnetic field $B$. The grey loop represents the raw data without paramagnetic correction; the red loop has been slope-corrected. (b) IRM acquisition (blue) and back-field demagnetization (orange) curves for the same sample. Commonly used parameters are indicated.

- low-field magnetic susceptibility ($\chi_{low\text{-}field}$),
- high-field magnetic susceptibility ($\chi_{high\text{-}field}$),
- low-frequency magnetic susceptibility ($\chi_{low\text{-}f}$),

- high-frequency magnetic susceptibility ($\chi_{high\text{-}f}$),

- frequency-dependent magnetic susceptibility ($\chi_{fd}$),

- volume-normalized magnetic susceptibility ($\chi$), and

- mass-normalized magnetic susceptibility ($\kappa$).

## 2.3.2 Hysteresis parameters

Magnetic hysteresis is a particular characteristic of ferromagnetic (*sensu lato*) materials. When an external magnetic field is applied to a ferromagnet, the atomic dipoles align themselves with the external field. Even when the external field is removed, part of the alignment will be retained and the material becomes magnetized. The relationship between the intensity of magnetization (*M*) of a ferromagnetic material and the applied magnetic field (*B*) is illustrated in Figure 2.6a. When increasing the applied field, the magnetization increases following a S-shaped curve. When the field becomes large enough, the magnetization will not increase further; this is the saturated magnetic state. If the applied field is then gradually reduced to zero, and then continues to be reduced to the negative saturated state, and then increased to the positive saturated state, a cycle that records the changes in *M* with *B* provides a so-called hysteresis loop. Compared to measurements of the in-field magnetization in a hysteresis loop, measurement of the change in remanent magnetization in a gradually increasing field produces an IRM acquisition curve (Figure 2.6b). In a gradually applied opposite field, a so-called backfield demagnetization curve is produced (Figure 2.6b; yellow). The commonly determined hysteresis parameters (Figure 2.6) are defined below.

- Saturation magnetization ($M_s$) is the maximum magnetization the sample can acquire in an applied magnetic field.

- Saturation remanent magnetization ($M_{rs}$) is the remanence when the applied field has been reduced to zero after inducing a saturation magnetization; it is the maximum remanent magnetization that a sample can acquire.

- Coercive force ($B_c$) is the value of the negative field at which the magnetization of the sample is reduced from saturation to zero.

- Coercivity of remanence ($B_{cr}$) is the backfield at which the total remanent magnetization is reduced from saturation to zero. It is always larger than the coercive force.

As discussed before, the magnetic domain state is grain size dependent. Day et al. (1997) demonstrated that the hysteresis properties of magnetite of known domain states follow a predictable trend on a plot of the ratios $M_{rs}/M_s$ versus $H_{cr}/H_c$. They defined three regions for SD, PSD and MD grains in what is now referred to as a Day plot (Figure 2.7). However, natural samples rarely contain only one grain-size distribution or even one magnetic mineral type. Dunlop (2002a, b) calculated theoretical mixing curves for bimodal grain size distributions of magnetite on a Day plot (Figure 2.7). Other factors, such as magnetostatic interactions, mineralogy, grain shape and degree of grain stress, can also influence the hysteresis properties of a sample, and hence will complicate interpretation of hysteresis parameters (Roberts et al., 2000; Tauxe et al., 2002; Muxworthy et al., 2003).
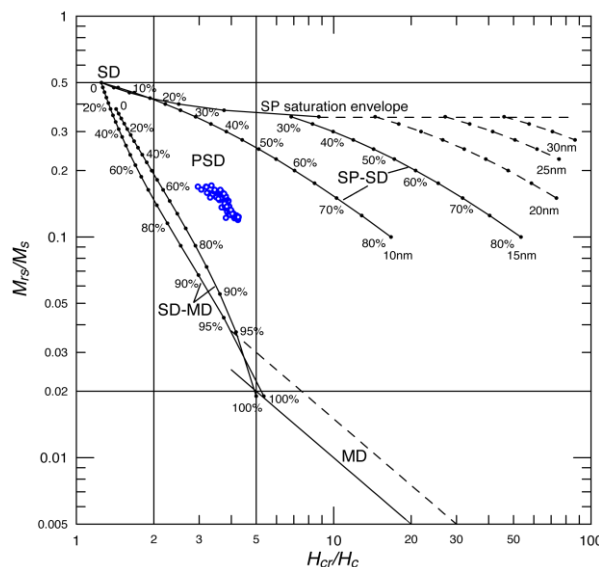


**Figure 2.7** An example of a Day plot (after Day et al., 1977); blue circles represent data from the BCY section, Chinese Loess Plateau. Dot-solid curves represent theoretical mixing lines for different domain states of magnetite from Dunlop (2002).

## 2.3.3 IRM acquisition curves

As discussed above, in a gradually increasing field, a sample will acquire an IRM as it progresses from a demagnetized to a saturated state (Figure 2.6b); this IRM acquisition process provides much useful information about the magnetic minerals in a sample. Robertson and France (1994) suggested that if a population of magnetic materials has a log-normally distributed coercivity spectrum and if the IRM is the linear sum of the IRM of all contributing grains, then an IRM acquisition curve can be "unmixed" into its constituent components. It is straightforward to rapidly measure

IRM acquisition curves using a vibrating sample magnetometer (VSM) or alternating gradient magnetometer (AGM). Several important developments in unmixing IRM acquisition curves have been made (e.g., Kruiver et al., 2001; Heslop et al., 2002; Egli, 2003; Heslop et al., 2007) since the original work of Robertson and France (1994).

A problem with analysis of IRM acquisition curves method is that measurements are discrete with systematic errors. When calculating a derivative, these errors are enlarged, which makes it difficult to judge how many components should be modelled and how good is the modelling. Egli (2003) proposed a useful method to avoid this problem. Discrete data are first fitted with a hyperbolic curve, and are then subtracted from the raw data to obtain a difference between the curves. The residual data are then filtered using a least-squares collocation method to produce one best fitting residual curve. The sum of these two curves produces the best modelling of the raw data; we can then calculate the derivative of this curve with minimized errors. Details of this mathematical procedure can be found in Egli (2003).

### 2.3.4 Inter-parametric ratios

Beside the $M_{rs}/M_s$ and $B_{cr}/B_c$ hysteresis ratios, several other inter-parametric ratios are commonly used in environmental magnetism.

- The S-ratio is the ratio of the IRM acquired in a back-field of magnitude $x$ to the SIRM or $M_{rs}$ (Bloemendal et al., 1992). In the traditional definition of the S-ratio, the back-field is equal to 300 mT, so that the S-ratio represents the relative concentration of magnetically "soft" and "hard" magnetic minerals such as magnetite and hematite, respectively.

- The hard IRM (HIRM) is defined as: HIRM = (SIRM + IRM$_{-x\,\text{mT}}$)/2, where $x$ is equal to 300 in the traditional definition of HIRM. This parameter is used to represent the absolute concentration of the high coercivity magnetic component, although it may not always provide a precise determination of the high coercivity component (e.g., Liu et al., 2008).

- $M_{rs}/\chi$ is the ratio of the saturation IRM to magnetic susceptibility. It is an indicator of magnetic grain size if only one magnetic mineral is present in a sample. It has also been used to indicate the presence of minerals other than

magnetite in the sample, such as magnetic iron sulphides, which often occur in a SD state in sediments (e.g., Snowball, 1991; Roberts, 1995).

- $\chi_{ARM}/\chi_{low-f}$ also provides information about magnetite grain size, where $\chi_{ARM}$ is the ratio of ARM to the applied DC field used to produce the ARM.

- Relative paleointensities are usually determined using the NRM measured along a sedimentary section, with normalization of the NRM by various parameters, such as $\chi_{low-f}$, ARM, SIRM or their values after a typical demagnetization treatment.

## 2.3.5 Magnetic minerals

Numerous magnetic minerals occur in nature and can be found in various environments. These minerals have contrasting magnetic properties that determine their ability to carry paleomagnetic signals. As described in Chapter 1, many magnetic minerals have been found in Chinese loess, such as magnetite, hematite, maghemite, and goethite. The basic magnetic properties and composition of geologically common magnetic minerals are listed in Table 2.1.

**Table 2.1** Physical properties of common natural magnetic minerals.

| Mineral | Composition | Density $(kg/m^3)$ | $M_s$ $(Am^2/kg)$ | $T_C/T_N$ $(°C)$ | $B_c$ $(mT)$ | Other |
|---|---|---|---|---|---|---|
| Magnetite | $Fe_3O_4$ | 5197 | 92 | 580 | 10's | $T_v = 110\text{-}120$ K |
| Hematite | $\alpha Fe_2O_3$ | 5271 | 0.4 | 675 | highly variable | $T_M = \sim250\text{-}260$ K |
| Maghemite | $\gamma Fe_2O_3$ | 5074 | 74 | 590-675 | | Breaks down to hematite |
| Goethite | $\alpha FeOOH$ | 4264 | <1 | 70-125 | very large | Breaks down to hematite |
| Greigite | $Fe_3S_4$ | 4079 | ~59 | >350 | <70 | Breaks down to hematite |
| Pyrrhotite | $Fe_7S_8$ | 4662 | <20 | 270 | 100's | Transition at 34 K |
| Titanomagnetite TM60 | $Fe_{2.4}Ti_{0.6}O_4$ | 4939 | 24 | 150 | 8 | |

Note: Data are from O'Reilly et al. (2000), Dunlop and Özdemir (1997), and Chang (2009).

# Chapter 3

# Hematite Formation During Pedogenesis in Chinese Loess/Paleosol Sequences

## 3.1  Introduction

Vast Chinese loess-paleosol deposits, which formed over the past 2.6 Ma, have recorded both paleoclimatic and paleomagnetic signals over different time scales (Heller and Liu, 1982, 1986; Kukla et al., 1988; An, 2000). Long-term paleoclimate variations from the Chinese loess can be correlated with those recorded by marine sediments (Heller and Liu, 1982, 1984; Liu, 1985; Kukla et al., 1988; Zhou et al., 1990; Deng et al., 2005). Loess deposited during cold and dry glacial periods has low mass-specific magnetic susceptibility ($\chi$). In contrast, paleosols that formed during warm and humid interglacial periods have enhanced $\chi$ values (Liu, 1985; Zhou et al., 1990; Maher and Thompson, 1991, 1992; Evans and Heller, 1994). This correlation, however, has been complicated by apparent offsets in the recording of magnetic polarity boundaries (Tauxe et al., 1996; Zhou and Shackleton, 1999; Spassov et al., 2003a). This longstanding problem has recently been clearly resolved by Liu et al. (2008) who demonstrated that local rainfall variations produce variations in pedogenic magnetic enhancement and that clearer identification of glacial/interglacial boundaries is obtained when using paleoclimatically sensitive parameters that are not affected by pedogenesis, such as quartz grain size.

Over the past two decades, the magnetic mineralogy of Chinese loess has been widely investigated to determine the mechanisms of magnetic enhancement in paleosols (Heller and Liu, 1986; Kukla et al., 1988; Zhou et al., 1990; Maher and Thompson, 1991, 1992; Rolph et al., 1993; Verosub et al., 1993; Kletetschka and Banerjee, 1995; Liu et al., 2005a, b). Most studies have emphasized the role of detrital

magnetite and the pedogenic formation of superparamagnetic (SP)/ single domain (SD) magnetite and maghemite (Zhou et al., 1990; Maher and Thompson, 1991; Hus and Han, 1992; Verosub et al., 1993; Liu et al., 2005a, b). The spontaneous magnetization of magnetite and maghemite is two orders of magnitude higher than that of hematite or goethite (Dunlop and Özdemir, 1997), which means that they dominate the magnetic signal. As a result, the presence and potential environmental importance of hematite and goethite in Chinese loess/paleosol sequences has been under-recognized.

Despite the fact that magnetite and maghemite have received more attention in studies of the Chinese loess sequences, hematite was recognized in early studies of the Chinese loess by Heller and Liu (1984) based on thermal demagnetization and optical microscopy studies. Heller and Liu (1984) interpreted the remanence carried by hematite as a chemical remanent magnetization. Later studies provide much more evidence for the widespread occurrence of hematite and goethite in Chinese loess sequences (see summary of Liu et al. (2007a)). Maher and Thompson (1992) calculated the concentration of hematite in both loess and paleosols (0.92 and 0.73 weight (wt.) %, respectively) using multiple regressions of remanence and susceptibility data. By analyzing isothermal remanent magnetization (IRM) acquisition data, Evans and Heller (1994) interpreted their component A as detrital hematite (0.88 wt. %). They argued that this component is essentially uniform across the Chinese loess plateau at least in loess unit L4. Detailed coercivity analyses for both different grain size fractions and bulk samples (Spassov et al., 2003b) have led to the suggestion that the hematite component has a detrital origin, and that pedogenic hematite, which causes the redness of paleosols (Chen et al., 2002), is too fine-grained (<0.03 μm) to carry a stable remanence. In contrast, Liu et al. (2004a) detected antiferromagnetic minerals from L2 to S1 in the Yuanbao section, and found that paleosols can have up to 2-3 times higher concentrations of remanence-carrying high coercivity minerals than loess and proposed that this is due to pedogenic SD hematite formation. Bloemendal and Liu (2005) also found that the "hard" IRM (HIRM) from both bulk samples and the carbonate-free sediment fraction are higher in paleosols, which indicates that SD hematite is present in paleosols although they suggested that hematite destruction also occurs in some paleosols. These studies demonstrate collectively that pedogenic hematite can grow through the stable SD blocking volume in Chinese paleosols. The problem with magnetic-remanence-related parameters is

that they can only reflect the SD (or larger) hematite component that can carry a stable remanence, and that they ignore SP hematite. Results from non-magnetic methods, such as diffuse reflectance spectroscopy (DRS), demonstrate that the total hematite concentration is variable through time (Balsam et al., 2004) and that it is linked to pedogenesis (Liu et al., 2006a; Torrent et al., 2006). On the basis of the weak spontaneous magnetization of hematite, a minor change in magnetization can indicate a relatively large change in hematite content.

Several magnetic and non-magnetic techniques have been developed to assess relative or absolute variations of hematite and goethite abundance in sediments. The HIRM and S-ratio (Stober and Thompson, 1979; King and Channell, 1991) are often used to detect variations in these high coercivity minerals. In contrast, Liu et al. (2007b) proposed the L-ratio to detect coercivity variations within high coercivity minerals, especially hematite. Mathematical un-mixing techniques enable separation of different coercivity fractions from IRM acquisition or alternating field (AF) demagnetization curves (e.g., Robertson and France, 1994; Stockhausen, 1998; Kruiver et al., 2001; Heslop et al., 2002; Egli, 2003), and have been successfully applied to Chinese loess (Spassov et al., 2003b). Pedogenic hematite formation provides important information about soil environments (Schwertmann, 1985; Stokking and Tauxe, 1990; Liu et al., 2006a, b; Torrent et al., 2006) and it can also be important for paleomagnetic and environmental magnetic studies of Chinese loess/paleosol sequences. In this study, we aim to distinguish between eolian and pedogenic hematite using magnetic methods and the second-order DRS technique (Torrent et al., 2006; Liu et al., 2006a), as well as using a mathematical un-mixing approach (Egli, 2003). We estimate hematite abundances in order to assess the importance of hematite formation in Chinese loess/paleosol sequences.

## 3.2 Samples

The Baicaoyuan section (BCY, 36.28°N, 105.21°E) is located on the northwestern Chinese Loess Plateau (Figure 3.1). We systematically sampled the last loess/paleosol (L1/S1) sequence at an average stratigraphic interval of 10 cm. All of the samples were collected after removal of the outer surface of the outcrop to obtain fresh samples. The L1/S1 sequence can be correlated with marine oxygen isotope

stage (MIS) 4/5. Previous studies demonstrate that the $\chi$ of L1 is uniform; the three $\chi$ peaks in S1 correspond to soil subunits S1SS1, S1SS2 and S1SS3, which correlate with MIS 5a, 5c and 5e, respectively (Deng, 2008). In order to focus on the effects of pedogenesis, we studied the interval from 10 to 18.6 metres below the modern terrace. Selected samples from Luochuan (LC, 35.4˚N, 109.5˚E) and Yuanbao (YB, 35.38˚N, 103.10˚E) were also investigated in this study (10 samples from LC and 8 from YB).
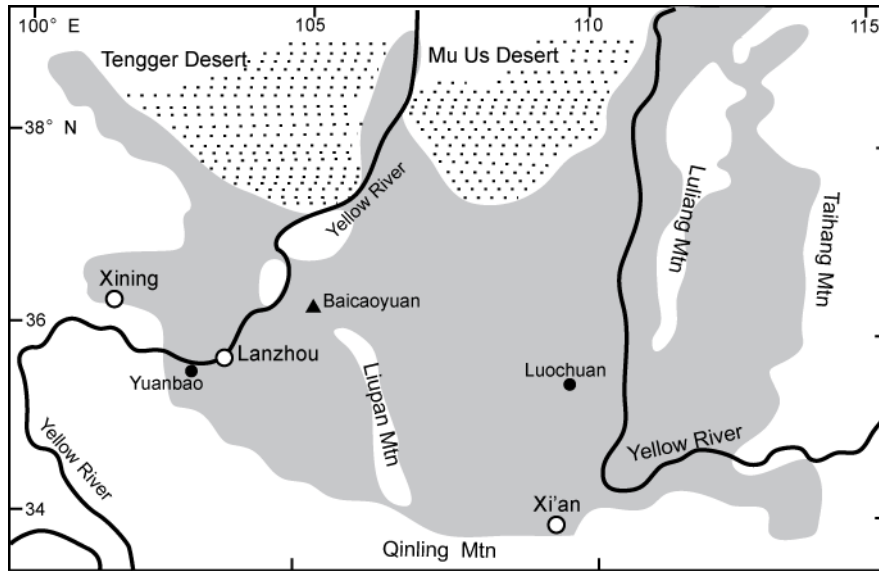


**Figure 3.1** Location map of the Chinese Loess Plateau (shaded) with the locations of the Baicaoyuan, Luochuan and Yuanbao sections (after Deng et al. (2008)). The stippled pattern indicates deserts. Unfilled circles represent the major cities.

## 3.3 Methods

### 3.3.1 Magnetic measurements

$\chi$ was measured using a Bartington Instruments MS2 magnetic susceptibility meter at low frequency (lf; 0.47 kHz) and high frequency (hf; 4.7 kHz). The absolute frequency-dependent susceptibility ($\chi_{fd}$) and the corresponding relative frequency-dependent susceptibility ($\chi_{fd}\%$) are: ($\chi_{fd} = \chi_{lf}-\chi_{hf}$; $\chi_{fd}\% = (\chi_{fd} / \chi_{lf})\times100\%$). All $\chi$ values are mass normalized, and we use $\chi$ to represent $\chi_{lf}$ throughout this paper. Room temperature magnetic hysteresis loops, backfield demagnetization curves and IRM acquisition curves were measured using a Princeton Measurements Corporation vibrating sample magnetometer (VSM). The maximum applied field was 1 Tesla (T). Saturation magnetization, $M_s$, saturation remanence, $M_{rs}$, and coercive force, $B_c$, were

obtained after paramagnetic correction for the high-field slope of the hysteresis loops. After imparting an IRM with a +1 T field, backfield demagnetization curves were obtained using fields of up to -1 T. The coercivity of remanence ($B_{cr}$) was obtained from these curves. The S-ratio was calculated as $IRM_{300\ mT}/M_{rs}$, where $IRM_{300\ mT}$ represents the IRM remaining after imparting a reversed DC field of 300 mT. All samples that were analyzed on the VSM were lightly ground into a powder, and were tightly compacted into non-magnetic gelatin capsules. All magnetic measurements were made at the National Oceanography Centre, Southampton.

## 3.3.2 Diffuse Reflective Spectroscopy (DRS) analysis

Thirty-nine selected sub-samples from the Baicaoyuan section were ground into a powder (<10 μm) for DRS measurements. DRS spectra were recorded from 380 to 900 nm in 0.5 nm steps using a Varian Cary 1E spectrophotometer equipped with a BaSO$_4$-coated integrating sphere 73 mm in diameter (Varian Inc., Palo Alto, California); the scan rate was set at 30 nm per minute. Measurements were made at the University of Córdoba. The second derivative spectrum of the Kubelka-Munk (K-M) remission function was calculated according to Torrent and Barrón (2003). Band intensities at ~425 nm ($I_{425}$) and ~535 nm ($I_{535}$) are proportional to the concentration of goethite and hematite, respectively (Scheinost et al., 1998). The samples were also analyzed using the method of Mehra and Jackson (1960) to determine the citrate-bicarbonate-dithionite (CBD)-extractable Fe (Fe$_d$). For CBD analysis, samples were ground to <2 mm. An extraction temperature of 25°C and an extraction time of 16 h were used. The citrate/bicarbonate extraction procedure was exactly the same as outlined by Mehra and Jackson (1960) except that no dithionite was added into the suspension. Fe$_d$, CBD-extractable Al (Al$_d$), and the citrate/bicarbonate-extractable Al (Al$_c$) and Fe (Fe$_c$) were all determined by inductively coupled plasma-mass spectrometry (ICP-MS) with a Perkin-Elmer ELAN DRC-e instrument at the University of Córdoba. Fe$_d$ was used to calculate the absolute concentration of hematite and goethite. The Al content is a major factor that controls the magnetic properties of hematite and goethite (Liu et al., 2006b, 2007b). The mol% Al in hematite/ goethite was therefore also calculated as: $(Al_d - Al_c)/((Fe_d - Fe_c) + (Al_d - Al_c)) \times 100$. Liu et al. (2004b) demonstrated that the contributions of ferrihydrite and maghemite to Fe$_d$ are limited and can be neglected for Chinese paleosols. Based on

the calibration curve $Y_s = -0.133 + 2.871X_s - 1.709X_s^2$ ($Y_s$ = hematite/ (hematite + goethite); $X_s = I_{535}/ (I_{425} + I_{535})$), $Fe_d$ is attributed to a combination of Fe in stoichiometric hematite and goethite. Then the relation $Fe_d$ = hematite/1.43 + goethite/1.59 can be used to calculate the absolute concentrations of hematite and goethite (Torrent et al., 2007).

# 3.4 Results

## 3.4.1 Rock magnetic parameters and DRS data

$\chi$ has been widely used as a paleoclimate index in studies of Chinese loess (e.g., Heller and Liu, 1982, 1986). High $\chi$ and $\chi_{fd}$ values are mainly caused by pedogenic formation of SP, SD and pseudo single domain (PSD) magnetite/maghemite, with increased pedogenesis normally occurring with increased rainfall (Zhou et al., 1990; Maher and Thompson, 1991, 1992; Hus and Han, 1992; Verosub et al., 1993; Liu et al., 2005a, b). $\chi$ and $\chi_{fd}$ therefore provide useful indications of pedogenesis. The three $\chi$ and $\chi_{fd}$ peaks for the Baicaoyuan section (Figure 3.2a, b) correspond to the three sub-paleosols (S1SS1, S1SS2 and S1SS3 from top to bottom, respectively) recognized by Deng (2008). $M_{rs}$ also has higher values in the sub-paleosols but with more noise compared to the $\chi$ signal (Figure 3.2c). HIRM is used to quantify the concentration of magnetic minerals with coercivity >300 mT, such as hematite, but this parameter ignores any hematite with coercivity <300 mT. HIRM has a large peak in sub-paleosol S1SS3 (Figure 3.2d). The S-ratio has an average value of 0.93, and varies between 0.91 and 0.95 (Figure 3.2e), which indicates that low coercivity magnetite/maghemite is dominant but that there must also be a significant high coercivity component. Sub-paleosol S1SS3 is magnetically enhanced more than S1SS2, which means that more pedogenic magnetite/maghemite was produced. It should therefore have a higher S-ratio if the concentration of high coercivity minerals is constant; however, sub-paleosol S1SS2 has a slightly higher S-ratio than S1SS3. This confirms the indication from HIRM values that a significantly greater content of pedogenic hematite was produced in sub-paleosol S1SS3 than in S1SS2. $B_{cr}$ values are relatively uniform in loess unit L1 with an average value of 57 mT. $B_{cr}$ values are lower in the paleosols, with a minimum value of 22.5 mT at 17.9 m (Figure 3.2f), because the bulk coercivity

of pedogenic magnetite/magnetite is much lower than that of the detrital component in the Chinese loess.

The hematite concentration determined from DRS data has three peaks that correspond to the sub-paleosol units (Figure 3.2k), with the highest values occurring within S1SS3. Although the goethite concentration is variable (Figure 3.2l), there is no clear relationship between goethite and the magnetic parameters. The Al content changes markedly at the boundary between L1 and S1 at ~13.5 m, with higher average values in paleosol S1 compared to those in loess L1 (Figure 3.2m).
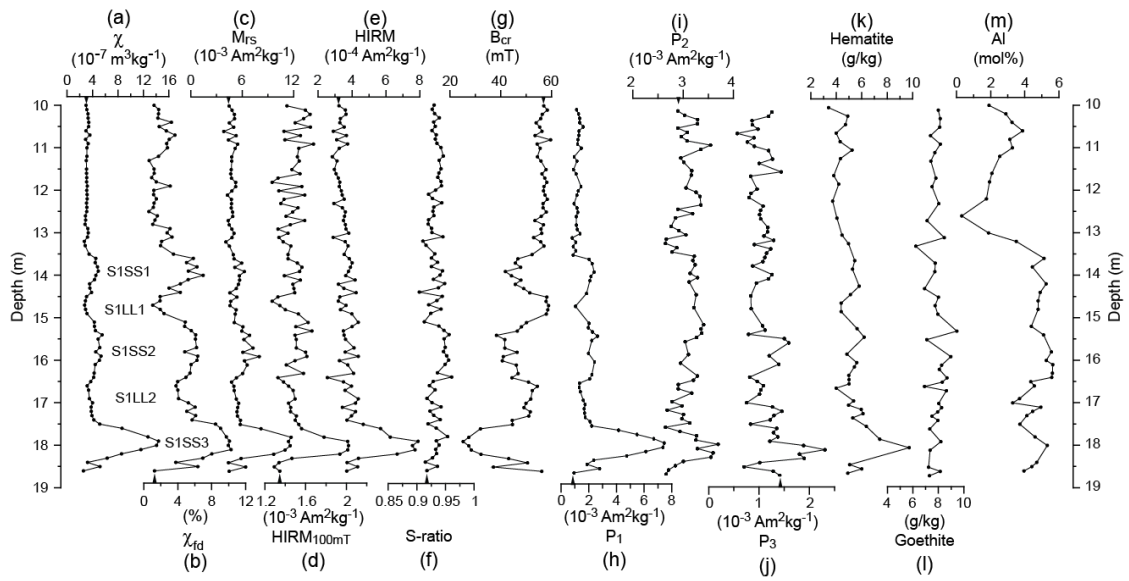


**Figure 3.2**      (a-g) Magnetic parameters, (h-j) IRM component analysis results, (k-l) DRS results, and (m) Al content for the interval spanning paleosol S1 and part of loess unit L1 for the Baicaoyuan section (see Figure 3.1 for location).

## 3.4.2 Analysis of coercivity components

Robertson and France (1994) demonstrated that IRM acquisition in monomineralic assemblages could be represented closely by a cumulative log-Gaussian (CLG) distribution. The bulk IRM acquisition curve can therefore be modelled using several individual CLG curves added linearly, where each CLG curve represents an independent coercivity component with different physical properties. Several studies have improved this method (e.g., Stockhausen, 1998; Kruiver et al., 2001; Heslop et al., 2002). Egli (2003) then used more parameters to control the shape of Skewed Generalized Gaussian functions (SGG), while Heslop and Dillon (2007) reported a non-negative matrix factorization (NMF) algorithm that can be applied without *a priori* knowledge. I used the MAG-MIX package of Egli (2003).
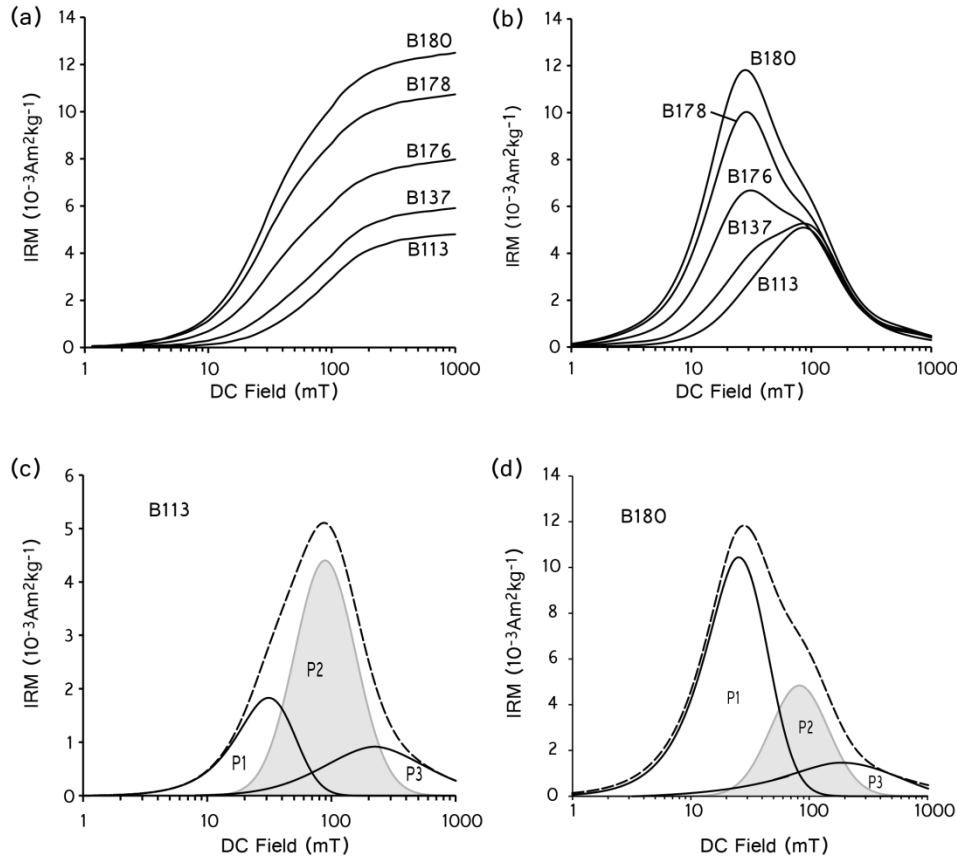
**Figure 3.3**     IRM acquisition and derivative curves for selected samples for Baicaoyuan. (a) IRM acquisition curves; (b) coercivity distribution curves; (c) and (d) component analysis results for samples B113 and B180, respectively.

All samples were magnetized from an AF demagnetized state with a gradually increasing DC field up to 1 T using a VSM, with 50 logarithmically spaced measurement steps. Mass normalized IRM acquisition data were input to Codica (the first part of the MAG-MIX package) for calculating IRM spectra. After removing obviously outlying data, the best-fitted hyperbolic tangent function and polynomial function for the residuals were used to represent the noise-free IRM acquisition curves. The differential data (on a $\log_{10}$ scale) for these curves were then output for component analysis using Geca (the second part of the MAG-MIX package). Detailed descriptions of the method can be found in Egli (2003) or in the MAG-MIX manual. The mass normalized IRM for paleosols is stronger than for loess samples. The gradient IRM curves shown in Figure 3.3b indicate that the magnetization spectra represent mixed signals. Loess samples such as B113 have the simplest curves and are dominated by a component with a peak at around 100 mT, but they still have a multi-component character. With progressively increasing pedogenesis, a component with a coercivity of ~25 mT becomes increasingly significant. I label the three components

with peaks at 25, 82, and 196 as $P_1$, $P_2$, and $P_3$, respectively. Loess that has been affected by pedogenesis can be treated as a paleosol, so that all samples can be modelled using the same components. Loess sample B113 and paleosol sample B180 were selected as pristine loess (Figure 3.3c) and mature paleosol (Figure 3.3d) end-members, respectively, in order to select reference modelling parameters. Four individual IRM acquisition curves were measured for these two samples using the same measurement settings. The averaged data were used for IRM analysis. Both samples can be modelled precisely using three components. All of the samples were therefore analyzed based on these reference parameters, and the magnetizations of the four components along the Baicaoyuan profile are shown in Figure 3.2h-j.

It has been demonstrated in many studies that pedogenic magnetite/maghemite particles occur across the SP to SD grain size range (e.g., Zhou et al., 1990; Eyre and Shaw, 1994; Liu et al., 2004b). SP particles do not carry a stable remanence; therefore the $P_1$ component with a peak at 25 mT only reflects the concentration of magnetite/maghemite with SD size. Eyre (1996) and Spassov et al. (2003a, b) reported higher coercivities of 30-35 mT for the low coercivity component in Chinese paleosols, but our value is consistent with the 21-29 mT range reported for synthetic SD magnetite (Maher, 1988). The high surface area to volume ratio of pedogenic particles makes them easy to oxidize into maghemite (van Velzen and Dekkers, 1999; Liu et al., 2003), which might explain the slightly higher coercivities documented by Eyre (1996) and Spassov et al. (2003a, b). Liu et al. (2005c) measured the temperature dependent $\chi_{fd}$ from 10 to 300 K and found that pedogenic particles have a uniform size distribution at different sites, and that SD magnetite/maghemite particles can contribute more than half the magnetization based on the volume fraction. As shown below, we interpret the $P_1$ component to represent pedogenic SD magnetite/maghemite with a small contribution from fine-grained detrital magnetite.

Component $P_2$ is present in all samples (with a peak at 82 mT). It dominates the loess samples and is also present in paleosols. It was described by Eyre (1996) as component 3 with a coercivity of around 115 $\pm$5 mT. Spassov et al. (2003b) identified two different components from the 5-20 μm and 20-50 μm sediment fractions with coercivities of 113 mT and 79 mT, respectively, and interpreted them to represent detrital maghemite and detrital magnetite with maghemite crust based on thermal demagnetization behaviour, respectively. These two components have similar

coercivity distributions, and are combined here to represent our $P_2$ component. I therefore interpret $P_2$ to represent coarse-grained detrital magnetite/maghemite. The high coercivity of this component can be explained by the high internal stress between the magnetite core and the maghemite crust (e.g., Cui et al., 1994; van Velzen and Dekkers, 1999; Liu et al., 2003).
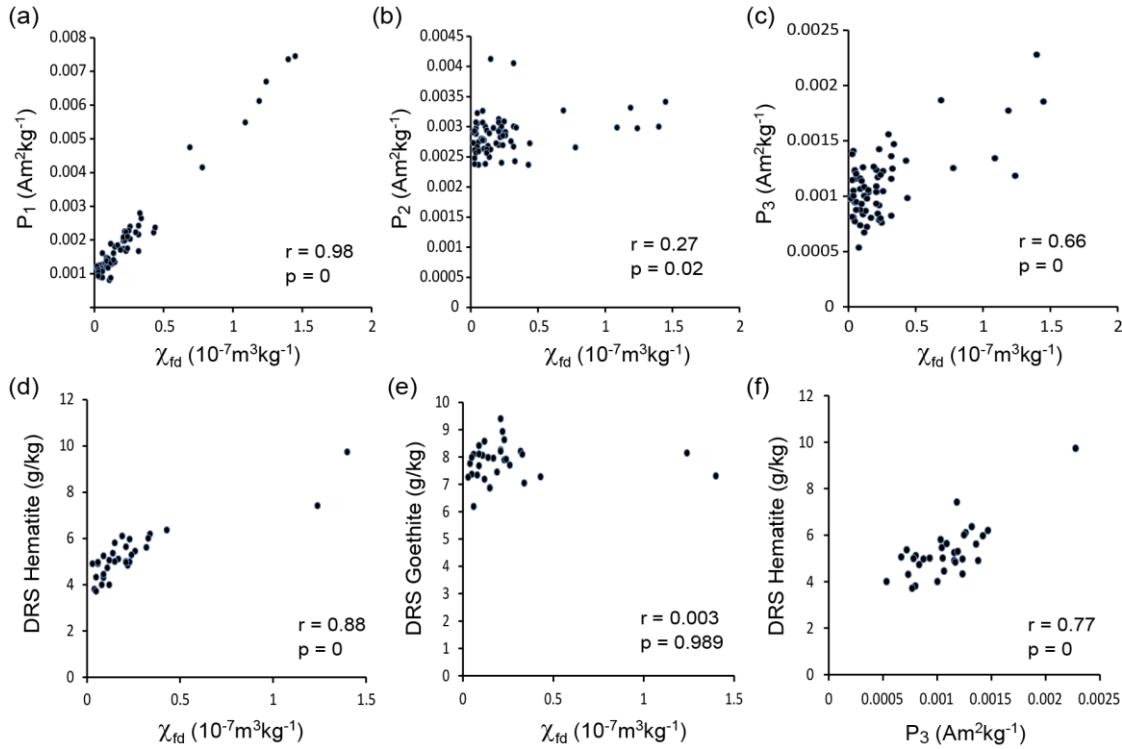


**Figure 3.4**    Rank correlation among different magnetic and physical parameters and the magnetic components identified in IRM acquisition curve analysis. $\chi_{fd}$ is the frequency dependent magnetic susceptibility, which is used to indicate SP pedogenic magnetite/maghemite. The non-zero intercept in (a) indicates that there is a background detrital magnetite contribution. $P_1$, $P_2$ and $P_3$ are the magnetizations of different components from IRM acquisition curve analysis. $P_1$ represents SD pedogenic magnetite/maghemite; $P_2$ represents detrital magnetite/maghemite; $P_3$ represent SD hematite (with both detrital and pedogenic origins). DRS-derived hematite represents the entire hematite content for a subset of the studied samples. DRS-derived goethite represents the goethite content in the sample. R represents the correlation factor, and p is the p-value. See text for discussion.

Component $P_3$ is identified in both loess and paleosols with a peak coercivity of 196 mT (Figure 3.3d). It has a clearly increasing trend in sub-paleosol S1SS3 (Figure 3.2j). The increasing hematite content in this sub-paleosol is also indicated by high HIRM values (Figure 3.2d). Spassov et al. (2003b) suggested this high coercivity component as detrital hematite and considered it to have a constant concentration between loess and paleosol samples. Pedogenic hematite, which has caused the reddish color of paleosols, has been considered too small to carry a stable remanence (Spassov et al., 2003b; and references therein). Nevertheless, the presence of

enhanced concentrations of high coercivity material in the reddest soil in the Baicaoyuan section (S1SS3) indicates that component $P_3$ must reflect pedogenic hematite in the SD size range.

Correlation between the magnetization of component $P_1$ and $\chi_{fd}$ (Figure 3.2b, h) strongly indicates that $P_1$ is dominantly a pedogenic component. The small but non-zero value of $P_1$ in the loess indicates that there is a small detrital contribution to $P_1$, with a magnetization of around $0.6 \times 10^{-3} Am^3kg^{-1}$ (Figure 3.2g, 3.4a); however, $P_1$ can still be an indicator of pedogenesis. We plot $\chi_{fd}$ versus the magnetization of components $P_2$, $P_3$, and the DRS determined hematite and goethite contents in Figure 3.4b-e. Except for component $P_2$ and DRS goethite, a positive correlation is observed in each case, which indicates that component $P_2$ is dominated by detrital magnetic minerals, while the other components are controlled by pedogenesis. The non-zero intercept on the *y* axis in Figure 3.4c-d indicates a detrital contribution to these components. We subtracted the value at the intercept when calculating the mass concentration of each component (Figure 3.5) in order to emphasize the pedogenic contribution.

## 3.4.3 Estimation of the mass concentration of each magnetic mineral phase

The large difference in magnetization between magnetite/maghemite and hematite/goethite often obscures the magnetic signal due to hematite/goethite when using magnetic parameters. Nevertheless, estimating the mass content of each mineral phase is useful when thinking about the magnetic assemblage and environmental processes. Maher and Thompson (1992) and Evans and Heller (1994) calculated the mass content of different mineral fractions and found similar hematite concentrations that are almost twice as high as that of magnetite/maghemite concentrations. We base our calculations on the results of our IRM acquisition curve analysis, and we use the intrinsic properties of magnetic minerals to estimate the mass concentration of different mineral fractions. Although the magnetite in the $P_1$ component has probably partially oxidized into maghemite, we use magnetite and maghemite values as end members to estimate a potential range of values for their contribution to component $P_1$. Based on data from Dunlop and Özdemir (1997), we use $M_s$ values of 92.68, 74.89 and 0.47 $Am^2/kg$ for magnetite, maghemite and hematite, respectively. We assume a

$M_{rs}/M_s$ ratio of 0.5 for SD grains to estimate $M_{rs}$. The magnetization of loess samples is dominated by coarse-grained magnetite/maghemite (Maher and Thompson, 1992), therefore we use an average $M_{rs}/M_s$ value of 0.13 for the 20 loess samples from depths between 10 and 12 m to simulate the PSD to MD magnetite/maghemite that represents component $P_2$.
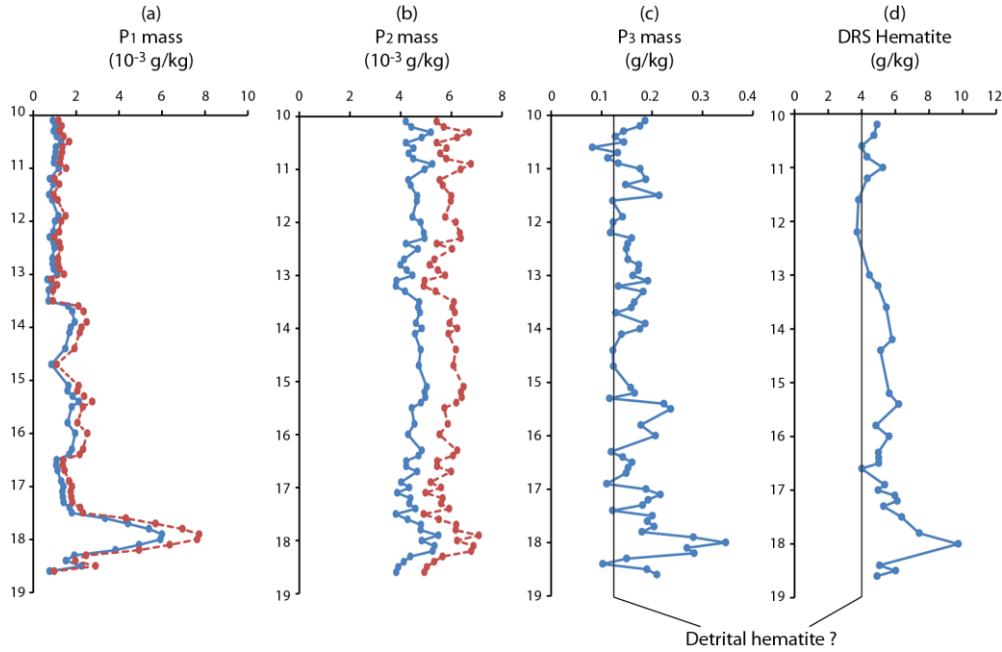


**Figure 3.5** Mass concentrations of different magnetic mineral components in the studied Baicaoyuan sequence. (a) The $P_1$ component, which represents SD pedogenic magnetite/maghemite (with a small detrital contribution), (b) the $P_2$ component, which represents detrital coarse-grained magnetite/maghemite, (c) the $P_3$ component and (d) total hematite from DRS measurements. Dashed red lines in (a) and (b) were estimated using values for maghemite, while solid blue lines were estimated for magnetite. The straight base line in (c) and (d) represents potential contributions from detrital hematite obtained from the correlations in Figure 3.4, while the grey shading represents the pedogenic hematite contribution.

The lower and upper limits of the mass concentration of the $P_1$ and $P_2$ components are estimated by using magnetite and maghemite as end-members, respectively (i.e., the mass value is much higher when using maghemite as the main contributor to either $P_1$ or $P_2$ because maghemite has a lower $M_s$ value). We estimate the hematite concentration in the $P_3$ component by assuming that the goethite indicated in Figure 3.2l does not carry a stable remanence, which seems reasonable because goethite concentrations do not correlate with any of the magnetic parameters. We then use the $P_3$ component to estimate the SD hematite concentration. The mass concentrations have the same pattern as the corresponding IRM-based magnetizations (Figure 3.2h-j), but with different units and scale (Figure 3.5). However, the mass

concentrations directly reflect the magnetic mineral contents rather than being obscured by large differences in $M_s$, especially for hematite. The mass of component $P_3$ has a similar variation pattern and has a positive correlation with the DRS-derived hematite concentration (Figure 3.4f), which suggests that these methods are robust. The SD hematite mass indicated by $P_3$ is more than 30 times that of magnetite/maghemite (Figure 3.5), and the total hematite concentration indicated by DRS is up to 1000 times that of magnetite/maghemite. We interpret the additional DRS-derived hematite to represent pedogenic SP hematite that does not contribute to remanence, as measured by $P_3$.
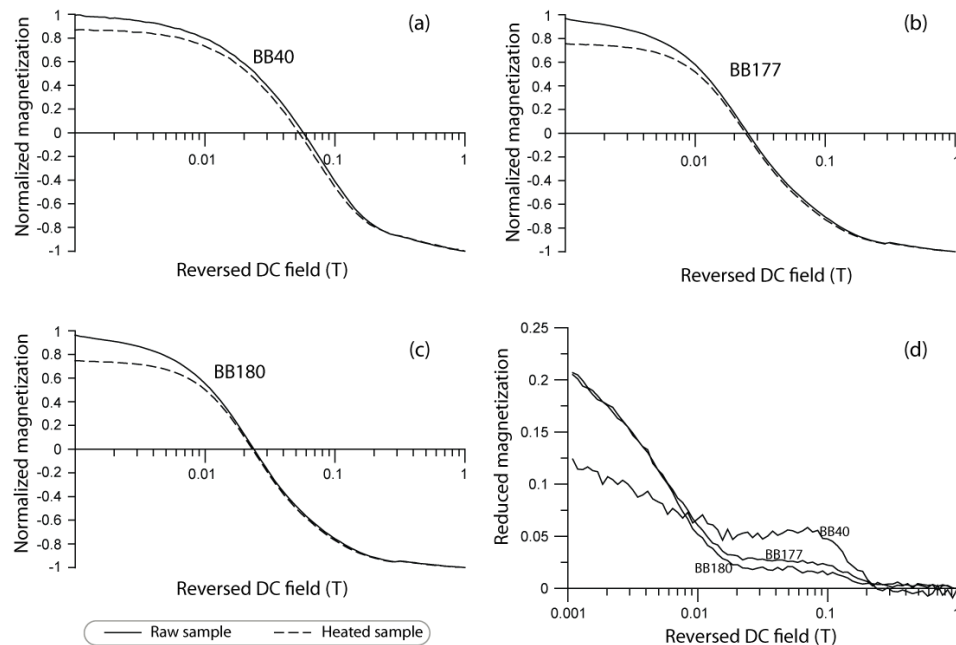


**Figure 3.6** Backfield demagnetization curves for three samples before (solid line) and after (dashed line) heating to 125°C. (a), (b) and (c) After normalization for samples BB40, BB177 and BB180, respectively; (d) the difference between the two curves before and after heating as a function of applied DC backfield.

## 3.5 Discussion

### 3.5.1 Does goethite contribute to the magnetization of Chinese loess?

Goethite is a common soil magnetic mineral that is known to occur in Chinese loess (e.g., Ji et al., 2004; Liu et al., 2006a; Torrent et al., 2007). Liu et al. (2006a) reported a HIRM anomaly within sub-paleosol S5SS1 at the Luochuan section to be

due to a low goethite concentration, and argued that HIRM is controlled by both goethite and hematite. Our DRS results support the interpretation that goethite is present in the Chinese loess. These results indicate that the absolute abundance of goethite is around 8 g/kg in the Baicaoyuan section (Figure 3.2l), which is more than the average hematite concentration (Figure 3.2k, 3.4f). It is therefore important to consider whether goethite contributes to the remanence of Chinese loess at ambient temperatures.

Samples BB40, BB177 and BB180 were selected on the basis of their different levels of pedogenic magnetic enhancement to assess whether goethite contributes to the magnetic signal at Baicaoyuan. Powder samples were tightly compacted into a specially designed quartz capsule, which were fixed on a sample rod. We applied a direct field of 1 T, and then measured the backfield demagnetization curves up to -1 T. After re-applying a 1 T field, the samples were heated to 125°C in a MMTD60 thermal demagnetization oven at a heating rate of 5°C/min and kept for 20 minutes at 125°C. After cooling, the samples were put into the VSM in their original orientation and backfield demagnetization curves were obtained without saturating the samples again. Any decrease in the backfield curves before and after heating should therefore be due to the unblocking of magnetite, maghemite, and hematite with unblocking temperature ($T_{unb}$) below 125°C and all goethite because its Néel temperature (Dunlop and Özdemir, 1997) was exceeded by the heating. In Figure 3.6, the applied backfield is shown with positive values in order to enable use of a logarithmic scale, and each curve is normalized by the absolute value of the final remanence at -1 T to avoid errors caused by minor mismatches in the orientation of the sample in the second measurement. The total magnetization is reduced by ~25% for samples BB177 and BB180, while it is only reduced by 12.5% for sample BB40. The reduced magnetization has mainly occurred in the low coercivity part (<200 mT) of the coercivity spectrum, while there is no measureable difference in the high coercivity part (>200 mT) where goethite would be expected to contribute if it was responsible for any of the remanence. These results suggest that goethite does not contribute to remanence (at least the HIRM) at ambient temperatures in the Chinese loess, which is consistent with the findings of previous studies (Spassov et al., 2003b; Liu et al., 2007a). Unlike hematite, goethite is probably not linked with pedogenesis. Its concentration appears to be relatively constant throughout the loess and paleosol

intervals in the studied section. Al substitution can significantly affect the Néel temperature and $M_s$ of goethite, which largely reduces the ability of goethite to carry a stable remanence at ambient temperatures (Özdemir and Dunlop, 1996; Liu et al., 2006b; Deng et al., 2006). We suggest that Al substitution in this case means that goethite does not contribute significantly to the magnetization of the studied section.

## 3.5.2 Implications of hematite formation in Chinese loess

Since Heller and Liu (1984) demonstrated the presence of hematite in Chinese loess, several studies have estimated the amount of hematite in these sediments. Hematite has a far greater concentration than magnetite/maghemite by mass (Maher and Thompson, 1992; Evans and Heller, 1994). Redness caused by ultra-fine-grained hematite pigmentation has been often used to identify paleosols within loess sequences in the field. However, the weak spontaneous magnetization of hematite makes it difficult to detect using magnetic methods. Several workers have reported detrital hematite (Evans and Heller, 1994; Eyre, 1996; Spassov et al., 2003b) and interpret pedogenic hematite to occur in the SP (0.01 to 0.1 μm) grain size range, so that no contribution is expected to the remanence from pedogenic hematite (Spassov et al., 2003b and references therein). Torrent et al. (2006) also reported that hematite is linked to magnetic enhancement, which is consistent with the results of Balsam et al. (2004) who observed a long-term hematite trend that correlates to magnetic susceptibility at Luochuan.

Based on our above arguments for why goethite does not contribute to the remanence in the Baicaoyuan section, we consider the high coercivity component $P_3$ to represent hematite. This component is affected by pedogenesis, as indicated by the peak in sub-paleosol S1SS3 (Figure 3.2 j). However, it is likely that detrital hematite is also present, because HIRM, the S-ratio and $P_3$ (Figure 3.2e, f, j) all indicate a magnetization due to hematite that exceeds 6% of $M_{rs}$ even in the loess unit (e.g., 10 m to 13 m). The hematite component that carries a remanent magnetization is therefore partly detrital as well as partly containing a fraction that grew through the stable SD blocking volume during pedogenesis. The hematite mass concentration determined from IRM acquisition curves is significantly different to the DRS-derived concentration (Figure 3.5c, d). We interpret this to be because the DRS method detects SP as well as SD hematite particles, and to a lesser extent particles that are not

activated magnetically with a 1 T DC field. We therefore conclude that hematite in the Chinese loess can have a significant pedogenic SP component, a detrital SD component, and a pedogenic SD component. Component $P_3$ and DRS-derived hematite both correlate with $\chi_{fd}$ (Figure 3.4c, d), which supports the results of Liu et al. (2004a) and Bloemendal and Liu (2005) who suggested that SD hematite can be produced by pedogenesis. We suggest that pedogenic SD hematite occurs largely in a particular grain size range with a peak coercivity of 196 mT on IRM acquisition curves. Pedogenic SD hematite has a mass abundance that is 2 times larger in the more intensely pedogenically altered sub-paleosol S1SS3 than in the loess (Figure 3.5c). If our assumption is valid that pedogenic SP hematite is responsible for the large difference in DRS-derived hematite concentration and $P_3$, then SP hematite must be the dominant product of pedogenesis, which represents >99% of the hematite by mass (Figure 3.5c, d). Compared to magnetite/maghemite, the mass concentration of hematite is much larger in both loess and paleosols, by a factor of 30 for SD hematite and by a much larger factor for the total hematite concentration by mass (Figure 3.5).

Unlike magnetite, which requires alternating reducing and oxidizing conditions to form (Maher, 1998), hematite can form via thermal transformation from goethite or maghemite or feroxyhyte, or through dehydration-rearrangement of ferrihydrite (Cornell and Schwertmann, 2000). Based on laboratory synthesis experiments, Schwertmann (1988) established that hematite forms in soils via dehydration-rearrangement of ferrihydrite rather than by other mechanisms. Balsam et al. (2004) suggested that hematite forms as a result of longer and warmer dry periods following shorter periods of soil wetness. It is important to better understand pedogenic processes in the Chinese loess and the paleoclimatic significance of magnetic parameters. The ferrihydrite via maghemite conversion into hematite hypothesis (Barrón and Torrent, 2002; Barrón et al., 2003; Schwertmann et al., 2004; Torrent et al., 2006, 2007) can explain the coexistence of maghemite and hematite in the Chinese loess. It needs to be thoroughly checked in future studies (Torrent et al., 2007), but it could explain why so much SP and SD hematite is produced during pedogenesis.

### 3.5.3 Widespread pedogenic process across the Chinese Loess Plateau

Temperature‑dependent and frequency‑dependent magnetic susceptibility results for locations across the Chinese Loess Plateau indicate that ultra-fine pedogenic magnetite/maghemite formed through a similar magnetic enhancement mechanism (Liu et al., 2004a). Correlation between DRS-derived hematite concentration and $\chi_{fd}$ indicates that hematite formation is linked to pedogenesis. Nevertheless, pedogenic hematite may not form under exactly the same mechanism as pedogenic magnetite/maghemite, which may require different temperature and precipitation conditions compared to magnetite/maghemite (Maher, 1998; Balsam et al., 2004). Our IRM component analysis results from three sections, Baicaoyuan (BCY), Yuanbao (YB), and Luochuan (LC), indicate the presence of similar magnetic mineral compositions (Table 3.1). These results suggest that the mechanism of magnetic mineral enrichment associated with pedogenic processes is likely to be widespread across the Chinese Loess Plateau.

**Table 3.1  The peak coercivity of each magnetic mineral component from IRM acquisition curve analysis for the three studied sections.**

| Section (Numbers) | Peak Coercivity (mT) | | |
|---|---|---|---|
| | $P_1$ | $P_2$ | $P_3$ |
| BCY  (77) | 24 $\pm$2 | 82 $\pm$4 | 196 $\pm$1 |
| YB  (8) | 28 $\pm$4 | 92 $\pm$5 | 199 $\pm$3 |
| LC  (9) | 21 $\pm$1 | 80 $\pm$5 | 203 $\pm$5 |

Note: BCY = Baicaoyuan; YB = Yuanbao; LC = Luochuan (See Figure 3.1 for locations). $\pm$ represent the standard deviation.

## 3.6  Conclusions

Although goethite exists in both loess and paleosol samples, it does not contribute to the stable remanent magnetization of the Chinese loess. Hematite therefore dominates the magnetization of high coercivity components (i.e., HIRM) in the studied Baicaoyuan Chinese loess section. IRM component analysis and DRS data indicate that SD and SP hematite, respectively, are produced in the Chinese loess during pedogenesis. The mass concentration of hematite estimated in this study indicates that both detrital and pedogenic hematite are important in Chinese loess. The

transformation of 2-line ferrihydrite via maghemite to hematite has been proposed as a potential mechanism for hematite enrichment in paleosols. The presence of comparable magnetic mineral components that are widely distributed in loess/paleosol sections indicates a consistent mechanism for magnetic enhancement across the Chinese Loess Plateau. Our results therefore provide important insights into the essential processes of pedogenesis, which has caused marked magnetic fluctuations that respond to paleoclimatic and paleoenvironmental changes.

# Chapter 4

# How Does Chinese Loess Become Magnetized?*

## 4.1  Introduction

Vast expanses (~500,000 km$^2$) of thick, ancient wind-blown dust deposits are preserved on the Chinese Loess Plateau in central China. These deposits represent one of the world's most outstanding terrestrial archives of paleoclimate change. Chinese loess sequences range between ~100 and 300 m in thickness and record aridity in desertified source regions in northwestern China and Mongolia during glacial periods, while intercalated paleosols reflect intensified summer monsoon conditions that supported soil formation during interglacial periods. These climate changes are recorded over the last 2.6 million years (Ma) in loess/paleosol sequences (Heller and Liu, 1982, 1984; Liu et al., 1988a; Rutter et al., 1990) and back to 22 Ma in the underlying Red Clay sequences (Guo et al., 2002). High loess accumulation rates preserve paleoclimate signals that can be analysed at high resolution, including millennial-scale climate changes (e.g., Liu et al., 2005a).

Paleomagnetic studies have proved crucial in establishing the chronology of paleoclimate variations in Chinese loess sequences (e.g., Heller and Liu, 1982, 1984; Liu et al., 1988a; Rutter et al., 1990). Identification of the positions of geomagnetic reversals over the past 2.6 Ma enabled correlation of magnetic susceptibility profiles to the marine $\delta^{18}$O record (Kukla et al., 1988). Magnetic susceptibility peaks occur within paleosols as a result of magnetite/maghemite formation during pedogenesis (e.g., Zhou et al., 1990); the intervening loess units have much lower magnetic susceptibilities. Despite this first-order success in establishing the loess chronology,

---

* The main part of this chapter has been published as: Zhao, X. and A. P. Roberts (2010). How does Chinese loess become magnetized? *Earth and Planetary Science Letters*, 292: 112-122.

which has been assisted by orbital tuning of paleoclimatically sensitive parameters such as magnetic susceptibility (Heslop et al., 2000), a major chronological conundrum has persisted. The last major geomagnetic reversal (Matuyama-Brunhes boundary) is widely recorded in glacial deposits in the Chinese loess, whereas it is located in interglacial deposits in marine sediments (e.g., Tauxe et al., 1996; Zhou and Shackleton, 1999). This conundrum has made it difficult to correlate paleoclimate signals in loess with those in other archives and to establish phase relationships between the respective signals. This chronological problem has been resolved by Wang et al. (2006) and Liu et al. (2008) who demonstrated that parameters such as magnetic susceptibility are too sensitive to local variations in rainfall and pedogenesis, which means that they can provide misleading information concerning the positions of boundaries between glacials and interglacials. In contrast, quartz grain size is insensitive to pedogenic alteration and is a useful parameter for determining the true position of magnetic polarity boundaries with respect to paleoclimatic boundaries. Liu et al. (2008) demonstrated that there is no offset in the position of the Matuyama-Brunhes boundary between marine and Chinese loess sequences if quartz grain size is used as a paleoclimate proxy for the Chinese loess. They thereby demonstrated that there is no need to invoke a deep post-depositional remanent magnetization (PDRM) lock-in (of up to 3 m) to explain paleomagnetic observations from the Chinese Loess Plateau (cf. Tauxe et al., 1996; Zhou and Shackleton, 1999).

Despite recent resolution of this long-standing conundrum, and despite the fact that paleomagnetic reversal stratigraphies have been successfully developed in Chinese loess sequences for nearly 3 decades since the pioneering work of Heller and Liu (1982), the mechanism by which Chinese loess acquires its paleomagnetic signal is still not understood. Part of the problem lies with the perception that there are significant delays in remanence acquisition in Chinese loess (of 2-3 m or 20-30 kyr), as discussed above (e.g., Tauxe et al., 1996; Zhou and Shackleton, 1999; Heslop et al., 2000). This conclusion has been difficult to reconcile with the observation that the Chinese loess often records high-frequency geomagnetic signals, including excursions (e.g., Pan et al., 2002; Yang et al., 2007b; Zhu et al., 2007), which would not be possible with deep PDRM lock-in (cf. Roberts and Winklhofer, 2004). In order to account for the previously hypothesized large downward shift of geomagnetic reversal boundaries in Chinese loess sequences (e.g., Tauxe et al., 1996; Zhou and Shackleton,

1999; Heslop et al., 2000), while enabling recording of high-frequency geomagnetic features (e.g., Pan et al., 2002), Spassov et al. (2003a) proposed a composite model in which the natural remanent magnetization (NRM) is a shallow PDRM that is augmented by a later pedogenic chemical remanent magnetization (CRM). Liu et al. (2008) conclusively removed the basis for invoking deep PDRM and CRM acquisition, although this is not to say that CRM does not remain a valid mechanism for NRM acquisition, particularly at shallow depths within paleosols where magnetite and maghemite are known to grow through the stable single domain blocking volume. Nevertheless, fundamental questions remain about the mechanism(s) by which loess records geomagnetic signals. If the NRM is acquired at shallow depths, is it acquired through a detrital remanent magnetization (DRM) or is it a PDRM or a CRM or is it a composite of several mechanisms? Constraining these questions is fundamental to the interpretation of paleomagnetic data from the Chinese Loess Plateau. Re-deposition experiments are therefore needed to help us understand how Chinese loess becomes magnetized.

During deposition, magnetic particles partially align with the ambient magnetic field, which produces a DRM in sediments. To understand the DRM acquisition mechanism in sediments, many laboratory redeposition experiments have been carried out (Johnson et al., 1948; King, 1955; Blow and Hamilton, 1978; Barton et al., 1980). Most previous redeposition studies have focussed on material that formed in aqueous environments, such as marine sediments, and lacustrine deposits, which involved experiments with water tanks for deposition. Although it is difficult to simulate nature with such a small apparatus and over short laboratory time scales, such work has provided important insights into DRM mechanisms. The magnetization of Chinese loess, which is a wind-blown deposit, has been studied for over 30 years. However, systematic investigation of remanence acquisition mechanism(s) in Chinese loess has not been undertaken. To understand how Chinese loess becomes magnetized, redeposition experiments are necessary. Of the >1,000 papers that have been published about Chinese loess, only one has reported loess laboratory redeposition experiments (McIntosh, 1993). To address this key problem in Chinese loess research, I have designed an aeolian dust deposition simulator to test the ability of re-deposited loess to record the ambient magnetic field. This device can cancel 95% of the ambient geomagnetic field, and produce a constant field with intensity up to 100 µT in any

direction, with 9 samples in the constant field region in which disaggregated loess is redeposited. In this Chapter, I describe the field control system and dust deposition system, and report results of more comprehensive re-deposition experiments.

# 4.2  Design of an eolian deposition simulator

## 4.2.1 Helmholtz coils

A three-axis Helmholtz system is the simplest and most frequently used coil configuration for providing a uniform field over large volumes in the laboratory. In its original form, a Helmholtz system consists of two equal, coaxial circular radius coils separated by a distance $2z$. It is possible to approximate a uniform field by adjusting the distance $z$. For a square coil with side $2a$, the field along the axis of the coil ($B_z$) is given by:

$$B_z = \frac{2\mu N i a^2}{\pi(a^2 + z^2)(2a^2 + z^2)^{1/2}},$$

where $N$ is the number of turns and $i$ is the current. After differentiation, $2z = 1.088a$, which enables a square coil to satisfy the Helmholtz condition. Based on the expression for $B_z$ for circular coils by Parry (1967), the expression for square coils is:

$$B_z = B_0 \left[1 - \frac{1}{a^4}\left(0.783z^4 - 1.668z^2(x^2 + y^2) - 1.95x^2y^2 + 0.458(x^4 + y^4)\right)\right].$$
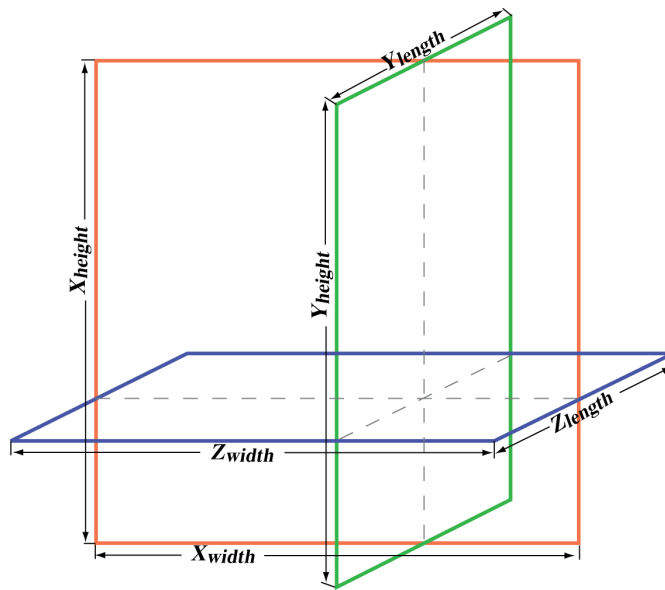


**Figure 4.1**     Sketch of the Helmholtz coil system developed for the eolian dust simulator.

**Table 4.1  Detailed parameters for the coils.**

| Index | Outer boundary length | Real coil side length | Cross-sectional width |
|---|---|---|---|
| $X_{height}$ | 490 | 476 | 4 |
| $X_{length}$ | 506 | 492 | 4 |
| $Y_{width}$ | 510 | 494 | 5 |
| $Y_{height}$ | 510 | 494 | 5 |
| $Z_{width}$ | 490 | 476 | 4 |
| $Z_{length}$ | 490 | 476 | 4 |

U-shaped aluminium was used to build the coil framework; three pairs of coils (six coils in total) were made for the three axes Helmholtz system. One pair was built using two aluminium U-shaped frames (length: 1000 mm, width: 16 mm, height: 10 mm) to provide the main supporting framework. The other two pairs were built with single aluminium frames (length: 1000 mm, width: 8 mm, height: 8 mm) that were set within the main framework. Each aluminium piece was cut in half into 500 mm lengths, with four pieces joined using a strong adhesive. Insulating tape was placed along the interior of the U-shaped frames to present short circuits from developing. 40 turns of lacquered wire were wound onto each coil. To assemble the coils according to Helmholtz conditions, each pair of coils is slightly different as shown in Figure 4.1 and Table 4.1.
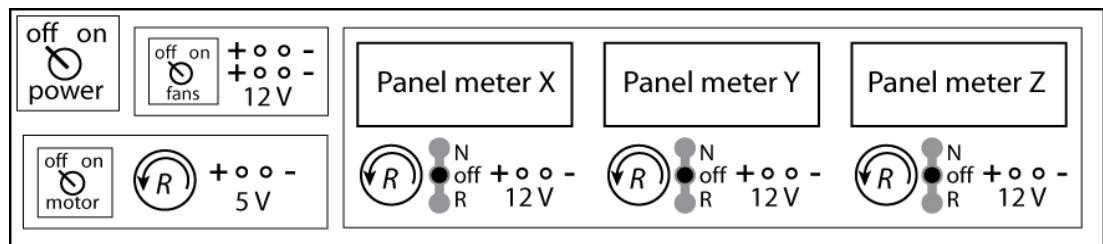


**Figure 4.2**    Sketch of the front panel of the power supply system for the Helmholtz coil system.

## 4.2.2 Power supply system

The power supply system includes a standard computer power supply and a control panel, which are enclosed in a case. This power supply requires 200-240 V AC input, and was set to output four 12 V independent voltages (three for the pairs of coils and one for the electric fans for the dust deposition simulator), as well as four 5

V independent voltages for the panel meters and rolling motor at the base of the hopper used to supply dust into the simulator (Figure 4.2).


## 4.2.3 Dust deposition simulator
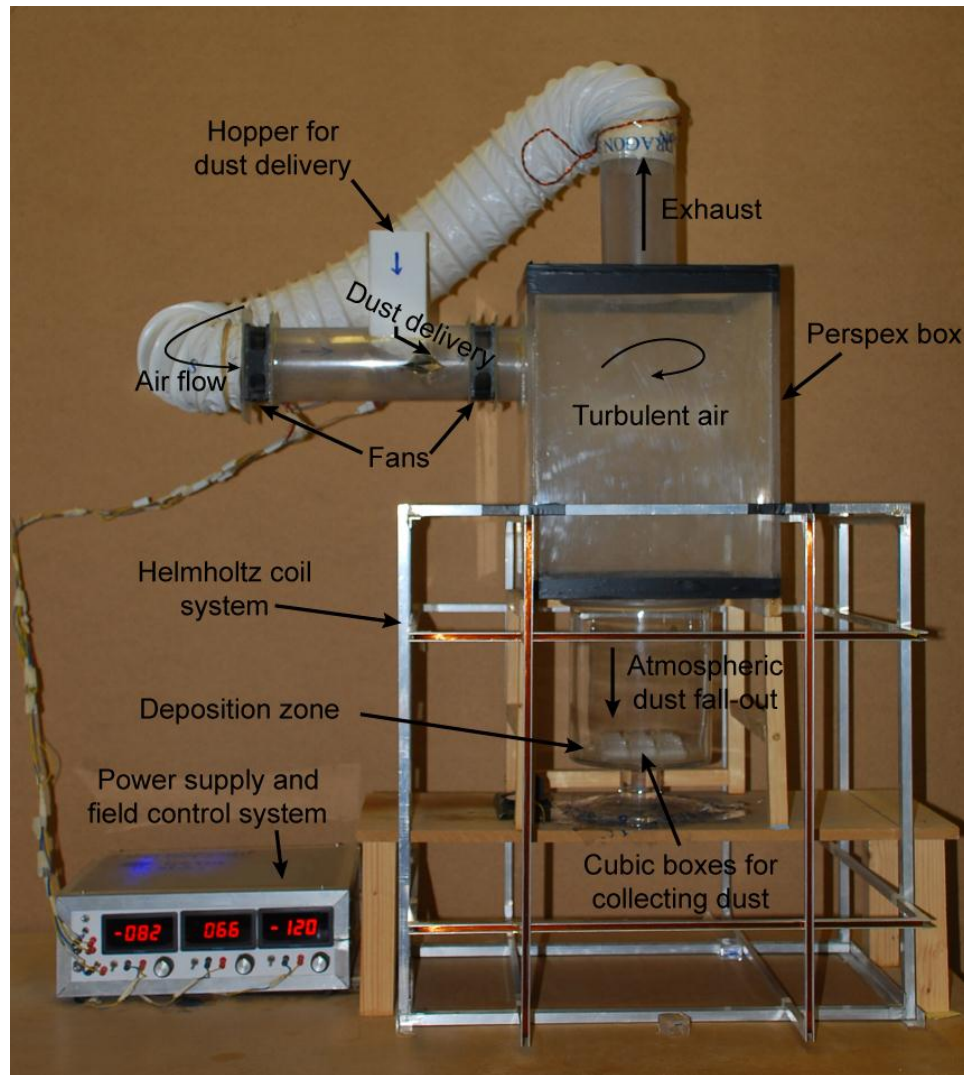


**Figure 4.3**        Photograph of the eolian dust deposition simulator used for the experiments reported in this paper. See text for explanation.

        To adequately replicate the natural dust deposition process, as described by Heller and Liu (1982) and Liu (1985), the dust deposition simulator should have the following three parts: a wind source, a dust circulation zone and a deposition zone (for sample collection). In practice, the system is designed as a closed loop to avoid the escape of dust into the laboratory, as well as to simulate stronger winds. Dry sediment was delivered into the inlet pipe via a hopper. A steady flow of sediment was released into the inlet pipe by use of a motor-controlled roller at the bottom of the hopper.

When the sediment falls from the hopper into the underlying pipe, a pair of fans blows the dust into a Perspex box, under which is situated a deposition chamber. This chamber is placed within the field control system. Nine empty plastic cubes were placed at the base of the chamber for collecting samples (Figure 4.3).

## 4.3  Methods

In order to simulate the loess deposition processes described by Liu et al. (1985), re-deposition experiments were performed on weakly consolidated L1 loess sediments from Yuanbao, Gansu province, western Chinese Loess Plateau. The loess was disaggregated to produce a uniformly fine-grained dust for the experiments. The experiments were performed in the eolian dust deposition simulator (Figure 4.3). An average of 4.0 g of sediment was deposited in each cube per experiment (dry sample masses ranged from 1.6 to 7.4 g). The sediment was deposited into the plastic cubes using a range of field directions. The field intensity was maintained for all experiments at 50 μT, which is a typical value for the present-day geomagnetic field on the Chinese Loess Plateau. Deposition was usually allowed to proceed for 3-4 hours for each experiment. Upon completion of the experiment, the field was switched off and the cubes were removed from the chamber and were taken into a magnetically shielded laboratory at the National Oceanography Centre, Southampton (NOCS) for measurement of the NRM. Magnetic measurements were made using a 2-G Enterprises superconducting rock magnetometer. After measuring (and sometimes repeatedly remeasuring) the initial NRM of the re-deposited sediments, static 3-axis stepwise alternating field (AF) demagnetization was performed using applied fields of 2.5, 5, 7.5, 10, 12.5, 15, 20, 25, 30, 40, 50, 60, 70, 80, and 100 mT on an AF demagnetization system that is arranged in-line with the magnetometer. AF demagnetization was conducted to assess the stability of the magnetizations. Principal component analysis (PCA) was used to determine the characteristic remanent magnetization (ChRM) from a best fit through the stepwise AF demagnetization data (Kirschvink, 1980). The uncertainty associated with this determination is given by the maximum angular deviation (MAD). AF demagnetization was conducted many times on the studied sediments, both before the original sediment was disaggregated and after each re-deposition experiment. The sediments have uniform magnetic properties, as indicated by the virtually identical coercivity spectra for all demagnetization runs.

A series of re-deposition experiments was carried out. The first involved dry deposition to simulate a pure eolian DRM and to assess its recording fidelity for a range of field settings. The second set of experiments involved dry deposition, after which the Perspex box was removed and water was gently sprayed through a fine nozzle from a spray bottle to provide a small amount of moisture to the deposited sediment. The water content was small and was not determined for this set of experiments. The field remained switched on during water spraying. Minor moisture was added to assess whether it enabled magnetic grain remobilization after deposition to improve recording efficiency. The third set of experiments involved dry deposition in zero-field. After deposition, the samples were measured in the magnetometer and then weighed. Water was then added to the samples so that the deposited sediments were water saturated. The samples were measured in the magnetometer again and were weighed again to allow calculation of the water content. Water content was estimated following the definition of Verosub et al. (1979) where: $H_2O\% = ((Mass_{total} - Mass_{dry})/Mass_{dry}) \times 100\%$. In many cases, water ponded above the sediment surface in the plastic cubes used to hold the samples, so $H_2O\%$ is not a true measure of water content in relation to sediment pore space. After weighing, the cubes were returned to the deposition chamber and the field was switched on. Covers were placed on top of the plastic cubes to maintain humidity and to minimize evaporation for either 12 or 24 hours, respectively. At the end of this period, the samples were allowed to dry within the same field. Drying took 2-3 days. Any stable remanence produced is likely to be a PDRM because the water content was sufficiently high that any depositional alignment was probably lost after addition of water. When dry, the samples were measured in the magnetometer and were subjected to progressive AF demagnetization. The above procedure for PDRM simulation is similar to that employed by Irving and Major (1964). The samples were then subjected to progressive acquisition of an anhysteretic remanent magnetization (ARM) with a DC bias field of 0.05 mT and a progressively increasing AF using applied fields of 2.5, 5, 7.5, 10, 12.5, 15, 20, 25, 30, 40, 50, 60, 70, 80, and 100 mT. The ARM was subjected to stepwise AF demagnetization using the same sequence of applied fields.

# 4.4  Results

## 4.4.1 NRM recording fidelity from re-deposition experiments

Simulation of a pure eolian DRM was performed in 18 dry deposition experiment runs (9 samples per run). Dry deposition enables faithful recording of the declination of the ambient field, except when the inclination is steep (Figure 4.4a). As expected for steep fields, any misalignment of particles away from the vertical produces declination scatter. Nevertheless, apart from this case, the declination of the ambient field is well recorded. In contrast, the measured inclinations for the redeposited loess are systematically shallow (Figure 4.4b).
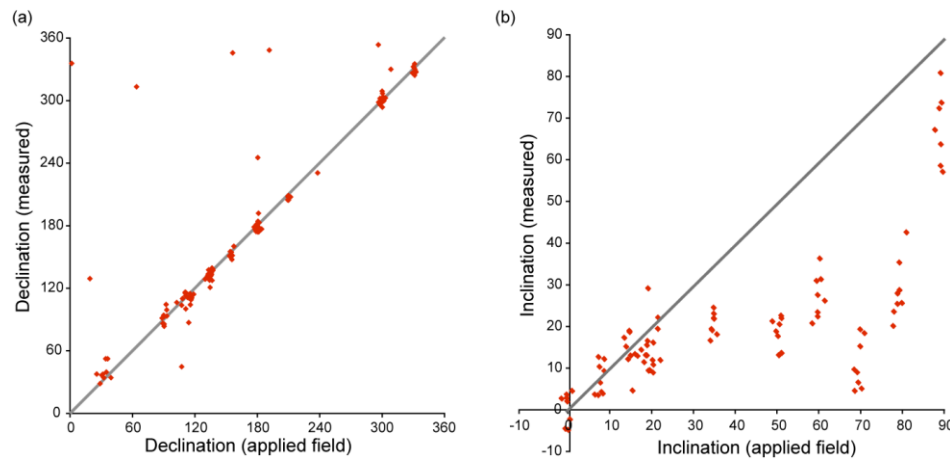


**Figure 4.4**      Recording fidelity of a DRM produced via dry deposition in the eolian dust simulator (Figure 4.3). (a) Measured NRM declination for re-deposited samples plotted versus the applied ambient field declination. (b) Measured NRM inclination for re-deposited samples plotted versus the applied ambient field inclination. The declination data that lie the furthest off the 1:1 line correspond to the steepest inclinations. A significant inclination error is observed. See text for discussion.

A second set of dry deposition experiments was undertaken (6 batches of 9 samples) to check whether addition of minor moisture could cause post-depositional realignment of particles to improve the DRM recording fidelity. With addition of minor moisture, the NRM (Figure 4.5a) and ChRM (Figure 4.5c) continue to record accurately the declination of the applied field. However, systematic inclination shallowing continues to be observed for both the NRM (Figure 4.5b) and ChRM (Figure 4.5d). Addition of minor water therefore does not enable significant post-depositional realignment of magnetic particles (Figure 4.5), although the observed inclination shallowing is less severe than in dry deposition experiments (Figure 4.4).

Despite the first-order similarity between the dry re-deposition experiments and those with minor added water (Figures 4.4 and 4.5), AF demagnetization results indicate a significant difference in the quality of the recorded magnetizations (Figure 4.6). Vector demagnetization diagrams for samples from the two sets of experiments are different, with the samples from the dry re-deposition experiments (with no added water) having less stable magnetizations. Even without demagnetization, these samples undergo a time-dependent exponential decay of magnetization (Figure 4.6a). This decay is less evident for samples with minor added water (Figure 4.6b) and it is absent for the PDRM experiment (Figure 4.6c). The loess sediment used for the experiments has consistently uniform magnetic properties, which precludes a viscous origin for the magnetization decay. This decay appears to be due to progressive physical randomization of particles resulting from vibrations associated with movement of the sample in and out of the magnetometer for the repeated NRM measurements. The fact that this decay is much less evident for samples with minor added water indicates that the water has provided some stabilization against vibration-related particle movement. The time-dependent magnetization decay for the pure DRM is probably not geologically meaningful because the particles will be fixed in position through compaction (and possibly cementation). Nevertheless, even though the recorded inclinations are systematically shallow for both sets of DRM experiments (Figure 4.4 and 4.5), the recorded ChRM is more stable even with minor added water (Figure 4.6b). Likewise, the DRM intensity is marginally higher and less variable for the experiments with minor added water (Table 4.2).

The third set of re-deposition experiments was intended to simulate a PDRM. Initial re-deposition in zero-field produced a weak remanence that became substantially stronger when the sample was water-saturated and placed in a 50-$\mu$T field. At high water contents, the sediment becomes a slurry, and there is little impediment to post-depositional realignment of the magnetic particles by the ambient field. When the water-saturated samples are dried, the recording fidelity of the ambient field is much superior (Figures 4.6 and 4.7; Table 4.2) to samples produced by dry deposition (Figures 4.4, 4.5 and 4.6). The declinations for 9 batches of 9 samples are tightly grouped (Figure 4.7a). Despite data scatter, there is no systematic inclination shallowing (Figure 4.7b).
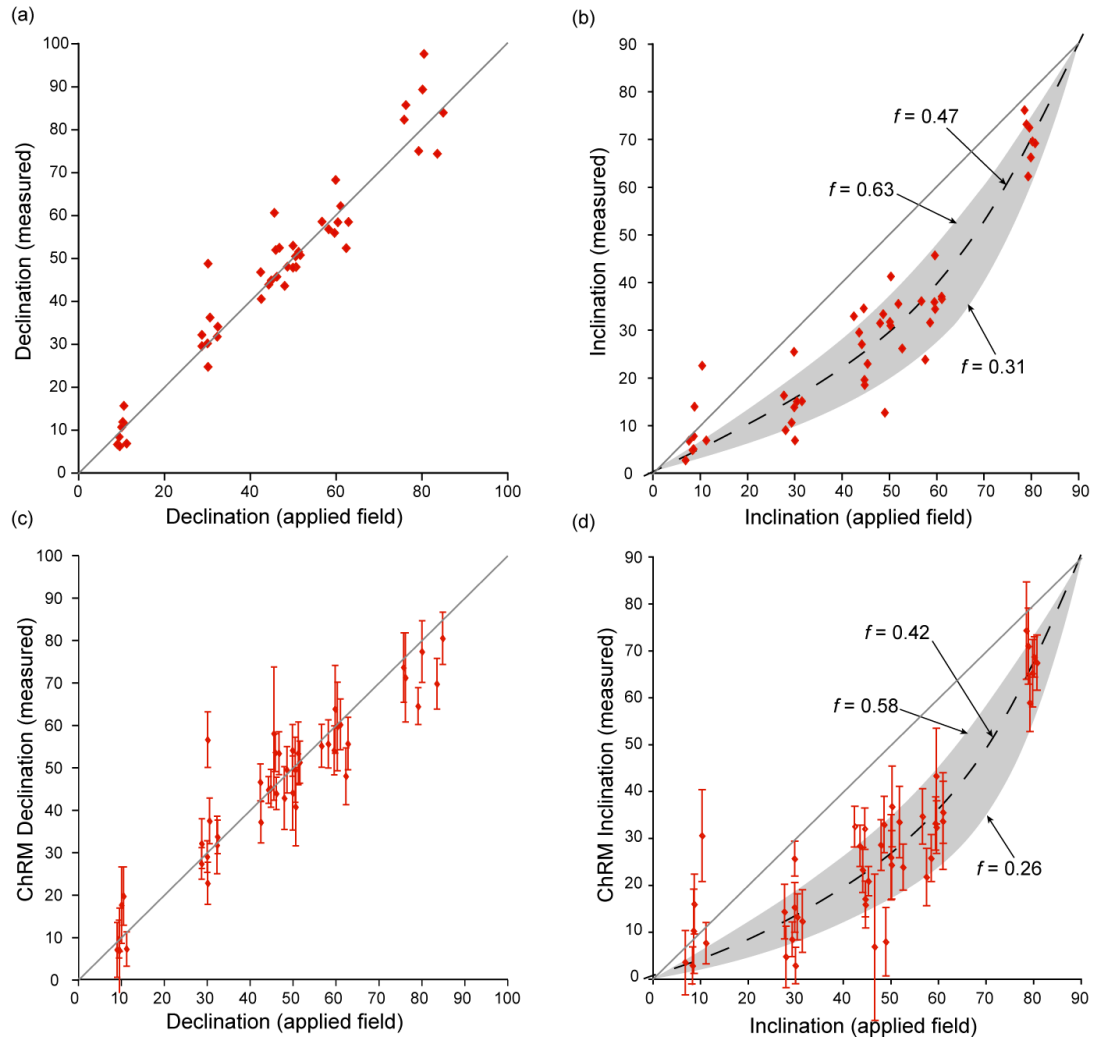
**Figure 4.5** Recording fidelity of a DRM produced via dry deposition with post-depositional addition of minor water. (a) Measured NRM declination for re-deposited samples plotted versus the applied ambient field declination. (b) Measured NRM inclination for re-deposited samples plotted versus the applied ambient field inclination. (c) Calculated ChRM declination for re-deposited samples plotted versus the applied ambient field declination. (d) Calculated ChRM inclination for re-deposited samples plotted versus the applied ambient field inclination. Error bars in (c) and (d) represent the MAD values for the PCA fits for the ChRM determinations. The dotted curve represents a best fit to the data for the inclination error formula of King (1955): $\tan I_o = f \tan I_f$ (see text for discussion), with the $1\sigma$ range indicated by grey shading.

Water content has a significant effect on magnetic recording fidelity in our experiments. This is evident in the marked difference between the DRM (Figures 4.4 and 4.5) and PDRM (Figure 4.7) results, respectively, as well as in the ChRM stability and remanence intensity for each type of magnetization (Figure 4.6; Table 4.2). This difference is reflected in the size of the error bars (which represent MAD values from the respective PCA fits for the ChRM determinations) in Figures 4.5 and 4.7, respectively (note the different declination ranges of these figures). We therefore present additional results to demonstrate the effect of water content by mass% on
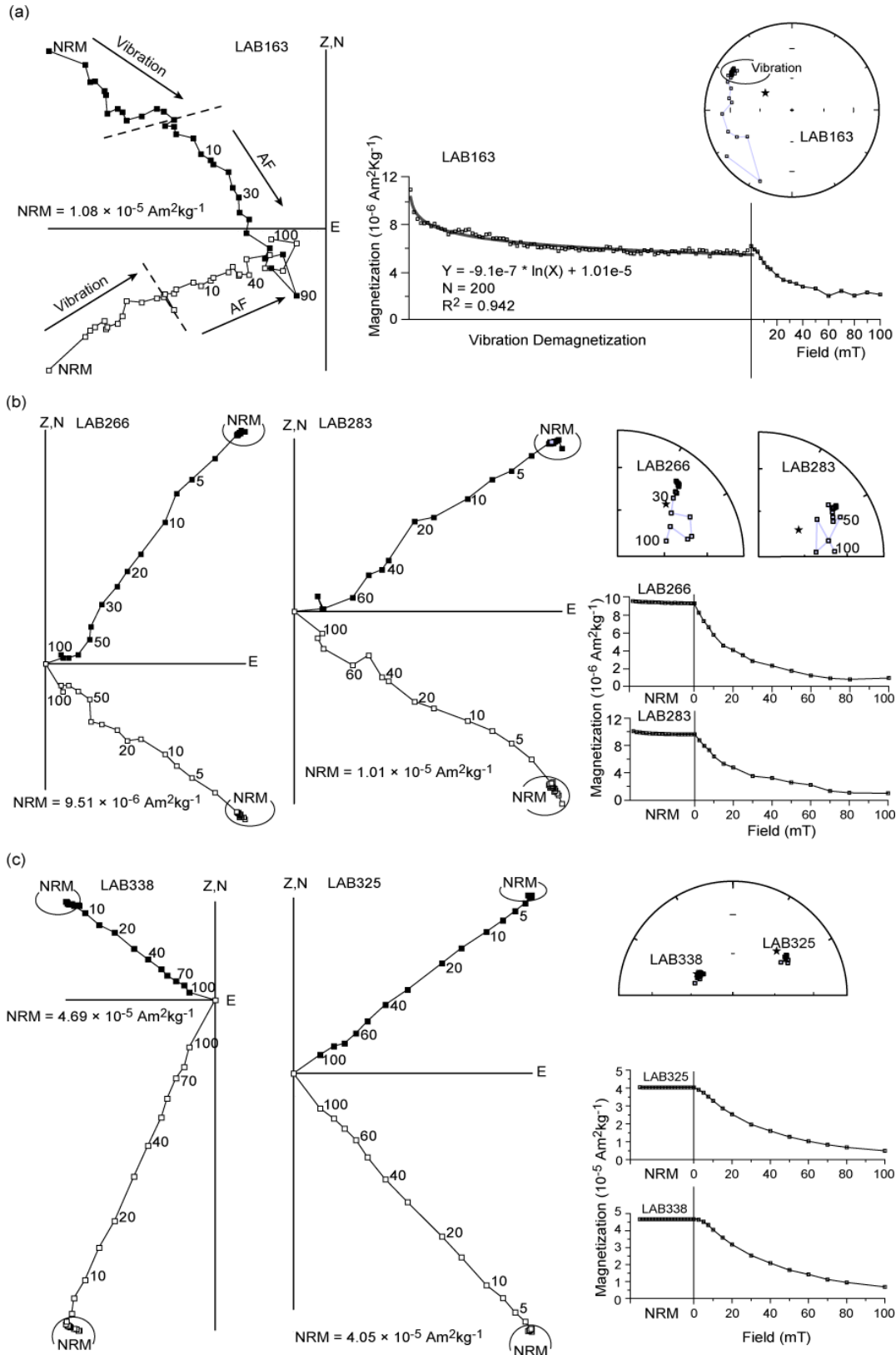
**Figure 4.6**      Vector component diagrams, intensity decay plots and equal area stereographic projections for stepwise AF demagnetization data for samples from: (a) dry re-deposition experiments (DRM), (b) re-deposition experiments with minor water added (DRM), and (c) re-deposition experiments with water saturation after deposition (PDRM). See text for discussion.

recording fidelity. It is important to note the magnetic uniformity of the sediment used for the re-deposition experiments, as indicated by the consistency of AF demagnetization spectra, as well as by consistent ARM intensities when normalized by mass (Figure 4.8a). Thus, any variation in the NRM/ARM ratio will be a result of variations in the efficiency of particle alignment during NRM acquisition. Water content is a key determinant of the DRM and PDRM intensity (Figure 4.8b, c; Table 4.2), and therefore of the NRM/ARM ratio (Figure 4.8c). When the water content is 40% or less, the NRM after addition of water is not significantly stronger than the NRM produced by dry deposition in zero-field (Figure 4.8b). The NRM/ARM ratio for such samples is low (~0.1-0.2) because of the inefficient alignment of magnetic particles (Figure 4.8d). As discussed above, the water content definition of Verosub et al. (1979) is not a true measure of water content in relation to sediment pore space; the high $H_2O\%$ values indicate that the sample was a wet slurry. Despite this definition, there is a key change in the magnetic recording quality at $H_2O\% = 40\text{-}50\%$. When the water content by mass exceeds 50%, the NRM increases significantly after adding water and applying the 50 $\mu$T field. The resulting NRM is so efficient that it is stronger than the ARM (Figure 4.8b). For water contents >45-50%, the NRM/ARM ratio consistently exceeds 1.0 (Figure 4.8d). These results indicate that there is a critical water content of ~40% (which effectively reflects water saturation), above which the alignment efficiency of magnetic particles with the applied field improves significantly.

The final effect that we note is that the efficiency of NRM acquisition improves with longer exposure to an applied field. Samples that were left in the 50-$\mu$T field in a water-logged state for 24 hours have stronger NRMs than samples that were allowed to stand for 12 hours or less (Figure 4.8c). We did not allow samples to stand for longer periods of time to further test the effects of time exposure to a field for water-saturated sediments (such observations were reported for PDRM experiments by Otofuji et al. (1982)).
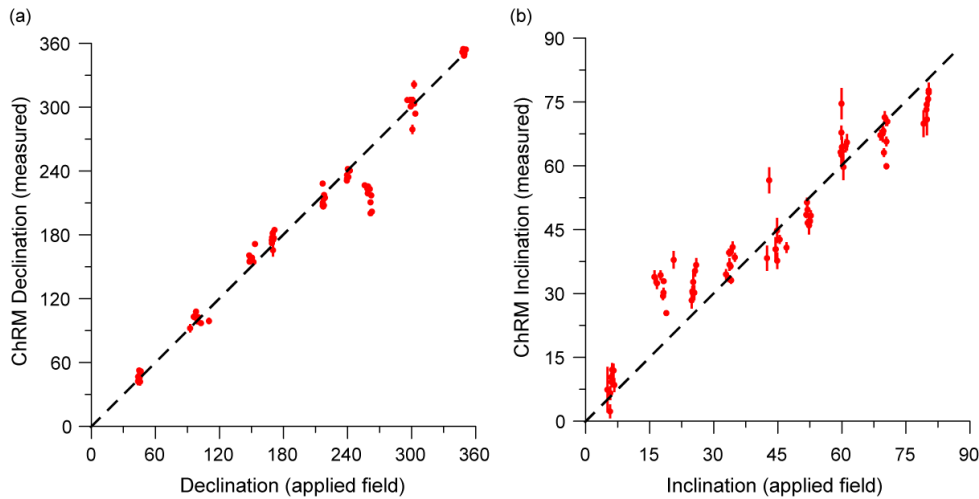
**Figure 4.7** Recording fidelity of a PDRM produced via dry deposition in zero-field followed by post-depositional water-saturation in a 50-µT field. (a) Calculated ChRM declination for re-deposited samples plotted versus the applied ambient field declination. (b) Calculated ChRM inclination for re-deposited samples plotted versus the applied ambient field inclination. Error bars represent the respective MAD values for the PCA fits for the ChRM determinations.

## 4.4.2 Paleomagnetic recording fidelity of Chinese loess

To address the question of how Chinese loess becomes magnetized, it is meaningful to compare the recording fidelity in our DRM and PDRM simulations with the long-term paleomagnetic recording fidelity of a range of Chinese loess sequences. In Figure 4.9, we plot published paleomagnetic data from long stratigraphic sections onto equal area stereographic projections. We plot data from loess intervals only; we explicitly exclude paleosol data and intervals with elevated magnetic susceptibility values because we wish to better understand paleomagnetic recording in loess and we wish to avoid complications related to possible acquisition of an additional CRM associated with pedogenic formation of magnetite, maghemite and/or hematite. Whilst it has been argued that pedogenesis can affect loess intervals as well as paleosols (e.g., Verosub et al., 1993), it is expected that the effects of pedogenesis will not be strong in loess intervals. We also exclude data from intervals that are interpreted to contain excursions and polarity transitions because our intention is to understand recording fidelity in non-transitional intervals. Data are plotted for the following stratigraphic intervals at the following localities: loess unit L1 (excluding sub-paleosol L1SS1) at Yichuan (Zhu et al., 2007), units L1, L2, L3, L4, L5, L6, L7, and the upper part of L8 (the problematical unit L9 was not included) at Sanmenxia (Wang et al., 2005), unit L1 (excluding sub-paleosol L1SS1 and the paleomagnetic

excursion interpreted to lie within it) at Xifeng (Zhu et al., 2007), units L1 and L2 at Lingtai (Zhu et al., 2000), unit L1 at Baicaoyuan (Deng et al., 2008), units L1, L2, L3, L4, L5, L6, L7, and the upper part of L8 (excluding interpreted paleomagnetic excursions and the Matuyama-Brunhes boundary interval) at Weinan (Pan et al., 2002), and units L5, L6, L7, and the upper part of L8 at Baoji (Yang et al., 2007b). For each location, we show the paleomagnetic data, the 95% cone of confidence about the mean direction, and the respective geocentric axial dipole (GAD) direction.

We aim to establish whether the paleomagnetic records for these distributed locations provide evidence for faithful recording of the time-averaged geomagnetic field. The time-averaged paleomagnetic direction sometimes coincides with the expected GAD direction (Figure 4.9). However, the mean paleomagnetic direction for thick intervals of Chinese loess, within the respective 95% confidence limits, often does not coincide with the expected GAD direction. In most cases, the inclinations are shallower than for the GAD field, and the mean declinations are generally deflected to the west of the expected GAD declination. Long paleomagnetic time series therefore indicate that Chinese loess can provide an accurate record of the time-averaged geomagnetic field, but that degraded paleomagnetic recording is also widespread. When paleomagnetic data are included for the paleosol units within these sequences, the average paleomagnetic directions are often even shallower than for the loess-only data shown in Figure 4.9. This suggests that CRM recording in paleosols merits further investigation, which is outside the scope of the present study.

## 4.5 Discussion

### 4.5.1 Laboratory simulation of DRM

Our initial experiments provide a simulation of DRM acquisition associated with eolian deposition under dry conditions. Faithful recording of the applied field declination, with systematically shallow inclinations (Figures 4.4 and 4.5), is typical for a DRM. The measured DRM data (Figure 4.5) follow the relationship given by the "inclination error formula" (King, 1955):

$$\tan I_0 = f \tan I_f,$$

where $I_o$ and $I_f$ are the observed and applied field inclinations, respectively, and $f$ is the so-called flattening factor. For the ChRM recorded in our re-deposition experiments, $f = 0.42$, which is in the middle of the $f = 0.2$ to $0.7$ range reported for a DRM (e.g., King, 1955; Tauxe, 2005). Shallow paleomagnetic inclinations are apparently commonly recorded across the Chinese Loess Plateau (Figure 4.9). It is therefore likely that a DRM is responsible for at least some of the NRMs recorded by the Chinese loess. However, our results also clearly demonstrate that a DRM cannot produce accurate recording of inclinations at the latitudes of the Chinese Loess Plateau (Figure 4.9). Therefore, for locations, or for significant loess intervals at specific locations, where the mean paleomagnetic direction is indistinguishable from the expected GAD direction, another remanence acquisition mechanism must have been operating.

## 4.5.2 Laboratory simulation of PDRM

The importance of water in the acquisition of a remanent magnetization has long been recognised for a PDRM in general (e.g., Irving and Major, 1964) and for loess deposits in China (e.g., Burbank and Li, 1985; McIntosh, 1993) and Belgium (Hus and Geeraerts, 1986). All of the evidence from our experiments indicates that the post-depositional presence of water is crucial, above a threshold water content of ~40% (which effectively corresponds to water saturation), for producing an efficient PDRM in eolian sediments. If a sedimentary sequence is magnetically homogeneous, and if the remanence was acquired under uniform conditions, one would expect the NRM/ARM ratio to provide a proxy estimate of the relative geomagnetic field strength (e.g., Tauxe, 1993). In our experiments, the sediment is magnetically homogeneous and the field strength was constant, therefore NRM/ARM variations provide an indication of variations in the conditions under which the remanence was acquired. Our laboratory analyses of consolidated Holocene and L1 loess samples from the Yuanbao section indicate that NRM/ARM ratios range between 0.08 and 0.65 (Table 4.2). If the NRM/ARM ratio of the Yuanbao loess can be related to the NRM/ARM ratio in our experiments (which they might not because of potentially large differences in magnetic particle alignment efficiency for different remanence acquisition mechanisms), and if our experiments provide any meaningful analogue for sedimentary conditions in the Chinese loess, the water content of the studied Chinese

loess sediments can be inferred to have spanned the range between inefficient DRM acquisition (NRM/ARM ≈ 0.1) and efficient PDRM acquisition (NRM/ARM > 0.4). Comparison of data from Chinese loess in relation to our re-deposition experiments indicates that a mixed DRM and PDRM mechanism best explains a significant amount of the recorded paleomagnetic signal. However, the fact that short-period geomagnetic features are often recorded (e.g., Pan et al., 2002; Yang et al., 2007b; Zhu et al., 2007) indicates that the PDRM must have shallow lock-in (Roberts and Winklhofer, 2004; Liu et al., 2008).

## 4.5.3 Bioturbation?

In marine environments, bioturbation is a key process that causes sediment irrigation and that allows the grain remobilization that is crucial to PDRM acquisition (e.g., Kent, 1973; Roberts and Winklhofer, 2004). It has been argued that a stirred remanent magnetization is a good analogue for a PDRM (Tucker, 1980; Payne and Verosub, 1982). The high NRM/ARM ratios of samples with water contents >50% (Figure 4.8c) indicate a good statistical alignment of magnetic particles with the applied field. Nevertheless, the PDRM acquisition process used here did not involve stirring and the NRM intensities, although strong, are not as strong as would be expected for a stirred remanent magnetization. We did not seek to simulate the effects of bioturbation by producing a stirred remanent magnetization because bioturbation is only considered to be important in paleosols or where mean annual precipitation exceeds 600 mm/year (Xiao et al., 1995). We therefore restrict our discussion about PDRM acquisition to the mechanical alignment of magnetic particles with the geomagnetic field in environments with water content >40%. We also note that Irving and Major (1964) successfully simulated a PDRM without bioturbation.
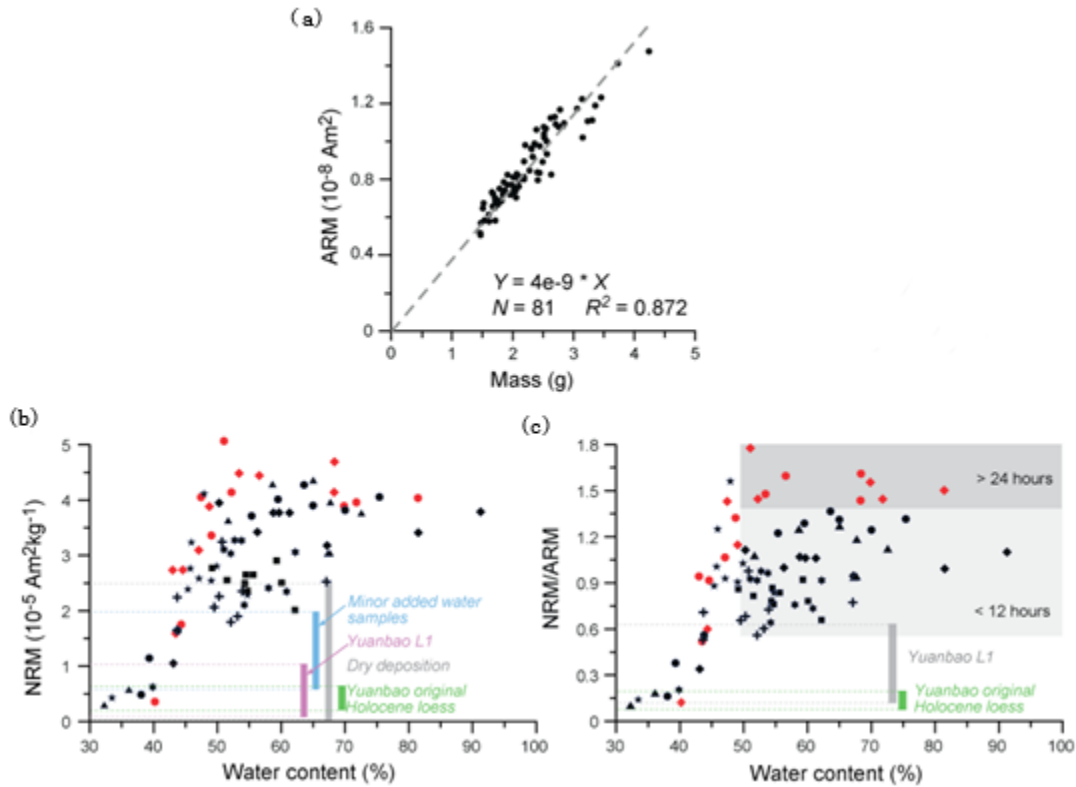
**Figure 4.8** Demonstration of the effects of variable water content by mass% on the magnetic recording fidelity of the DRM and PDRM. (a) Constant ARM per unit mass demonstrates the magnetic uniformity of the sediments. (b) Variation of NRM with water content. (c) Variation of NRM/ARM with water content by mass%. The different shading patterns for water content >50% indicate the NRM/ARM values for NRM acquisition after exposure in a field of <12 hours (black symbols) and >24 hours (red symbols), respectively. The different symbols indicate different sample batches. The range of values for (b) NRM and (c) NRM/ARM are shown for the original Holocene loess parent material from Yuanbao and for the L1 loess from Yuanbao, along with the range of NRM values for the two sets of DRM experiments.

## 4.5.4 Compaction-induced inclination flattening?

Widespread inclination flattening in Chinese loess, as indicated in Figure 4.9, could have caused DRM acquisition (Figure 4.4) or compaction. Tauxe (2005) noted that both DRM and compaction produce inclination flattening of the same form. Anson and Kodama (1987) argued that experimentally applied compaction pressures that produce inclination flattening are not applicable in natural sediments until depths of several hundred metres. In contrast, Arason and Levi (1990) observed noticeable compaction-induced inclination shallowing at depths of 60-85 m. Several of the loess sections from which data are plotted in Figure 4.9 extend to shallow maximum depths of 14 m (Baicaoyuan, Lingtai, Xifeng and Yichuan), so compaction-induced inclination shallowing would not be expected. Data from Baoji, Sanmenxia and

Weinan extend down to loess units L7 or L8 at maximum depths of 50-70 m. Inclination errors in Figure 4.9 are more significant for shallow sampling intervals than for deeper intervals. While there is significant inclination flattening at Baoji, the mean inclination at Sanmenxia is steeper than the GAD inclination and at Weinan it is similar to the GAD inclination. These observations are difficult to reconcile with compaction-induced inclination shallowing. Furthermore, application of the elongation-inclination method (Tauxe, 2005) to correct for inclination shallowing consistently yields unrealistically steep inclinations at the respective site latitudes. We therefore conclude that the observed inclination errors (Figure 4.9) are more reasonably explained by DRM recording than compaction.

## 4.5.5 DRM and PDRM remanence intensities

Inspection of Table 4.2 reveals a conundrum concerning the NRM intensity of the loess parent material that was re-deposited to produce the simulated DRM and PDRM. The NRM of the original loess is weak and ranges between 2.45 and 6.6 x $10^{-6}$ $Am^2kg^{-1}$. In contrast, the mean intensity of the simulated DRM is stronger than the upper range of loess NRM values (at 9.21 x $10^{-6}$ $Am^2kg^{-1}$), as is the entire range of PDRM intensities. This suggests that the simulated DRM and PDRM are both more efficient than the real NRM acquisition mechanism. It should, however, be borne in mind that the NRM of natural samples will contain a viscous component that has weakened the NRM from its original intensity. A DRM therefore remains a likely candidate as the NRM acquisition mechanism for Chinese loess. In contrast, the simulated PDRM is too efficient in terms of both directional recording fidelity and remanence intensity to be viable as a dominant mechanism for magnetizing the Chinese loess. Conversely, however, the degree of inclination shallowing evident in Figure 4.9 is not as large as in our simulated DRM (Figure 4.4 and 4.5). It is therefore highly likely that some water was present during remanence acquisition for significant stratigraphic intervals of the Chinese loess to produce the only partially degraded paleomagnetic records in Figure 4.9. A time-varying mixture between PDRM and DRM mechanisms therefore seems likely. If a PDRM has been in operation, then some aspect of loessification is likely to have given rise to a decrease in remanence intensity over time that we have not been able to reproduce in our laboratory re-deposition experiments. Future work is needed to understand this.
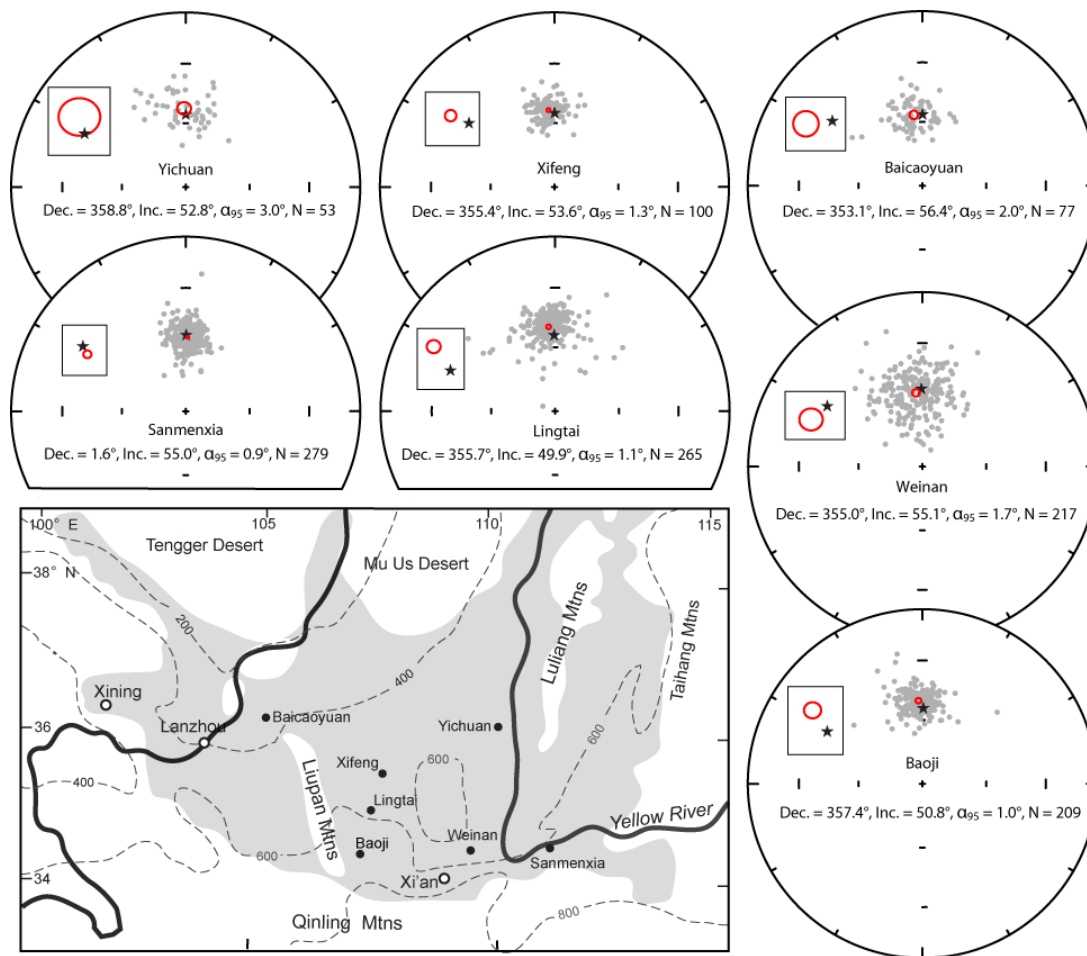
**Figure 4.9**        Map of the Chinese Loess Plateau with locations for which paleomagnetic directions are summarized on equal area stereographic projections. Shading indicates the areal extent of the Chinese loess deposits and the dashed contour lines indicate present-day rainfall (in mm/year). Paleomagnetic data are shown only for loess intervals of the respective sections. Red ellipses indicate 95% cones of confidence about the mean paleomagnetic directions. Black stars indicate the respective GAD directions. A threefold expansion of the area in the vicinity of the red ellipses and black stars is shown for clarity (insets). Time-averaged paleomagnetic directions are expected to coincide with the GAD directions if the loess faithfully records the geomagnetic field. Data sources are: Yichuan (Zhu et al., 2007), Sanmenxia (Wang et al., 2005), Xifeng (Zhu et al., 2007), Lingtai (Zhu et al., 2000), Baicaoyuan (Deng et al., 2008), Weinan (Pan et al., 2002), and Baoji (Yang et al., 2007b). See text for details of the stratigraphic intervals from which data are plotted.

## 4.5.6 Loess deposition and rainfall on the Chinese Loess Plateau

The Chinese Loess Plateau had an arid and dusty environment during glacial periods, but preservation of loess after deposition is not guaranteed. Any deposited loess would have been vulnerable to deflation and re-suspension. Addition of moisture, through rainfall, would provide cohesion to the sediment and would enhance resistance to deflation of the loess substrate. However, the probability of erosion will be increased by desiccation and strong winds. Unlike marine sediments, which are

generally expected to undergo reasonably continuous deposition, loess has been demonstrated to undergo episodic and highly variable deposition on interglacial and sub-glacial timescales, with non-deposition or erosion being common (e.g., Stevens et al., 2006, 2007). On annual timescales, dust delivery is not uniform and is associated with extreme weather events, with large dust outbreaks from loess source regions being most frequent in spring (Roe, 2009). Rainfall would not have been abundant on the Chinese Loess Plateau during glacial times, but rainfall after a dust deposition event is likely to have aided preservation of the deposited dust. Crucially, our results indicate that moisture is required for loess to faithfully record geomagnetic field variations. The fact that inclination errors are common in Chinese loess (Figure 4.9) might suggest that water contents were often below the critical ~40% threshold required to produce a PDRM and that a DRM must be responsible for a significant amount of the paleomagnetic signal recorded by the Chinese loess. Nevertheless, time-averaged paleomagnetic directions that are indistinguishable from the expected GAD field direction at some localities and NRM/ARM ratios that exceed 0.4 indicates that in other cases, a PDRM must be responsible for a significant amount of the paleomagnetic signal recorded by the Chinese loess. We therefore conclude that the Chinese loess is magnetized by a combination of DRM and PDRM mechanisms, with water content providing the key control on which remanence acquisition mechanism is dominant. We note, however, that there is no particular correlation between long-term paleomagnetic recording quality and the present day rainfall distribution shown in Figure 4.9. Loess sequences from the more arid northern parts of the Chinese Loess Plateau are often targeted for paleomagnetic studies to avoid pedogenic effects. It should be noted that reduced rainfall in these areas probably also contributes to reduced PDRM recording fidelity. The complex combination of remanence acquisition mechanisms, including DRM, PDRM, and CRM mechanisms, and their likely variation through time, not to mention episodic deposition/preservation, provides a significant complication for interpretation of short-period geomagnetic fluctuations from the Chinese loess. Regardless, efficient PDRM lock-in is likely to be associated with moisture availability, and the recording of short-period features such as geomagnetic excursions (e.g., Pan et al., 2002; Yang et al., 2007b; Zhu et al., 2007) means that the lock-in depth must be shallow (cf. Roberts and Winklhofer, 2004).

# 4.6 Conclusions

To address the lack of a convincing explanation for how Chinese loess becomes magnetized, we conducted laboratory re-deposition experiments using disaggregated loess. We simulated dry deposition of eolian sediments to produce a DRM without post-depositional modification. The simulated DRM provides a faithful record of the applied field declination, but with systematic inclination flattening. Post-depositional addition of minor water slightly improves recording of the applied field, but inclination flattening persists. We then simulated a PDRM by adding water in varying concentrations after dry deposition of eolian sediments. Reliable recording of the applied field occurs when the sediment is water-saturated. We also synthesized paleomagnetic data from Chinese loess sequences to test actual paleomagnetic recording against our laboratory simulations. Time-averaged paleomagnetic directions for loess sequences are often indistinguishable from the expected geocentric axial dipole (GAD) field, but in other cases inclinations are shallower than for a GAD field. We therefore conclude that the Chinese loess is magnetized by a combination of DRM and PDRM mechanisms, with water content providing the dominant control on the remanence acquisition mechanism. Where pedogenesis causes growth of magnetite, maghemite and/or hematite through the stable single domain blocking volume, an additional chemical remanent magnetization (CRM) will occur. The magnetization of Chinese loess therefore appears to be controlled by a complex, time-varying combination of DRM, PDRM and CRM mechanisms. This complexity has important consequences for the paleomagnetic recording fidelity of the Chinese loess, particularly for determination of short-period geomagnetic fluctuations, although PDRM lock-in is likely to be shallow because short-period features such as geomagnetic excursions are often recorded in the Chinese loess.

**Table 4.2** Remanence intensities for data from natural samples from Yuanbao and for redeposition experiments using the same sediments.

| Sample type | Remanence type | Remanence intensity ($Am^2kg^{-1}$) | | | | Number of samples |
|---|---|---|---|---|---|---|
| | | Maximum | Minimum | Mean | SD[7] | |
| Natural Holocene discrete samples[1] | NRM | 6.60E-06 | 4.78E-06 | 5.86E-06 | 4.05E-07 | 8 |
| Natural Holocene U-channel sample[2] | NRM | 5.89E-06 | 2.45E-06 | 3.43E-06 | 4.02E-07 | 122 |
| Natural L1 U-channel samples[3] | NRM | 1.17E-05 | 1.71E-06 | 5.19E-06 | 1.18E-06 | 1345 |
| Dry redeposition[4] | DRM | 2.52E-05 | 4.45E-07 | 9.21E-06 | 4.27E-06 | 159 |
| Minor added water after redeposition[5] | DRM | 1.97E-05 | 6.44E-06 | 1.24E-05 | 2.71E-06 | 48 |
| Water saturated after redeposition[6] | PDRM | 5.07E-05 | 1.05E-05 | 3.14E-05 | 7.38E-06 | 75 |
| Natural Holocene discrete samples[1] | ARM | 3.39E-05 | 2.71E-05 | 3.08E-05 | 2.03E-06 | 8 |
| Natural Holocene U-channel sample[2] | ARM | 3.98E-05 | 2.44E-05 | 2.97E-05 | 2.80E-06 | 122 |
| Natural L1 U-channel samples[3] | ARM | 2.53E-05 | 1.17E-06 | 1.78E-05 | 1.37E-05 | 1345 |
| Water saturated PDRM samples[6] | ARM | 3.57E-05 | 2.51E-05 | 3.10E-05 | 2.00E-06 | 75 |
| Natural Holocene discrete samples[1] | NRM/ARM | 0.21 | 0.16 | 0.19 | 0.01 | 8 |
| Natural Holocene U-channel sample[2] | NRM/ARM | 0.15 | 0.08 | 0.12 | 0.02 | 122 |
| Natural L1 U-channel samples[3] | NRM/ARM | 0.65 | 0.13 | 0.29 | 0.06 | 1345 |

1. Results from 8 discrete samples from the Holocene loess section at Yuanbao (i.e., the parent material for the redeposition experiments).

2. Results from a single U-channel sample (length of 1.22 m) from the Holocene loess section at Yuanbao. (parent material).

3. Results from U-channel samples (length of 13.45 m) from pedogenically unaltered L1 unit at Yuanbao.

4. Results from 18 batches of 9 samples (N = 162); 3 samples were destroyed prior to measurement to give N = 159.

5. Results from 6 batches of 9 samples (N = 54); 6 samples were destroyed prior to measurement to give N = 48.

6. Results from 9 batches of 9 samples (N = 81); 6 samples were destroyed prior to measurement to give N = 75.

7. SD = standard deviation.

# Chapter 5

# Can the Chinese Loess Record Variations in Relative Geomagnetic Paleointensity?

## 5.1  Introduction

The Chinese Loess Plateau contains one of the world's most outstanding terrestrial archives of paleoclimate change (Liu, 1985; Kukla et al., 1990; Wang et al., 1990; An et al., 1991; Ding and Liu, 1992; Heller and Evans, 1995). Paleomagnetic studies have been crucial in establishing the chronology of paleoclimate variations recorded by Chinese loess sequences (Heller and Liu, 1982, 1984; Rolph et al., 1989; Maher and Thompson, 1991). Identification of the position of geomagnetic reversals for the past 2.6 Ma has enabled correlation of magnetic susceptibility profiles to the marine $\delta^{18}O$ record (Kukla et al., 1990; Ding et al., 2000). Magnetic susceptibility peaks occur within paleosols as a result of magnetite/maghemite formation during pedogenesis; the intervening loess units have much lower magnetic susceptibilities (Kukla et al., 1990; Maher and Thompson, 1991; Heller and Evans, 1995). Despite this first-order success in establishing the loess chronology through orbital tuning of paleoclimatically sensitive parameters such as magnetic susceptibility (Lu et al., 1999; Heslop et al., 2000; Ding et al., 2002), a consistent chronology for the Chinese loess still does not exist. For example, the last major geomagnetic reversal (the Matuyama/Brunhes boundary) is usually reported to lie in glacial deposits in the Chinese loess, whereas it is located in interglacial deposits in marine sediments (Zhou and Shackleton, 1999). Although this problem has been solved through correlating quartz grain size with marine paleoclimate records (Liu et al., 2008), dating uncertainties remain and can make it difficult to correlate loess signals with other paleoclimate records and to establish phase relations between these records (Stevens

et al., 2006, 2007). Attempts to correctly correlate and interpret paleoclimate records from the Chinese loess depend on having a robust chronology.

In the past two decades, numerous relative geomagnetic paleointensity studies have been made on marine sediments (Tauxe and Valet, 1989; Valet et al., 1994; Yamazaki et al., 1995; Guyodo and Valet, 1996; Channell et al., 1997; Roberts et al., 1997; Brachfeld and Banerjee, 2000; Horng et al., 2003; Suganuma et al., 2008). Pedogenesis, which causes neoformation of at least two main magnetic mineral components in Chinese loess (Heller and Evans, 1995; Maher, 1998; van Velzen and Dekkers, 1999; Zhu et al., 2001), makes it difficult for Chinese loess to satisfy the criteria for relative paleointensity studies, as summarized by Tauxe (1993). However, several attempts to determine relative paleointensity have been published for the Chinese loess (Zheng et al., 1995; Zhu et al., 1999; Pan et al., 2001; Liu et al., 2005a). Zheng et al. (1995) first estimated relative paleointensity variations using the ratio of the natural remanent magnetization (NRM) to the anhysterestic remanent magnetization (ARM) after thermal demagnetization at 300°C for the last interglacial interval (paleosol S1) from the Huanxian section in the northern Chinese Loess Plateau. Zhu et al. (1999) also assumed that the same ratio provides an estimation of relative geomagnetic paleointensity for the last glacial interval (loess L1) from the Weinan section. Pan et al. (2001) systematically investigated the reliability of "relative paleointensity" signals recorded in the Lingtai section; they used both the traditional normalized NRM/ARM method and the pseudo-Thellier method (Tauxe et al., 1995) to estimate relative paleointensity. Spectral analyses and coherence tests indicate that the signals recorded in the studied section are complex. Liu et al. (2005a) compared both thermal and alternating field (AF) demagnetization curves of NRM, ARM and saturation isothermal remanent magnetization (SIRM), and argued that the AF-demagnetized SIRM is a more suitable parameter for relative paleointensity normalization. Zhu et al. (1999) and Pan et al. (2001) focussed on the L1 interval to avoid serious pedogenic effects on the magnetic mineralogy, while Zhang et al. (1995) and Liu et al. (2005a) concentrated on the S1 interval.

Even a superficial understanding of magnetization processes within Chinese loess makes it difficult to consider that it can reliably record relative geomagnetic paleointensity. Longer records, comparison among results from multiple localities, and a better understanding of magnetization processes in loess are required to provide

a more robust test of whether relative paleointensity can be determined and whether it can be used to develop robust chronologies for the Chinese loess. In this study, we investigate detailed records of sediment grain size and magnetic parameter variations for the last glacial/interglacial period, spanning from 120 to 20 ka, at Yuanbao. Comparisons between normalized remanence records from Chinese loess and marine records are discussed to assess the suitability of Chinese loess for studies of relative geomagnetic paleointensity.

## 5.2  Geological setting and samples

The Yuanbao section (35.64°N, 103.14°E) is located on the fourth terrace of the Daxiahe River (Figure 1.1), which is one of the main tributaries of the Yellow River on the northwestern Chinese Loess Plateau (Chen et al., 1997). The mean annual temperature is about 6-7°C, and annual precipitation is about 500 mm (Liu et al., 2005a). Loess deposits in this region are relatively coarse-grained, and pedogenesis is weak compared with the central Chinese Loess Plateau (such as at the well-known Luochuan section). Sedimentation rates in the northwestern Chinese Loess Plateau are also much higher than in southeastern parts. In total, 150 m of loess has been deposited on the terrace.



**Figure 5.1**    Photos of field sampling. (a) Overview of the upper Yuanbao section, and (b) sampling details for one interval at yuanbao.

We sampled a loess interval that spans most of the last glacial-interglacial period. At least 20 cm of surface sediment was removed to avoid weathered material

when sampling and a smooth vertical surface was cut into the outcrop using a plumb line to ensure that the face was vertical. Perpendicular to the smooth surface, two 2-cm-deep parallel vertical grooves were cut. The grooves were maintained at a constant 2 cm spacing to form a 2-cm-wide loess strip. U-shaped sample holders were carefully pushed into the grooves, and were marked with the sample number and orientation. Each sample was then removed from the outcrop by running a fishing line behind the sample. Each U-channel sample is 75 cm long, and was sealed at both ends with laboratory film. In total, 41 U-channels were sampled at the Yuanbao section, and additional discrete samples were collected at 10 cm intervals for grain size analysis. Fourteen samples for optically stimulated luminescence (OSL) dating were also collected at selected depths along the section using a steel pipe, which was sealed with black tape at both ends.

## 5.3  Methods

### 5.3.1 Magnetic measurements

The U-channel samples were first subjected to low-field magnetic susceptibility measurements using a Bartington Instruments MS2 sensor that is connected to a laboratory-constructed automated long-core susceptibility measurement system. Remanence measurements were made with a 2-G Enterprises cryogenic magnetometer installed in a magnetically shielded laboratory (Roberts, 2006). In order to obtain detailed demagnetization spectra, the NRM of the samples was subjected to stepwise alternating field (AF) demagnetization at applied fields of 5, 10, 15, 20, 25, 30, 40, 50, 60, 70, 80, 90 and 100 mT. An ARM was imparted with a constant AF of 100 mT, and a direct current bias field of 0.08 mT. Stepwise AF demagnetization of the ARM was carried out using the same field steps as for the NRM. An IRM was imparted using a 2-G Enterprises pulse magnetizer with an inducing field of 1 T, and was then AF demagnetized using the same field steps as for the NRM. IRM was then imparted again at 1 T and an $IRM_{-300\,mT}$ was imparted using a field of 300 mT that was applied in the opposite direction to the $IRM_{1\,T}$. All measurements were made at 1-cm intervals at the National Oceanography Centre, Southampton (NOCS).

## 5.3.2 Grain size analysis

For grain size analysis of bulk sediments, 30% $H_2O_2$ was added to loess samples and maintained overnight to remove organic matter. Samples were then boiled for about 10 minutes after 10% HCl was added to remove carbonate. After cooling, 10 ml of 5% $(NaPO_3)_6$ was added to each sample, and the sample was then placed in an ultrasonic vibrator to disperse the particles (Sun et al., 2006a). The slurries were diluted to appropriate concentrations and measured with a Malvern Mastersizer S Laser instrument at the Institute of Earth Environment, Chinese Academy of Sciences, Xi'an, China.

## 5.3.3 OSL dating

In order to obtain age control points, 14 samples were processed for OSL dating at the Luminescence Laboratory of the Cold and Arid Environment and Engineering Research Institute, Chinese Academy of Sciences, Lanzhou, China, using an automated Risø TL/OSL-DA-15 reader (Markey et al., 1997; Zhao et al., 2010). We only obtained 6 valid OSL ages because the oldest samples had too strong a signal to be measured. The valid OSL ages are shown in Figure 5.2 and are used to help establish an approximate age model for the studied section.

# 5.4 Results

## 5.4.1 Grain-size distributions

Deposition of Chinese loess is associated with dust storms driven by the east Asian monsoon system (Liu, 1985). Therefore, the grain size distribution of Chinese loess contains information about past monsoons (Lu et al., 1996; Chen et al., 1997; Ding et al., 1999; Fang et al., 1999; Porter, 2001; Ding et al., 2002). Coarse silt-sized particles are generally associated with the winter monsoon; the mean grain size or the percentage of >40 μm diameter grains is often used to represent the winter monsoon intensity, which matches well with loess/paleosol cycles and also with climatic proxies recorded by marine sediments (Lu et al., 1996; Chen et al., 1997; Ding et al., 1999). Based on quartz grain size variations, Liu et al. (2008) demonstrated that the Matuyama/Brunhes boundary recorded in Chinese loess occurs without phase lag

compared to that recorded in marine sediments, which indicates that quartz grain size is much more suitable than magnetic susceptibility for recording paleoclimate changes. Sun et al. (2004) studied different intervals from different Chinese loess sections, and demonstrated the existence of bimodal or multi-modal grain size distributions. Bimodal or multi-modal grain size distributions are widespread in Chinese loess, including the Red Clay that stratigraphically underlies the loess sequences (Sun et al., 2004; Sun et al., 2006a). It has been demonstrated that different mathematical functions can be used to successfully separate grain size components from the total grain size distributions (Weltje et al., 1997; Sun et al., 2004; Parker and Bloemendal, 2005; Prins et al., 2007; Chen et al., 2009), including Weibull and Gaussian functions and an end-member fitting method. We follow Sun et al. (2004) in using the Weibull function to un-mix the grain size distribution. We obtained three grain-size components, compared to only the two of Sun et al. (2004), but which gives similar results to those modelled using Gaussian functions by Chen et al. (2009). Although Sun et al. (2006b) did not un-mix their results, their distribution curves all indicate the presence of a third grain size component. We name the components in our results the fine, medium and coarse components (details can be found in Appendix I). The fine component is uniform throughout the section, so we only discuss the medium and coarse components in this Chapter.

The 0.01-0.05 mm fraction was called the "loess fraction" by Liu (1985) after comparison of Chinese loess data with results of experiments in which it was demonstrated that grains of this size are easily carried by wind. In our Weibull distribution model, the "loess fraction" is treated as the coarse component with a mean grain-size of 30 μm. The grains in this component are difficult for wind to lift, which means that they rarely reach high altitudes and do not travel far (Tsoar and Pye, 1987). This component dominates loess samples, with average volume percentages reaching up to 80%, while it represents as little as 43% in paleosol samples (Figure 5.2). The coarse fraction is transported by the near-surface winter monsoon winds (An and Xiao, 1990; Sun et al., 2004), therefore parameters indicative of the coarse component are commonly used as indices for the winter monsoon (Lu and An, 1998; Fang et al., 1999; Ding et al., 2002; Sun et al., 2006b).

The medium grain size component is negatively correlated with the coarse component (Figure 5.2), which suggests that it is mainly controlled by the summer

monsoon. Although part of this component is transported by wind, part is also pedogenic in origin (Sun et al., 2006b). The pedogenic grains can be easily removed by chemical treatment, while quartz is resistant to this treatment process. Therefore, quartz grain size is used as an indicator of winter monsoon variations. Sun et al. (2006b) analysed the grain size of loess and Red Clay samples, and found that the medium component is significantly reduced after treatment, while the coarse (quartz-dominated) component does not change much. Despite differences in the amplitude of variations, there are no phase lags or other significant differences between the mean quartz grain size and the bulk mean grain size (Sun et al., 2010). Liu (1985) described a ratio of coarse to medium grain size fractions, and suggested that this ratio can be used as an indicator of post-depositional pedogenic modification. Here we use a medium/coarse ratio, which undergoes stratigraphic variation with a similar pattern as magnetic susceptibility variations (Figure 5.2g, h). Using the coarse component as the denominator in this ratio provides normalization for the original eolian input material, so that the medium/coarse ratio provides a measure of pedogenic particles and therefore of magnetic mineral enhancement in paleosols.

## 5.4.2 Age model

Paleosol unit S1 is related to marine oxygen isotope stage (MIS) 5, and three sub-paleosols S1SS1, S1SS2 and S1SS3 within S1 correlate with MIS 5a, 5c and 5e, respectively (Liu et al., 2005a), which are represented by three peaks in both grain size and magnetic susceptibility (Figure 5.2). Loess unit L1 has three sub-units L1LL1, L1SS1, and L1LL2, which correlate with MIS 2, 3 and 4, respectively. Based on these control points, we used bulk sediment grain size and magnetic susceptibility variations to correlate the studied loess sequence with the GRIP and SPECMAP oxygen isotope data to obtain an approximate age model for the Yuanbao section for the interval from 120 to 20 ka, which is consistent with previous results (Chen et al., 1997; Liu et al., 2005a). However, the OSL ages are generally too young compared to the correlation to the GRIP $\delta^{18}$O series.
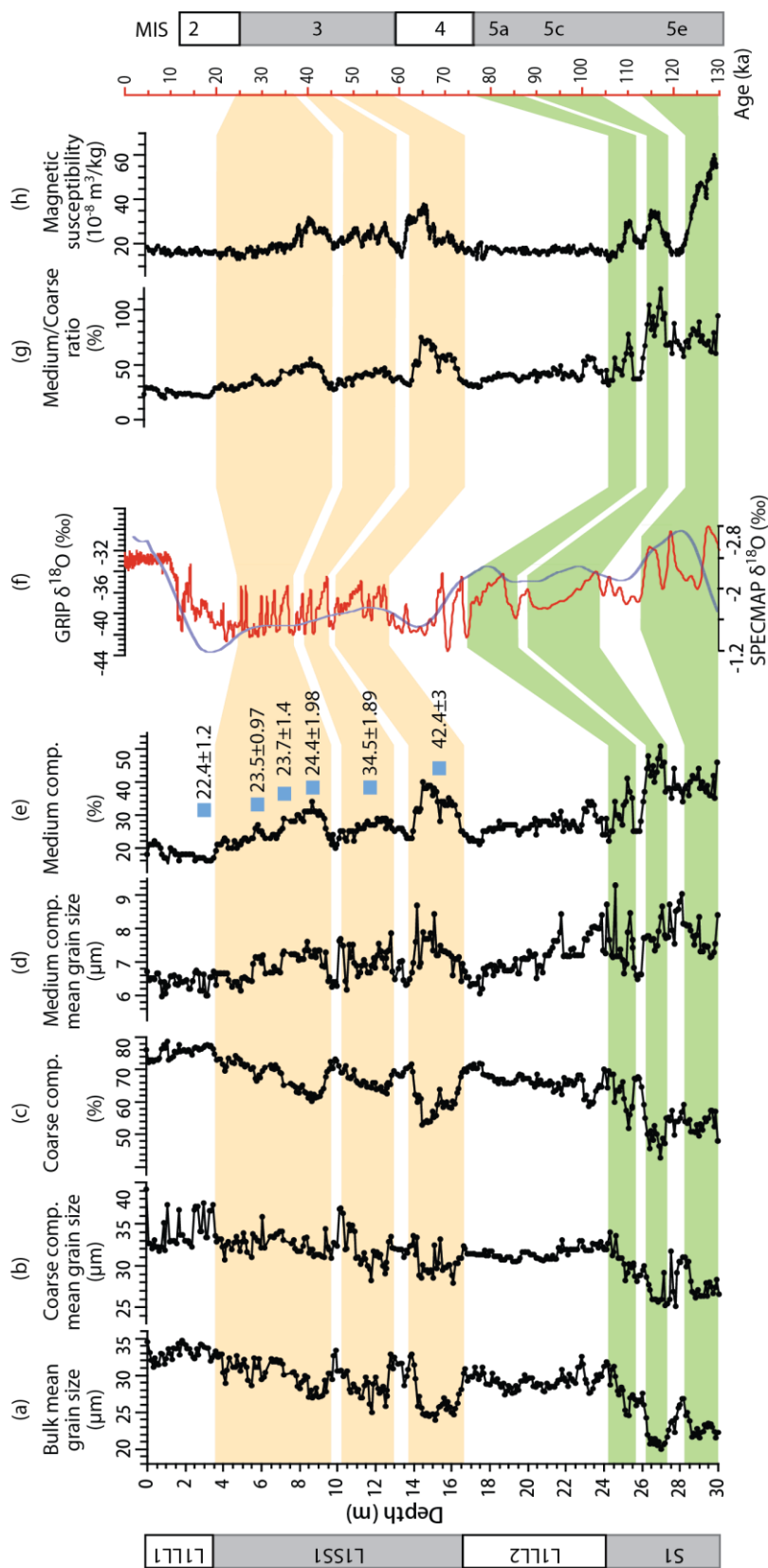
**Figure 5.2** Correlation of (a) bulk mean grain size, (b-e) grain size components, (g) the ratio of medium and coarse grain size components, and (h) the low-field magnetic susceptibility with (f) the relevant part of the GRIP ice core δ$^{18}$O series (red). The colour bands indicate tie points that are used to construct an age model using correlation of grain size and magnetic data to the millennial-scale δ$^{18}$O variations in the GRIP δ$^{18}$O record. The red axis is age for the GRIP data. The blue line in (f) represents the SPECMAP δ$^{18}$O data (Imbrie et al., 1989). Blue squares represent the OSL ages with standard deviation (and are generally too young compared to the correlation to the GRIP δ$^{18}$O series) (Johnsen et al. 2001).

## 5.4.3 Paleomagnetic results

Principal component analysis (Kirschvink, 1980) indicates that samples from the Yuanbao section have a stable characteristic remanent magnetization (ChRM). Relatively stable viscous remanent magnetization (VRM) and pedogenic chemical remanent magnetization (CRM) components represent noise for paleomagnetic studies of the Chinese loess. Stepwise AF demagnetization is useful for removing such secondary magnetization components and for identifying the primary component. The influence of pedogenesis on Chinese loess can be detected using magnetic susceptibility, ARM or IRM data. ARM and SIRM data at successive demagnetization levels (Figure 5.3) contain evidence of strong magnetic enhancement within paleosol or sub-paleosol intervals. A univectorial ChRM component is isolated with peak AFs of 40 mT (Figure 5.4). At this demagnetization level, ARM and SIRM data also become more uniform (Figure 5.3), which indicates that the secondary overprints are removed. Paleomagnetic declinations and inclinations vary around a mean that is close to but not coincident with the time-averaged geomagnetic field direction. The declinations are on average deflected to the east by around 15°, which represents a larger average deflection than can be explained by any error with compass
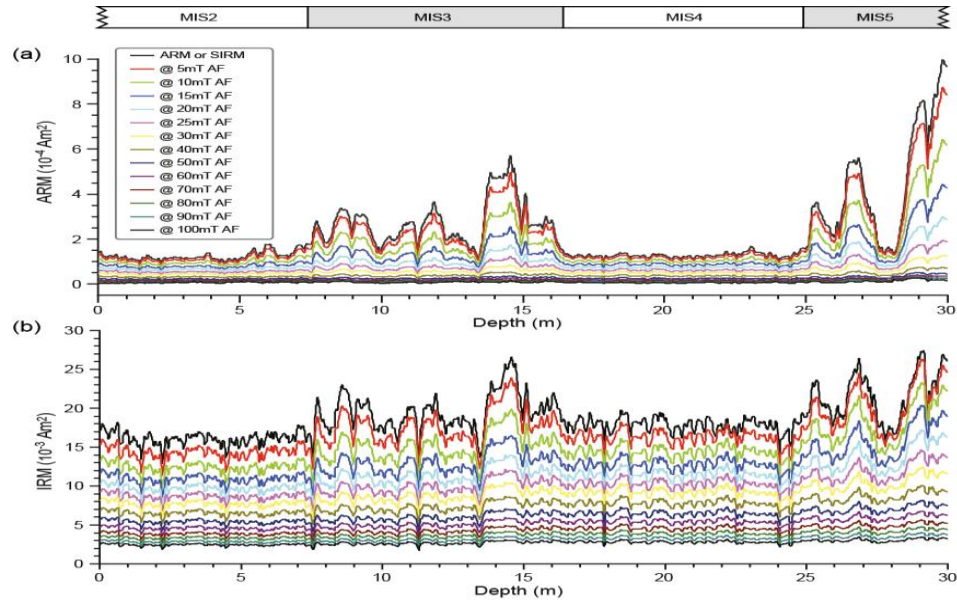


**Figure 5.3**     Intensity of remanent magnetization after each progressive AF demagnetization step (as labelled in the legend) for: (a) ARM and (b) IRM for the Yuanbao section. MIS5 (marine oxygen isotope stage 5) relates to Chinese loess soil unit one (S1), and MIS3 correlates to the sub-paleosol within loess unit L1. Both ARM and IRM are clearly affected by climate, with pedogenic magnetic mineral enhancement evident during MIS3 and MIS5. The gradual stepwise AF demagnetization results indicate that the climatic influence is largely removed at 40 mT and above.

measurements in the field. The inclinations average around 60°, which is coincident with the time-averaged field direction, but significant inclination error is observed within the following stratigraphic intervals: 3-8 m, 20-21 m and 27-28 m (Figure 5.4). This is consistent with the results of Zhao and Roberts (2010) who showed that inclination error can be large in loess intervals where dry deposition dominates and where lack of post-depositional addition of water does not enable particle realignment parallel to the ambient geomagnetic field direction. The maximum angular deviation (MAD) values for the principal component regression fit to the ChRM are also low (Figure 5.4c), except for samples from around 3 m, and are generally smaller than 6°.
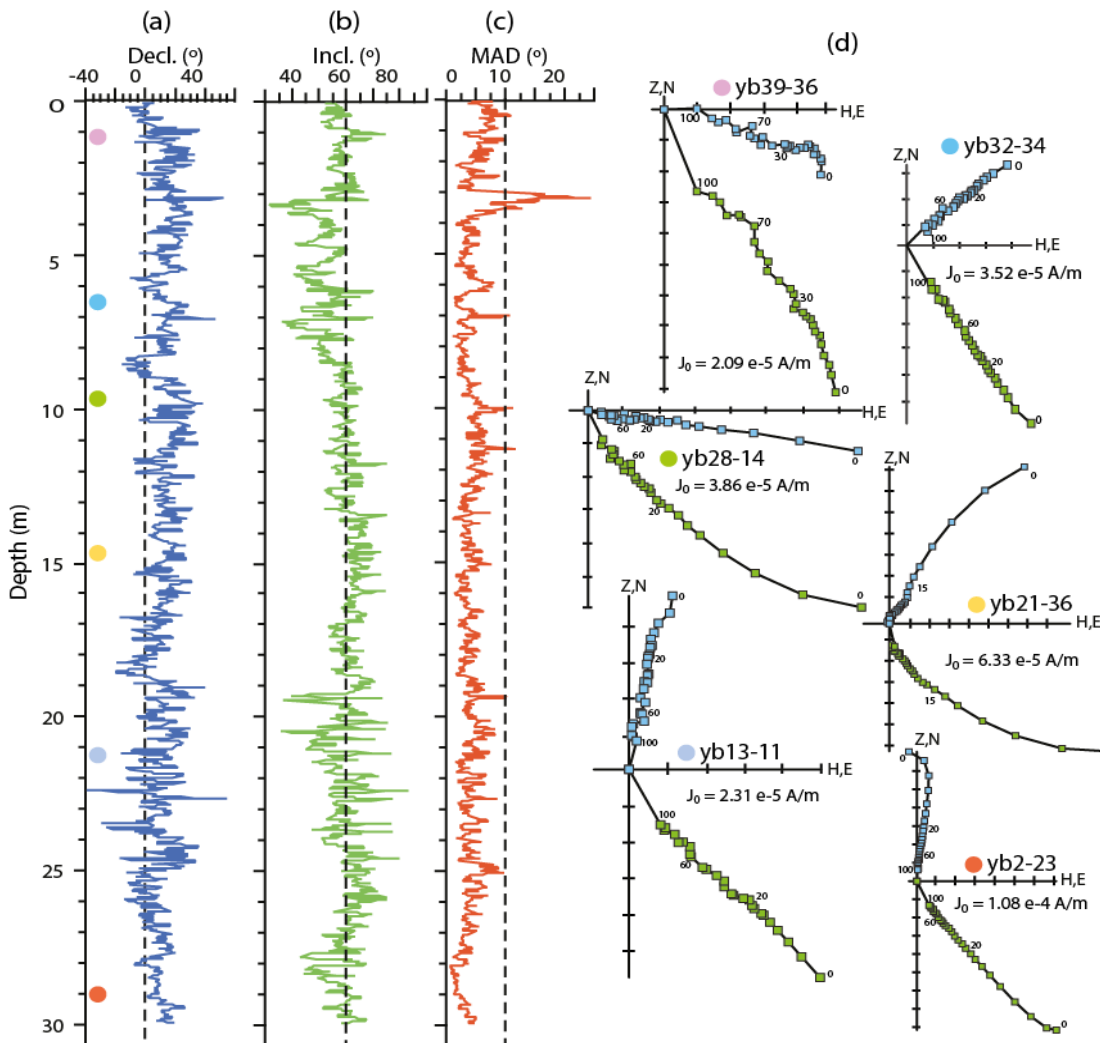


**Figure 5.4** ChRM results for the Yuanbao section. (a) Declination and (b) inclination of the ChRM after principal component analyses. (c) MAD values associated with the linear best fit to the ChRM vector. (d) Representative vector component diagrams for samples from selected depths (without declination correction). Blue squares represent the declination, while green squares represent the inclination. Coloured circles indicate the depths of the respective samples.

This indicates that a stable ChRM component has been isolated. No geomagnetic excursions are observed in the studied interval in the Yuanbao section. Typical demagnetization diagrams are plotted in Figure 5.4d. Most of the samples have a slight secondary component, which can be distinguished from the ChRM direction. The small MAD values indicate that we have isolated reliable ChRM directions, although what type of remanence has been recorded is not clear. As indicated by Zhao and Roberts (2010), it is possible that the ChRM represents a depositional remanent magnetization (DRM), a post-depositional remanent magnetization (PDRM), a CRM, or a complex composite magnetization.
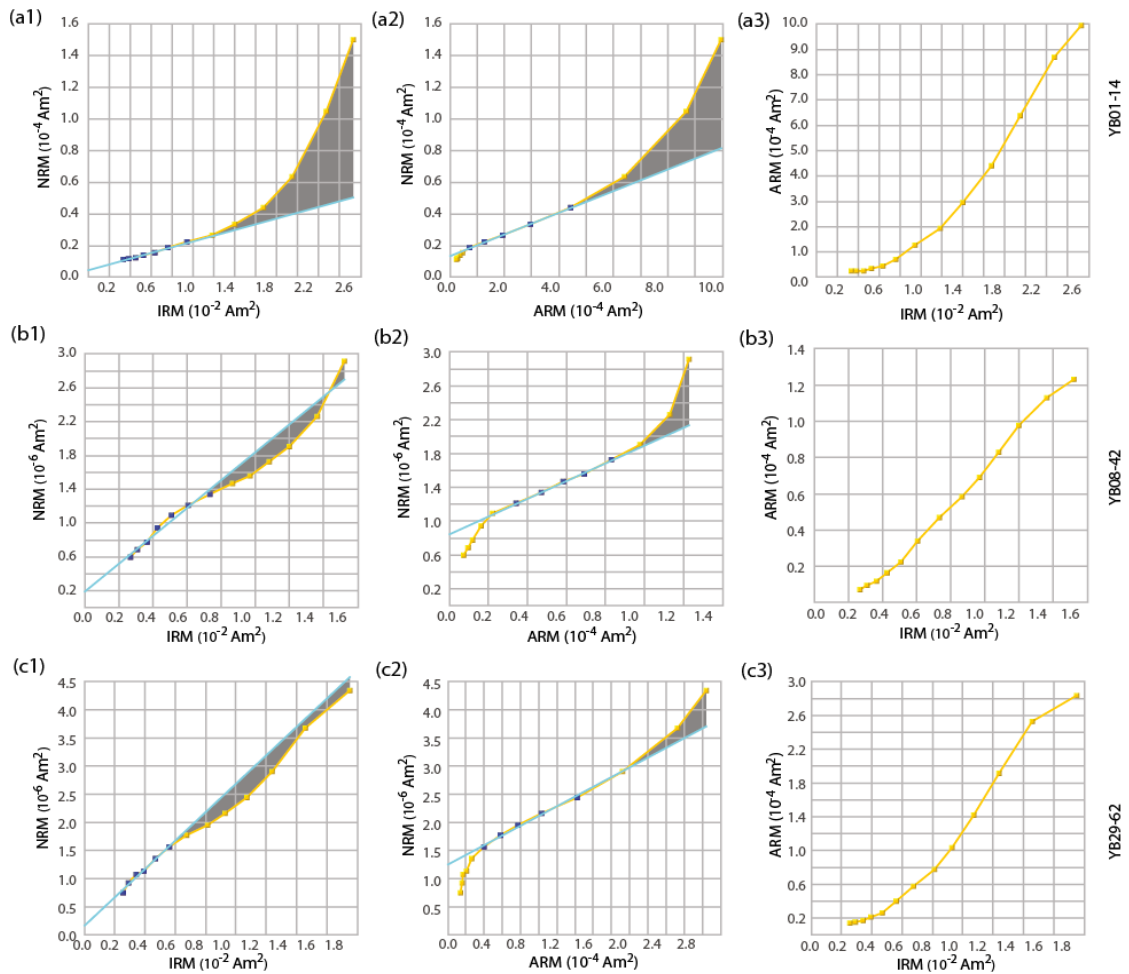


**Figure 5.5**       Representative cross-plots for respective pairs of NRM, IRM and ARM demagnetization data. The slopes of the lines were fitted using selected data points (dark), as typically used in pseudo-Thellier estimations of relative paleointensity. The grey area indicates the area used to estimate VRM and/or CRM components.

## 5.4.4 Normalized remanence records

Conventional relative paleointensity estimation methods employ normalization of a single NRM value (i.e., after demagnetization at a specified level) by the

low-field magnetic susceptibility, or by ARM or IRM data from the corresponding demagnetization step (Zheng et al., 1995; Zhu et al., 1999). Tauxe et al. (1995) described the so-called pseudo-Thellier method, in which a best-fit slope is fitted to stepwise-demagnetized NRM and stepwise-acquired ARM data at the same demagnetization levels. The slope is used to give a value that represents the border characteristics of the magnetic grain size distribution within the sample that is considered to provide a more robust estimation than conventional normalizations that only use a single demagnetization step. Valet and Meynadier (1998) compared different methods, and concluded that either ARM acquisition or demagnetization can be used and will produce the same relative paleointensity variations. Liu et al. (2005a) used the slope between NRM and IRM for AF demagnetization steps above 60 mT to estimate relative paleointensity for the S1 interval at the Yuanbao section, and argued that their results are reliable. Demagnetization at 60 mT was argued to remove any effects of pedogenesis, as we have also argued from the results in Figure 5.3. Here we have followed the same method as Liu et al. (2005a) to test whether relative paleointensity can be accurately determined for Chinese loess samples. The NRM, ARM and IRM were demagnetized using the same 13-step AF demagnetization procedure, and the slopes for respective data pairs are plotted in Figure 5.5. The correlations between NRM and IRM are different to those between NRM and ARM. On NRM versus IRM plots, there is a clear linear trend that is directed close to the origin of the plots after AF demagnetization at 40 mT. This linear component is present over a significant fraction of the intensity spectrum for both NRM and IRM. In contrast, in NRM versus ARM plots, while there appears to be a linear trend after AF demagnetization at 40 mT, there is always a deflection from linearity of the ARM at higher demagnetization steps, and a large non-zero intercept (Figure 5.5a2, b2, c2). For NRM and ARM, the linear trend is better for demagnetization data between 15 and 50 mT (Figure 5.5a2, b2, c2). We calculated all three slopes using the jackknife statistical method recommended by Tauxe and Gallet (1991), and refer to them as NRM/IRM, NRM/ARM and NRM/ARM2, respectively, where ARM2 refers to the slope of data above 50 mT. The general lack of a linear relationship between IRM and ARM (Figure 5.5a3, b3, c3) indicates that they are not recorded by the same magnetic mineral fraction.

## 5.4.5 VRM and/or CRM estimations

VRM and CRM represent secondary overprints that need to be removed to identify the DRM and/or PDRM in Chinese loess. These un-wanted secondary overprints can be removed by thermal or AF demagnetization (e.g., Zheng et al., 1995; Zhu et al., 1999; Pan et al., 2001). However, VRM and/or CRM can also provide useful information about paleoclimate because the formation of minerals that carry these remanences can be influenced by paleoclimatic variations. For example, formation of ultrafine magnetite during pedogenesis in Chinese loess is an important process that gives rise to VRM and/or CRM acquisition (Zhou et al., 1990). Kok and Tauxe (1999) presented a VRM area model based on the pseudo-Thellier relative paleointensity method. We used their approach to calculate the area between the data curve and the best-fit line used for remanence normalization to represent the VRM and/or CRM component(s) in Chinese loess samples (Figure 5.5). Due to the complex demagnetization behaviour, the VRM area lies above the best-fit line for paleosol samples (Figure 5.5a), while it lies under the best-fit line for loess samples (Figure 5.5c). For samples that have been affected moderately by pedogenesis, such as sample YB08-42, the area is defined on both sides of the best-fit line (Figure 5.5b). We define the area above the best-fit line as positive, while the area under the line is negative. Two sets of area calculations based on NRM/IRM and NRM/ARM data, respectively, are plotted in Figure 5.6 together with magnetic susceptibility to demonstrate their inter-relationship. These data can be used to assess the influence of paleoclimate on VRM and/or CRM. Only positive values are observed for the NRM/ARM case, which correlate well with magnetic susceptibility variations (Figure 5.6a). The positive areas relate to higher magnetic susceptibilities in both cases, while the negative areas are only present for NRM/IRM data and relate to low magnetic susceptibilities.

## 5.4.6 Spectral analyses and coherence tests

To examine whether climatic influences have been removed or limited by our normalization methods, the normalized remanences and low-field magnetic susceptibility records have been subjected to spectral analyses, including coherence testing between normalized remanences and the low-field magnetic susceptibility (Guyodo et al., 2000; Grinsted et al., 2004). The magnetic susceptibility data have a periodicity of about 16 ka throughout the studied section, but it is not significant at the

95% confidence level, and a statistically significant 6 ka periodicity between 40 and 55 ka (Figure 5.7a). The normalized remanences have similar spectra in which higher frequency periods of about 1.5 ka and 3 ka are present at 25-35 ka, 80 ka and 105-115 ka, respectively (Figure 5.7b, c, d). NRM/ARM has significant coherence with magnetic susceptibility at a period of 8.2 ka at 40-60 ka, and at about 16 ka throughout the studied section (Figure 5.7e). NRM/ARM2 and NRM/IRM have a similar coherence with magnetic susceptibility, with statistically significant periods of about 8 ka at 35-60 ka, and no coherence in the 16 ka period at 40-100 ka (Figure 5.7f, g). Pairs of normalized remanences are all highly coherent (Figure 5.7h is an example between NRM/IRM and NRM/ARM), which indicates that all of the normalizations are dominantly recording the same signal.
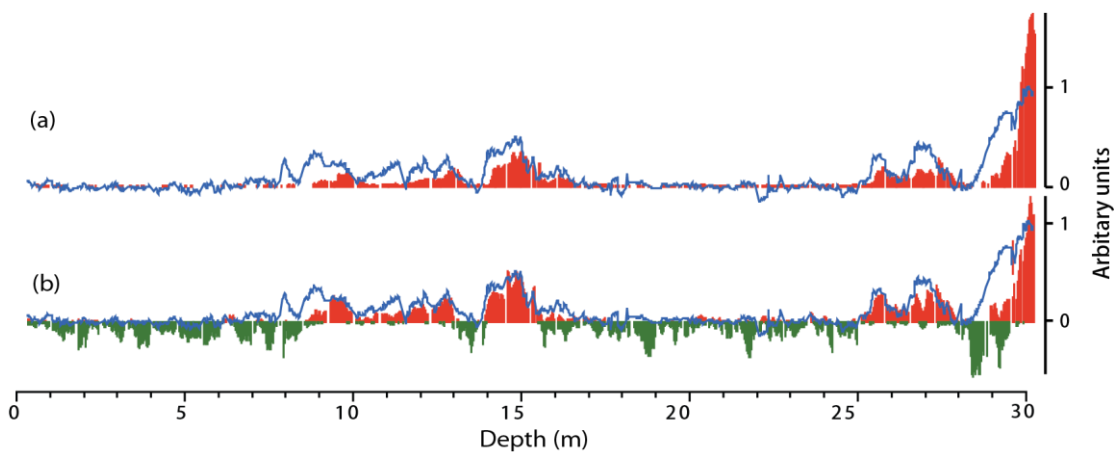


**Figure 5.6**     Correlation of VRM (red/green) for the studied Yuanbao section with the low-field magnetic susceptibility (blue line). The VRM estimations in (a) and (b) are from ARM and IRM, respectively. Red represents the area above fitted NRM/IRM or NRM/ARM lines (in Figure 5.5), while green represents the area under these lines. VRM is clearly larger in intervals affected by pedogenesis (in which magnetic susceptibility is higher). Sagging of the NRM/ARM line is indicated by the green lines in (b), which appears to result from the lower coercivity distribution in IRM compared to NRM in the coarse-grained loess intervals. Note: the *y* axis has arbitrary units.

**Figure 5.7**     Local wavelet power spectrum (LWPS) of: (a) low-field magnetic susceptibility (Mag-sus), (b) NRM/ARM, (c) NRM/ARM2, and (d) NRM/IRM. Squared wavelet coherence (WTC) between: (e) Mag-sus and NRM/ARM, (f) Mag-sus and NRM/ARM2, (g) Mag-sus and NRM/IRM, and (h) NRM/IRM and NRM/ARM. Values of normalized wavelet power and squared wavelet coherence are indicated using different colours, in which progression from blue to red indicates increasing values. A 5% significance level against red noise is shown as thick contours in all figures. The cones of influence where edge effects make the analysis unreliable are marked by the semi-transparent areas. The arrows in WTC represent the relative phase relationship, with in-phase pointing right and anti-phase pointing left. The Cross Wavelet and Wavelet Coherence Matlab package was used (Grinsted et al., 2004).
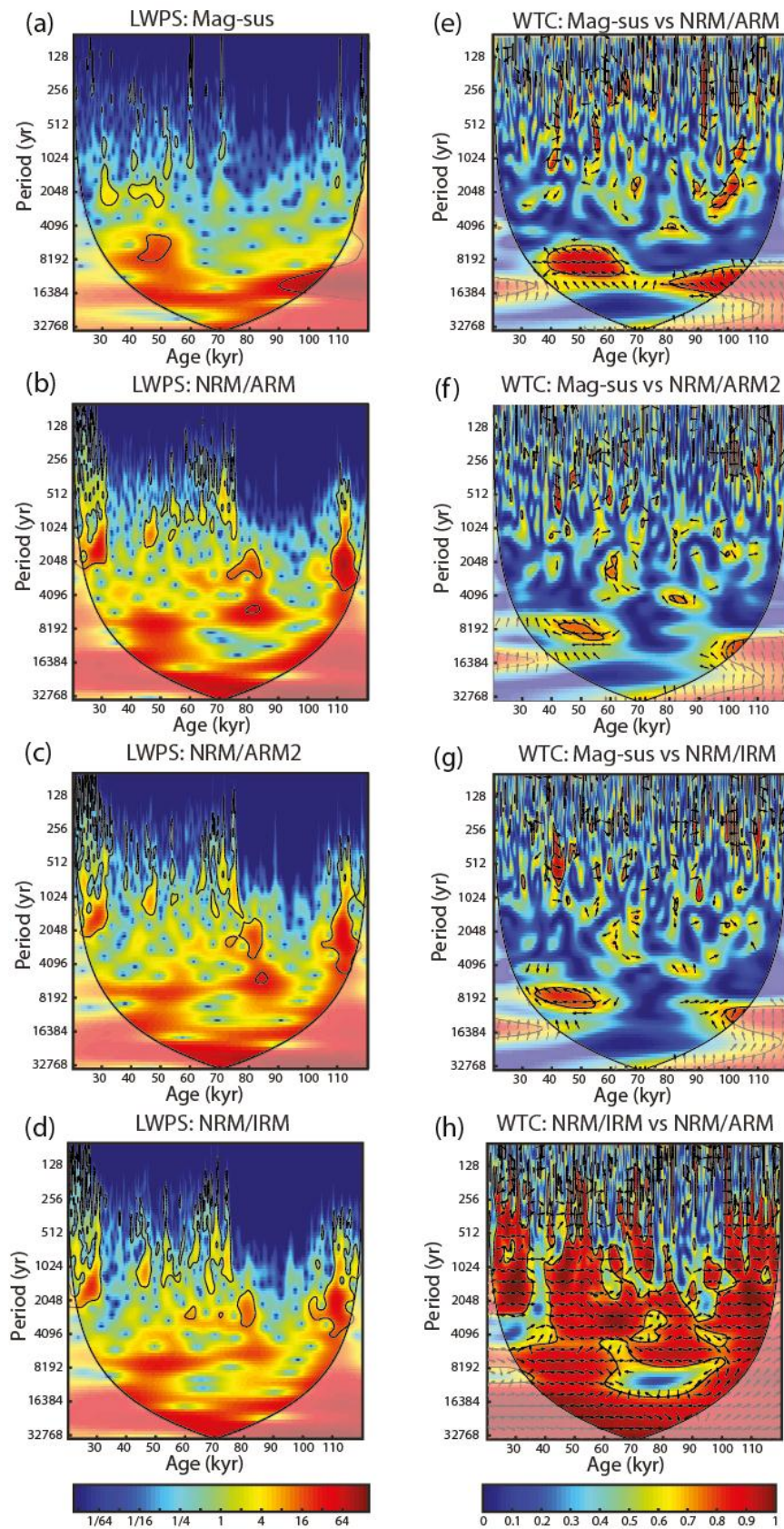
# 5.5 Discussion

## 5.5.1 What minerals are responsible for the magnetization of Chinese loess?

Magnetic mineral component analyses (Spassov et al., 2003; Chapter 3) for Chinese loess samples indicate that at least 3 magnetic mineral components exist in the Chinese loess. These are pedogenic magnetite/maghemite (component P1), detrital magnetite/maghemite (P2) and hematite/goethite (P3). The coercivity of P1 spans from 0 to 100 mT, with a peak at around 25 mT, while that of P2 spans from 10 to 200 mT with a peak at around 100 mT (Figure 3.3). Chinese loess samples can be almost magnetically saturated in a 1 T inducing field (Chapter 3). Therefore, the SIRM reflects information associated with all magnetic minerals within a sample. In contrast, the peak AF used in ARM acquisition is 100 mT; therefore the ARM will only reflect information from magnetic minerals with coercivity less than 100 mT. Components P1 and P2 have overlapping coercivity distributions, with cross-over of their distributions at around 40 mT (Figure 3.3). The good linear relationship between NRM and IRM for AF demagnetization steps above 40 mT (Figure 5.5a1, b1, c1), and between NRM and ARM for AF demagnetization steps between 15 and 50 mT (Figure 5.5a2, b2, c2) indicate that the remanences used here are mainly carried by components P2 and P1, respectively. The lack of linear correlation between NRM and ARM for AF demagnetization steps above 40 mT (Figure 5.5a2, b2, c2) indicates that the ARM is mainly controlled by P1, and is slightly affected by P2. For AF demagnetization steps between 15 and 50 mT, both NRM and IRM include information from component P2, therefore a non-linear correlation between NRM and IRM can be expected. The non-zero intercept in NRM versus ARM plots after AF demagnetization at 100 mT (Figure 5.5a2, b2, c2) also indicates contributions from high coercivity magnetic minerals (such as hematite and goethite).

Component P2 has been considered to represent the detrital magnetic component; therefore, a DRM and/or PDRM can be expected to be recorded during deposition or soon after by this component. Detrital magnetite grains in the Chinese loess are reported to have undergone low-temperature oxidation (Liu et al., 2003) in which the outer surface of magnetite was oxidized into maghemite (e.g., Cui et al., 1994; van Velzen et al., 1999). This oxidation occurs before deposition, but the effects

of surficial maghemitization on DRM or PDRM recording are not known. Component P1 is responsible for the magnetic enhancement of paleosols, which resulted from neoformation during pedogenesis. This component is therefore most likely to carry a CRM. Consideration of the magnetic minerals present in the Chinese loess and their mode of formation/occurrence and whether they have undergone significant post-depositional modification is fundamental to considering the possibility of recording relative paleointensity within Chinese loess, as discussed below.

## 5.5.2 Comparison of normalized remanences with those from other loess records

There is only a limited literature on attempts to obtain relative paleointensity records from Chinese loess, but it is still useful to collate and compare existing records to evaluate the potential for relative paleointensity determination in Chinese loess. Zheng et al. (1995) used the NRM/ARM ratio after thermal demagnetization at 300°C to represent the relative paleointensity for paleosol S1 in the Huanxian section, and compared the results with stacked paleointensity records from the Somali Basin and Mediterranean Seas (Meynadier et al., 1992; Tric et al., 1992) based on an age model from matching magnetic susceptibility and marine $\delta^{18}O$ curves. They concluded that there is some degree of correlation between the two types of normalized remanence records. Their record spans from 130 to 74 ka (Figure 5.8c), and has a minimum at around 110-120 ka that was thought to relate to the Blake excursion. Liu et al. (2005a) also focused on the S1 interval from the Yuanbao section, and used the slope of the best-fit line between the NRM and IRM at AF demagnetization steps of 60 mT and above. The chronology for their section was based on peak matching between magnetic susceptibility data and the SPECMAP $\delta^{18}O$ record. There are three peaks in their normalized remanence record (Figure 5.8b), which they correlated with $^{36}Cl$ flux peaks in a Greenland ice core. Zhu et al. (1999) and Pan et al. (2001) investigated loess interval L1 (spanning from 10 to 74 ka) at Weinan (Figure 5.8d) and Lingtai (Figure 5.8a), respectively, to avoid significant influences from pedogenesis in paleosol S1 (Figure 5.8a, d). All of the normalized remanence records except for that of Pan et al. (2001) were published with respect to depth, and have been re-scaled in Figure 5.8 based on the age control points provided in the original papers. Even if one were to stretch and squeeze the records to "tune"

features to improve correlations, there is no obvious correspondence among these records, including the normalized remanence record obtained in this study. This could partially be a result of the poor chronological control on the respective records and because different normalization methods were used. However, it also indicates that there is little consistency among the normalized remanence records.
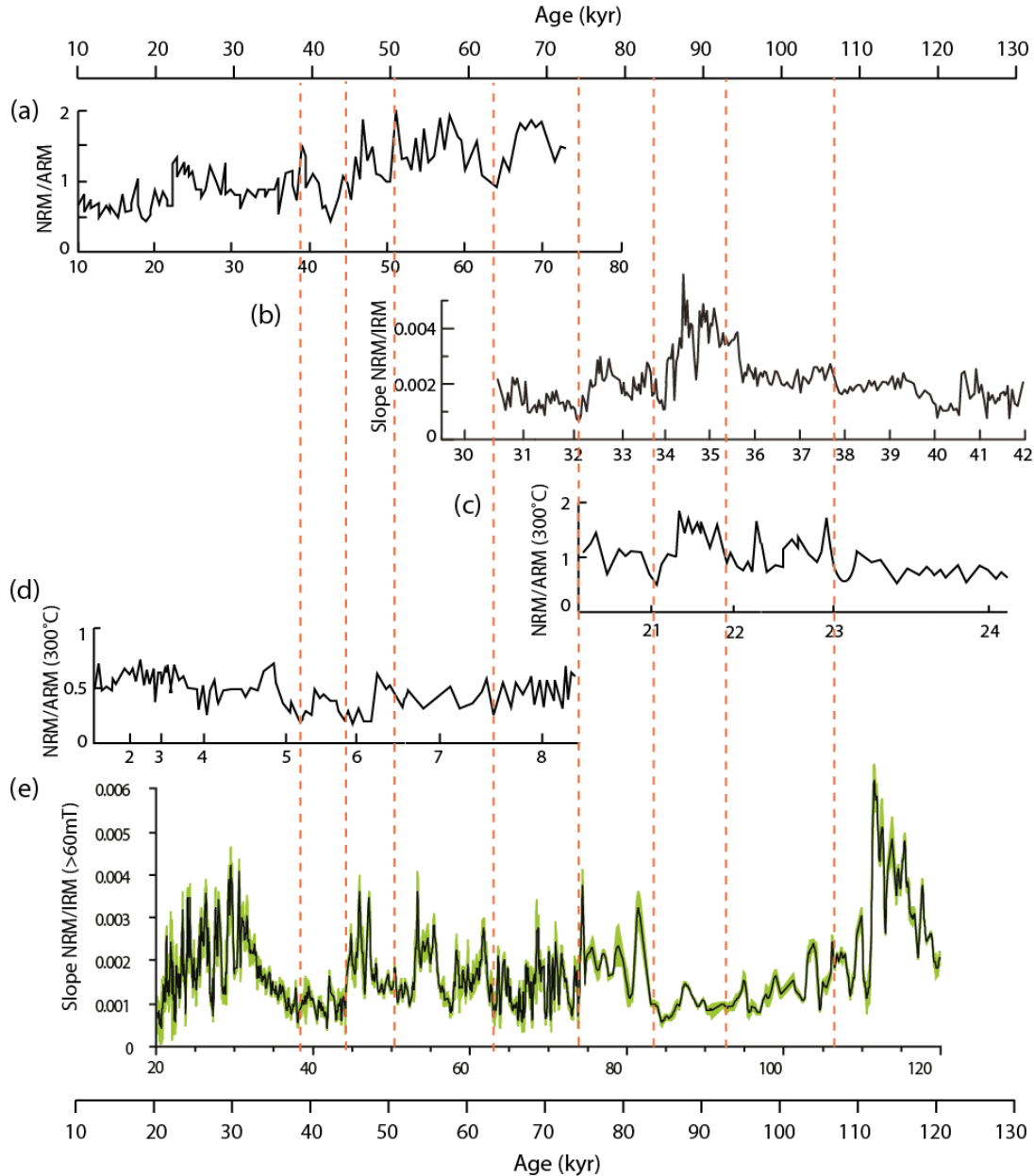


**Figure 5.8**        Comparison of different published normalized remanence records from the Chinese loess. (a) Lingtai section L1 (Pan et al., 2001a), (b) Yuanbao section S1 (Liu et al., 2005a), (c) Huanxian section S1 (Zheng et al., 1995), (d) Weinan section L1 (Zhu et al., 1999), and (e) Yuanbao section (L1+S1) from this study. There is no obvious correlation among the records. Vertical dashed red lines are reference lines for comparsion. For records not reported with respect to age in the original studies (i.e., b, c, d), the horizontal axes refer to depths, which have been scaled to age for this figure.
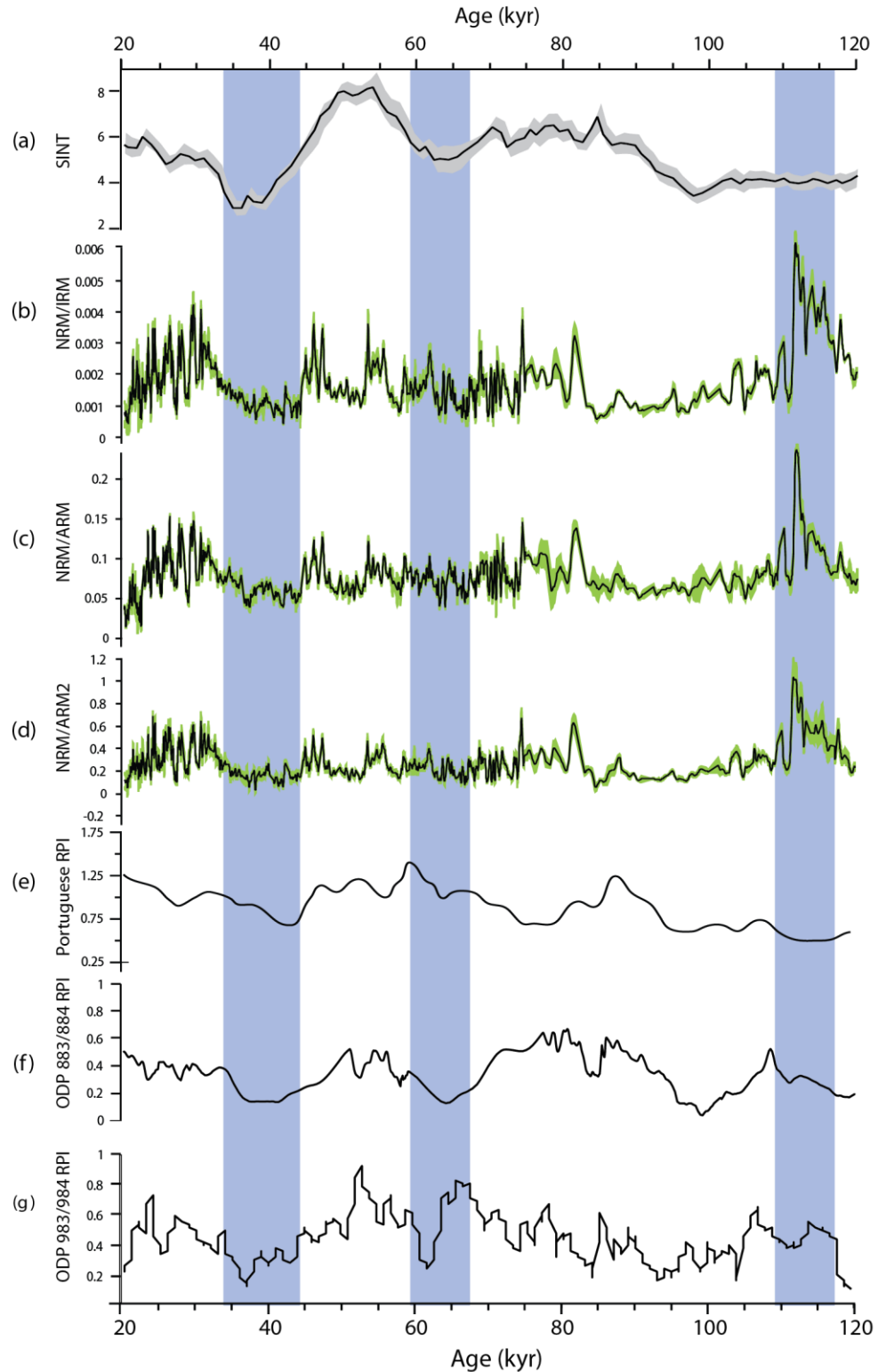
**Figure 5.9**    Comparisons of normalized remanence records from the Yuanbao section with different relative paleointensity records. (a) Part of the SINT-800 data set (Guyodo and Valet, 1999); (b-d) NRM/IRM, NRM/ARM and NRM/ARM2 for the Yuanbao section; (e) Portuguese margin marine stack (Thouveny et al., 2004), (f) North Pacific ODP 883 and 884 stack (Roberts et al., 1997) using the age model of Roberts (2008), and (g) the high-resolution paleointensity record from ODP sites 983/984 (Channell, 1999). All data are plotted on the same age scale. Blue vertical bars indicate major paleointensity minima in the SINT-800 record of Guyodo and Valet (1999).

### 5.5.3 Comparison of normalized remanences with marine relative paleointensity records

In evaluating the suitability of the Chinese loess for recording relative paleointensity variations, it is useful to compare our record from Yuanbao with published marine relative paleointensity records. In Figure 5.9, the three normalized remanence records from the studied Yuanbao section are plotted along with the SINT-800 global stack (Guyodo and Valet, 1999), a Portuguese margin stack (Thouveny et al., 2004), a North Pacific stack from ODP sites 883/884 (Roberts et al., 1997) using the revised age model from Roberts (2008) and the high-resolution paleointensity record from ODP sites 983/984 (Channell, 1999). The Yuanbao records contain high frequency variations that probably reflect the higher sedimentation rates of the loess compared to marine sediments. All of the records have low values at around 40 ka that relate to the Laschamp excursion and at 100 ka. The marine records have higher values during 40-90 ka with low values at around 60 ka. The Yuanbao loess records have much more frequent variations during 20-30 ka and 45-85 ka. A peak at around 113 ka is not present in the marine records. Overall, agreement between normalized remanence records from the Chinese loess and marine relative paleointensity records is poor. It is concluded that the Chinese loess has not reliably recorded relative paleointensity signals. Reasons for this are explored below.

### 5.5.4 Interpretation of normalized remanence results

Spectral analysis and coherence tests indicate that the three normalized remanence records from Yuanbao are consistent with each other despite the different normalizers used. The significant coherence between NRM/ARM and magnetic susceptibility at some periods over some time intervals indicates that they are both affected by the same pedogenic processes to some extent. This is probably because NRM/ARM was obtained using data from lower AF demagnetization steps at which pedogenic influences were not completely removed. Although the NRM/ARM2 and NRM/IRM records are less coherent with magnetic susceptibility, the strong coherence between NRM/IRM and NRM/ARM indicates that all of the normalized remanence records are still affected by environmental factors. NRM/IRM and NRM/ARM2 were calculated using data from higher AF demagnetization steps, which were considered by Liu et al. (2005a) to be a detrital signal that is free of

pedogenic influence. As discussed above, the NRM of Chinese loess may involve a DRM, PDRM, CRM or VRM or unknown combinations of these remanence acquisition mechanisms (Pan et al., 2001; Spassov et al., 2003; Zhao and Roberts, 2010). The dominant mechanism remains unclear and is likely to vary through time and space (Zhao and Roberts, 2010). On the basis of our data, CRM seems to be present and will at least seriously modify the detrital record if an original DRM or PDRM is preserved. Poor recording of relative paleointensity signals in Chinese loess was also observed in normalized remanence records that used thermal demagnetization data (Zhu et al., 1999; Pan et al., 2001). In contrast, inferred acceptable correlations between normalized remanence data from paleosol S1 and marine records as presented by Zheng et al. (1995) and Liu et al. (2005a) can only be explained if this interval is dominated by PDRM acquisition associated with higher rainfall during interglacial periods. Such a conclusion would be consistent with laboratory redeposition experiments (Zhao and Roberts, 2010; Wang and Løvlie, 2010). However, it is difficult to imagine how a paleosol interval could only record a PDRM with no CRM acquisition despite significant pedogenesis. As shown in Figure 5.8, correlation of these records is not convincing.

### 5.5.5 What do low paleointensity values mean?

During geomagnetic polarity transitions and excursions, low field intensities are expected (e.g., Valet and Meynadier, 1993; Channell and Kleiven, 2002; Roberts, 2008). Efforts to find geomagnetic excursions recorded in Chinese loess have had variable success (e.g., Pan et al., 1999; Fang et al., 1999). In the absence of anomalous paleomagnetic directions, low intensities have been considered to provide evidence of excursion(s). Does this mean that every low intensity event represents a geomagnetic excursion in the Chinese loess?

There are no obvious paleomagnetic directional anomalies in the Yuanbao section during 35-45 ka and 85-100 ka in which low normalized remanences are observed (Figure 5.4). These low intensity intervals coincide with warmer periods associated with MIS 3 and MIS 5, respectively. Based on laboratory redeposition experiments, Zhao and Roberts (2010) argued that the presence of water will increase the realignment efficiency of magnetic particles during the PDRM acquisition process. In terms of their findings, detrital particles in paleosols should be more efficiently

aligned compared to a PDRM in loess samples. However, this does not take into account the effects of pedogenesis.

The frequent major polarity swings that are often recorded within intervals of Chinese loess in which the geomagnetic field reversed polarity have been demonstrated to be recording artifacts (Jin and Liu, 2010). This indicates that both the direction and intensity have not been well recorded. During intervals with weak fields, all remanence acquisition mechanisms will have reduced efficiency; therefore intensity minima are likely to be observed. However, this is not always the case, as indicated by the normalized remanence peak at 113 ka in S1 at Yuanbao, which contrasts with a paleointensity minimum in marine sedimentary records (Figure 5.9). It will remain difficult to adequately interpret such low intensity intervals in Chinese loess until the acquisition of DRM, PDRM and CRM in Chinese loess are better understood. The evidence from Yuanbao suggests that relative paleointensity is not accurately recorded by either loess or paleosol units.

### 5.5.6 Complexity of relative paleointensity recording by Chinese loess

The amount of precipitation decreases from the northwestern to southeastern Chinese Loess Plateau (Figure 4.9). Laboratory redeposition experiments indicate that water content is an important factor that affects the efficiency of magnetization of Chinese loess (Mcintosh, 1993, Zhao and Roberts, 2010, Wang and Løvlie, 2010). Rainfall after settling of dust should improve the quality of the recorded magnetization. However, the mean grain size of Chinese loess also decreases from the northwest to southeast, which makes it difficult to rule out if these factors significantly affected relative paleointensity recording by the Chinese loess. Chinese loess has also suffered possible regional post-depositional reworking and other loessficiation processes (Liu, 1985). More work needs to be done to clarify the significance of these factors to relative paleointensity recording.

## 5.6  Conclusions

An approximate age model was established for the Yuanbao section in this study based on OSL age control and matching of sediment grain-size with marine and ice

core $\delta^{18}O$ curves. Lack of accuracy of OSL dating and the arbitrary nature of proxy correlation mean that the age model is approximate only. Nevertheless, this age model is considered suitable for evaluating whether Chinese loess can record variations in relative paleointensity. Although reliable ChRM directions have been successfully isolated from the Yuanbao section, the lack of similarity among normalized remanence records from the Chinese loess and relative paleointensity records from marine sediment indicates that it is difficult to extract magnetic intensity information that is free of the effects of pedogenesis, even in sections that were pre-selected because they would be expected not to be significantly affected by pedogenesis. More effort is needed to adequately understand the mechanism(s) of remanence acquisition in Chinese loess. While laboratory redeposition experiments are useful, they do not completely address questions concerning remanence acquisition mechanisms in Chinese loess and much more work is needed to better understand how Chinese loess becomes magnetized. We conclude, however, on the basis of the above results that complex mixtures of remanence acquisition mechanisms in the Chinese loess means that we currently cannot recover paleointensity information from these sediments.

# Chapter 6

# Summary and Conclusions

## 6.1  Conclusions

### 6.1.1 Magnetic minerals present in the Chinese loess

The presence of several magnetic minerals in the Chinese loess was confirmed by IRM acquisition analyses. SD magnetite/maghemite was produced or subsequently oxidized during pedogenesis, which contributes most of the observed magnetic mineral enhancement. Detrital PSD-MD magnetite/maghemite seems not to have been affected by pedogenesis, with variations in this component probably reflecting original variations in detrital inputs. Hematite in Chinese loess has both detrital and pedogenic origins. The concentration of pedogenic hematite is related to the intensity of pedogenesis. Partial thermal demagnetization experiments demonstrate that goethite does not contribute to remanence at room temperature. The concentrations of different magnetic mineral components were calculated based on unmixing IRM acquisition curves, except for the concentration of SP magnetite/maghemite. The total hematite concentration was obtained from DRS analyses, which include SP to SD hematite with both detrital and pedogenic origins. In paleosols that underwent intense pedogenesis, pedogenic hematite can grow through the magnetic SP/SD blocking volume (Chapter 4).

### 6.1.2 Eolian dust deposition simulator

In order to carry out laboratory redeposition experiments for Chinese loess, an eolian dust deposition simulator was built. This instrument enables control of the redeposition process and of the applied magnetic field. The redeposition component of the device enables simulation of dust emission and deposition, which is designed as a closed-wind-tunnel system in which the wind is driven by two parallel electric fans. The dust was collected using standard plastic paleomagnetic cubic boxes. The

magnetic field was produced using a 3-axis Helmholtz coil system. The field direction and intensity can be controlled by modifying the electrical current by rotating a knob on the control box. Each coil has independent power, which allows the operator to easily set the desired field. This system enables simulation of the dust deposition process in a given magnetic field to examine the recording fidelity of Chinese loess samples. Different experimental procedures were used to simulate a pure DRM and a PDRM with this system (Chapters 3).

### 6.1.3 Significance of Dust Deposition Simulator

The ability to reconstruct records of relative paleointensity variations is important to better understand the behaviour of the ancient geomagnetic field. Studies of marine sediments have provided useful information about such paleomagnetic field variations. However, acquisitions of data from continental sediments, such as Chinese loess, are useful for constructing geomagnetic field models. To enable determination of such records, the most important thing is to clearly understand the magnetic remanence mechanism of Chinese loess which provides the basis for recording relative paleointensity signals. The dust deposition simulator developed in this study enables dust redeposition experiments, which can simulate the processes by which Chinese loess becomes magnetized. In this study, I have successfully simulated the dust deposition process, and the associated magnetization processes in Chinese loess.

### 6.1.4 DRM and PDRM in Chinese loess

Understanding the mechanism(s) of remanence acquisition is the most important unresolved question for paleomagnetic research on the Chinese loess. DRM and PDRM were expected because of commonsense consideration associated with the settling of magnetic particles out of dust storms as part of the initial process of Chinese loess formation. CRM was also expected on the basis of widely documented neoformation of fine-grained magnetic particles in paleosols. As presented in Chapter 4, redeposition experiments were carried out on disaggregated Chinese loess to examine whether a DRM or PDRM could be acquired during or after deposition. Addition of water to the samples clearly affects the realignment efficiency of the PDRM, and there is a critical water content below which realignment does not occur. Results of pure DRM experiments indicate that the declination can be recorded

accurately, but that the recorded inclination has large errors. Addition of minor water helps to fix the sediment, which improves the directional recording quality to some degree, but it cannot effectively reduce inclination error. Water saturation in the redeposited samples significantly improves the inclination records by allowing efficient realignment of magnetic particles. Published paleomagnetic data from different locations indicate that there is obvious inclination shallowing of ChRM in natural Chinese loess samples, although it is not as large as documented in our DRM experiments. It is therefore likely that both DRM and PDRM mechanisms are involved in nature. Although the magnetic mineralogy is complex and the role of CRM/VRM is variable in the Chinese loess, this study has confirmed the possibility of DRM and PDRM recording by Chinese loess, and indicates that a PDRM can provide good directional recording when significant water is present after deposition.

## 6.1.5 Geomagnetic intensity records from Chinese loess

Despite the fact that the Chinese loess has successfully recorded geomagnetic polarity reversals and excursions, the possibility of recording relative paleointensity variations has been less intensely studied. Three normalized remanence records have been determined using the pseudo-Thellier method for the last loess/paleosol sequence at the Yuanbao section. The similarity among the three normalized remanence records is demonstrated by spectral analyses and coherence tests. This means that all three normalized remanence records are mainly controlled by the same factors. Comparison with published data from different Chinese loess sections does not suggest that it is possible to correlate the records. This is consistent with complex magnetic remanence acquisition that leads to difficulty in separating primary paleomagnetic information from the bulk mixed detrital and pedogenic signal. Comparison with marine relative geomagnetic paleointensity records also indicates a lack of consistency. It is therefore difficult to conclude that Chinese loess can provide reliable relative paleointensity records, which contrasts with the interpretations of Pan et al. (2001) and Liu et al. (2005a).

Laboratory redeposition experiments (Zhao and Roberts, 2010; Wang and Løvlie, 2010) demonstrate that the Chinese loess can acquire a DRM during deposition, and a PDRM when the sediment is water-saturated after deposition. If the ChRM is a DRM or PDRM, and AF demagnetization is effective in removing

secondary magnetic overprints, it should be possible to detect relative paleointensity variations from the Chinese loess. However, the similarity between NRM/IRM from higher AF demagnetization levels and NRM/ARM from medium demagnetization levels indicates two alternative interpretations. One is that pedogenesis has affected the magnetic mineral assemblage across the whole coercivity range; normalized remanence records would therefore be representative of the mixed magnetic signal after pedogenesis. The other alternative is that the overprint is a VRM that can be removed by AF demagnetization at 15 mT; normalized remanence would therefore represent the original paleointensity information. On the basis of production of SD magnetite/maghemite during pedogenesis, and the lack of similarity between normalized remanence records from across the Chinese Loess Plateau and with marine relative paleointensity records, the first interpretation is more likely. It is therefore concluded that normalized remanence records from the Chinese loess even from sections that are expected to have experienced minimal pedogenesis, will not provide meaningful estimations of geomagnetic relative paleointensity (Chapter 5).

## 6.2 Future work

### 6.2.1 CRM laboratory simulation

The complexity of normalized remanence records from the Chinese loess, as demonstrated in Chapter 5, confirms that the magnetization of Chinese loess is a complex time-varying combination that probably includes DRM, PDRM, CRM and VRM. Both the production of SP-SD magnetite (and hematite) and oxidation from magnetite to maghemite have the potential to produce a CRM. To better understand Chinese loess magnetization mechanisms, laboratory simulation of CRM is necessary in addition to redeposition experiments. This kind of experiment could provide information not only about the CRM acquisition process, but also about overprinting of the primary component, and about magnetic mineral phase transformations, which will provide a better understanding of the magnetic enhancement mechanism and remanence acquisition mechanisms. CRM simulation can also provide help to understand remagnetization in red soils (e.g., Liu et al., 2010) and greigite-bearing sediments (e.g., Roberts et al., 2005).

### 6.2.2 Magnetic remanence acquisition in weak fields

Low relative geomagnetic paleointensity values have often been used as an indicator of geomagnetic excursions. But not all low intensity intervals represent excursions, such as the low relative paleointensity interval at around 100 ka. It is easy to imagine how weak fields would reduce the efficiency of remanence acquisition. In Chapter 4, we tested the magnetic recording fidelity for DRM and PDRM acquisition using different magnetic field directions, but the field intensity was fixed at an average geomagnetic field value of 50 µT. The DRM and PDRM acquisition efficiency in different field intensities needs to be tested, which will be useful to understand paleomagnetic recording in weak fields, such as during excursions and polarity transitions. CRM and VRM acquisition in weak fields also needs to be simulated.

### 6.2.3 Remanence acquisition modelling

To better understand the physical theory of magnetic remanence acquisition in Chinese loess, computer modelling will help to examine which factor(s) contribute to and dominate the process. For example, what factors limit development of inclination error in DRM, how does water content improve particle alignment, which factors affect PDRM efficiency, etc.? Computer modelling can also provide useful information on remagnetization processes, as well as on oxidation of magnetite to maghemite.

## 6.3  Summary

Paleomagnetic analysis of Chinese loess lacks rigorous understanding of fundamentally important issues such as the type of remanent magnetization carried by loess and its acquisition mechanism(s). This PhD project aimed to contribute to filling this gap. After identifying the magnetic components present in the Chinese loess, and after undertaking laboratory redeposition experiments and detailed normalized remanence analyses, it is concluded that the Chinese loess is magnetized by a complex time-varying combination of DRM, PDRM, CRM and VRM mechanisms. This complexity means that significant work is necessary to understand individual records

from the Chinese loess. The story of the magnetization of Chinese loess is not closed. Much more work will continue to be needed.

# Appendix I

# Grain size Distribution Decomposition Program

## I.1 Introduction

Bimodal or multi-modal grain size distributions are widespread in Chinese loess, including the Red Clay that stratigraphically underlies the loess sequences (Sun et al., 2004; Sun et al., 2006b). It has been demonstrated that different mathematical functions can be used to successfully separate grain size components from the total grain size distributions (Sun et al., 2004; Parker and Bloemendal, 2005; Prins et al., 2007; Chen et al., 2009), including Weibull and Gaussian functions and an end-member fitting method. In this study, we follow Sun et al. (2004) by using Weibull functions to model the grain size distribution of Chinese loess. A Java program was written for this purpose, which has a user-friendly interface and basic statistical functions. For simplicity, we transformed the grain size data into a logarithmic scale to satisfy the requirements for a Weibull distribution.

## I.2  Theory

In probability theory and statistics, the Weibull distribution is a continuous probability distribution. The probability density function of a Weibull random variable $x$ is:

$$f(x;a,b) = \begin{cases} \dfrac{b}{a}\left(\dfrac{x}{a}\right)^{b-1} \exp\left(-(x/a)^b\right) & x \geq 0, \\ 0 & x < 0, \end{cases}$$

where $a > 0$ is the shape parameter and $b > 0$ is the scale parameter of the distribution. This is the traditional two-parameter Weibull distribution (cf., Kittl (1984)). As the studied grain size distributions always have more than two components, a modified

four-parameter Weibull function was used in this study (Ling et al., 2009):

$$f(x; a, b, c, d) = c\left[\frac{b}{a}\left(\frac{(x+d)}{a}\right)^{b-1} \exp\left(-((x+d)/a)^b\right)\right] \quad x \geq -d,$$

where the additional $c > 0$ is a weighting parameter and $d$ is the offside parameter that is used to enable data smaller than 0 to be transformed into a logarithmic scale for modelling with a Weibull function. Considering that most samples contain three grain size components, we simply write the function as:

$$f(x) = f(x; a1, b1, c1, d1) + f(x; a2, b2, c2, d2) + f(x; a3, b3, c3, d3),$$

where the numbers after the parameters $a$, $b$, $c$ and $d$ represent the component number. In theory, the sum of the three weighted parameters should equal 1.



**Figure A.I.1**      An example of input data format for the grain size decomposition program.

# I.3 Program

The sequence of steps required to operate the software developed for decomposing grain size distributions is described below.

## I.3.1 Input data format

Input data must be in a plain text file, which includes logarithmically spaced grain sizes (in μm) in the first column. The volume percentages of relevant grain size

data for each measured sample are tabulated in the remaining columns. An example of the data format is shown in Figure A.I.1.

## I.3.2  Load and display the data

To load a data file, click progressively on File→Open→select file→open (Figure A.I.2a). The *text area* on the left displays all the sample names (Figure A.I.2b). Click any sample name, and the respective data will plot on the right-hand panel (Figure A.I.2).
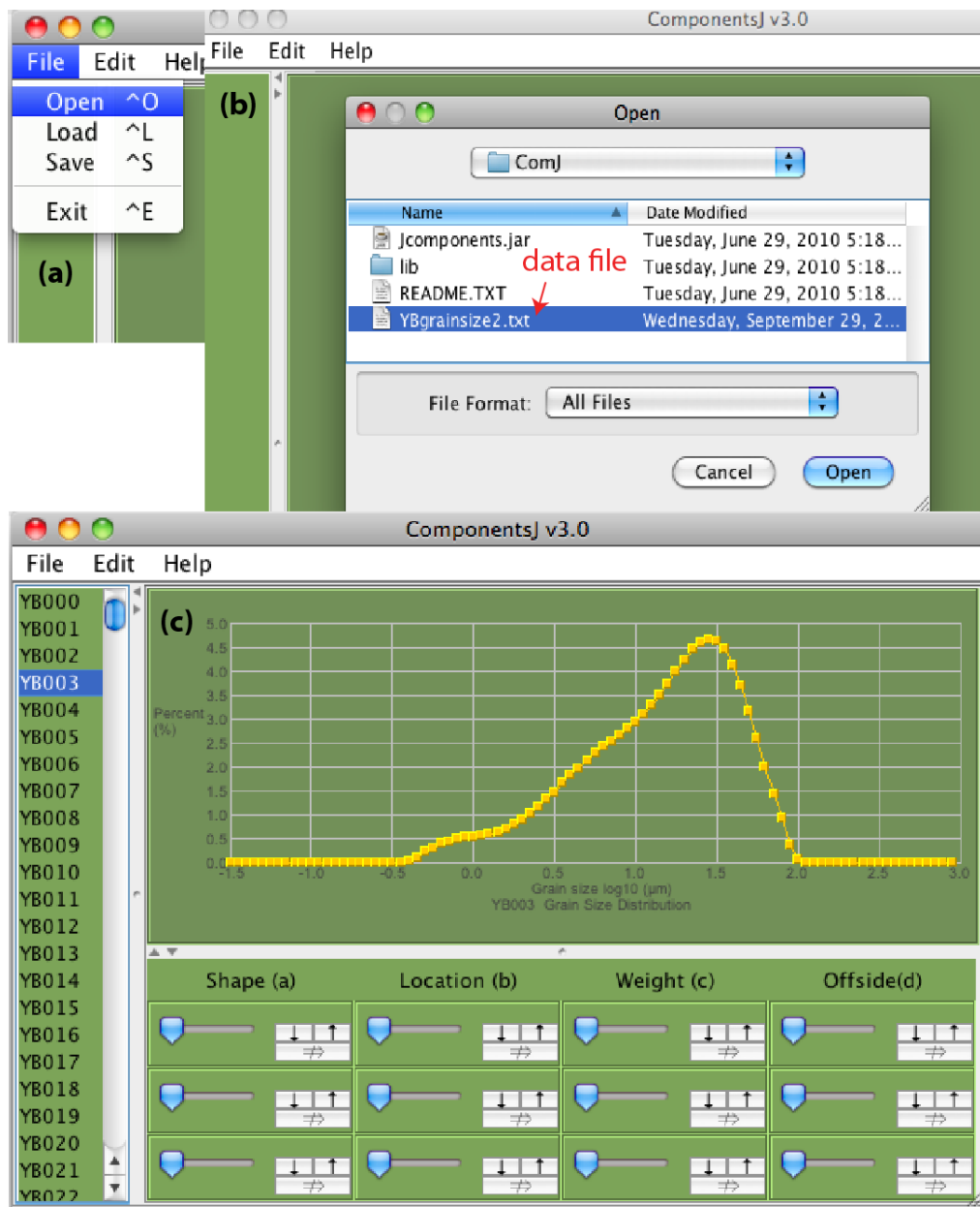


**Figure A.I.2**    Load and display a data file. (a) Open, (b) select the data file, and (c) display the data for the selected sample YB003 (yellow squares represent the data points).

## I.3.3 Activate component

Using the program interface, it is possible to manually adjust parameters for three components. Each component can be activated by dragging any of the parameter-adjusting-slides (Figure A.I.3).
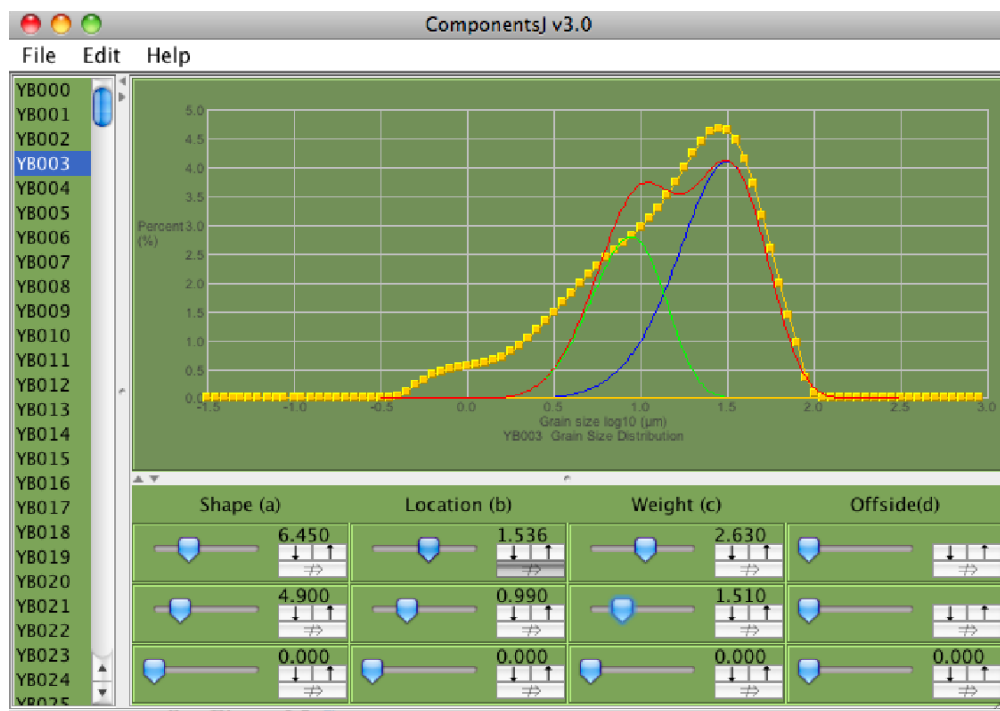


**Figure A.I.3**     Dragging the blue slides activates the respective components. In this example, the first two components have been activated. The blue line represents component 1, while the green line represents component 2, and the red line represents the combined result. The modelling parameters are displayed on the respective panels.

## I.3.4 Modifying parameters for component fitting

There are two ways to modify parameters for each component. Either drag the slides or click the arrow buttons. The trigger button can change the arrow button step length by clicking on or off (Figure A.I.4).
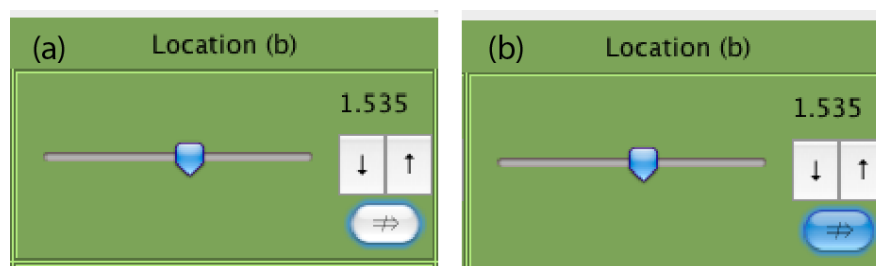


**Figure A.I.4**     The parameter selection panel. Either dragging the slide button or clicking the arrow buttons can modify the selected parameter value. The trigger button was off in (a), while it is activated in (b).

## I.3.5  Statistical results

The four parameters (*a*, *b*, *c*, *d*) for each component are automatically calculated. Additionally, the skewness, kurtosis and mean value of each component are also calculated. All results can be saved automatically in a text file.

## I.3.6  Save plot

By clicking the right mouse button, and then clicking *Save as* in the pop-up menu, the plot will be save as a PDF version, which allows modification of the plot for future use (Figure A.I.5).
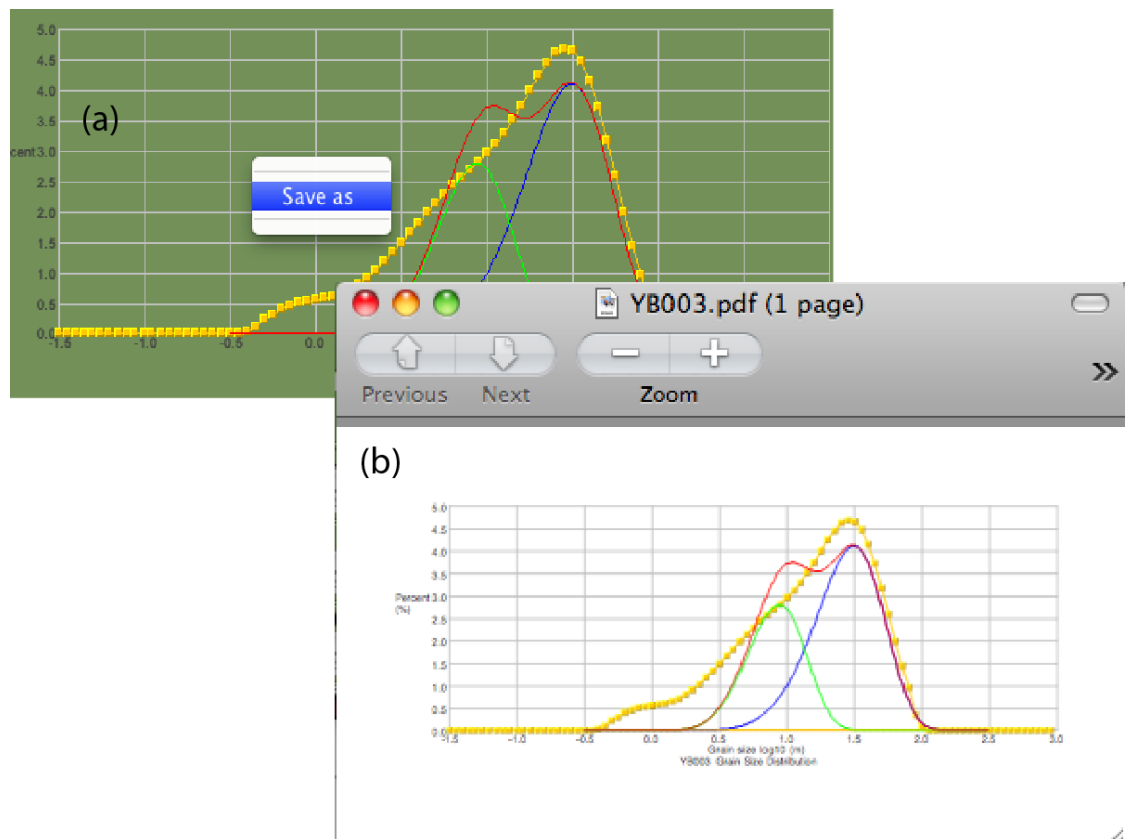


**Figure A.I.5**    Save the plot as a PDF version. (a) Click the right mouse button and save the plot as a PDF version. (b) The saved PDF file.

# Appendix II

# Relative Geomagnetic Paleointensity Analysis Software

## II.1 Introduction

Relative geomagnetic paleointensity estimation from sediments involves normalization of the NRM with a parameter that is expected to represent the concentration of magnetite in the sample. Conventional methods use a single NRM value after demagnetization at a specified level normalized by the respective normalizers, such as the low-field magnetic susceptibility, ARM and IRM. Tauxe et al. (1995) proposed a pseudo-Thellier method, which uses the slope of a best-fit line through data from multiple demagnetization steps to replace the normalization based on a single demagnetization step. Here I describe a Java program (RPI processor) for batch sample analysis, which enables automatic cross plotting between pairs of remanent magnetization data, and provides line fitting and VRM area estimations (Chapter 6). The jackknife method (Tauxe and Gallet, 1991) was used along with a least squares method, which provides two sets of results for comparison.

## II.2 How to use the program

### II.2.1 Input data format

The relevant NRM, ARM and IRM data at the same demagnetization level are required and need to be converted to the format shown in Figure A.II.1. An additional program was written to convert raw data from the magnetometer into this format. The file should have two header lines, with the sample name in the first line and title for the columns in the second line. The numbers in the first column provide an index for the data. Magnetic remanence data are tabulated in the remaining columns.

```
ds/RIP/plot/YB01-NRMD-0.06

YB01-NRMD-0.06
index          NRM          IRM          ARM
1             1.50E-04     2.49E-02     9.76E-04
2             1.06E-04     2.24E-02     8.51E-04
3             6.57E-05     1.92E-02     6.25E-04
4             4.65E-05     1.65E-02     4.32E-04
5             3.61E-05     1.38E-02     2.90E-04
6             2.92E-05     1.17E-02     1.90E-04
7             2.43E-05     9.35E-03     1.25E-04
8             1.97E-05     7.54E-03     7.15E-05
9             1.70E-05     6.28E-03     4.56E-05
10            1.54E-05     5.24E-03     3.46E-05
11            1.36E-05     4.48E-03     2.65E-05
12            1.24E-05     3.82E-03     2.51E-05
13            1.17E-05     3.30E-03     2.40E-05
```

**Figure A.II.1**   An example of a data file for sample YB01-NRMD-0.06 to illustrate the required data format. Two header lines and an index column are present as well as the magnetic remanence data.

## II.2.2  Open and load data

Data files are opened by clicking File→Open. The sample name will then be displayed on the left-hand *text area*. The program produces a list file in the root path, which allows the data to be opened by clicking File→Load the next time the data need to be inspected (Figure A.II.2).
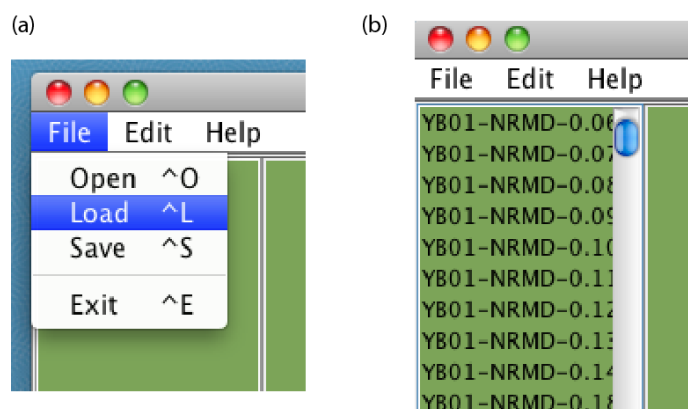


**Figure A.II.2**   Open or Load data file. (a) The File menu, and (b) imported data files for the respective sample displayed in the left-hand *text area*.

## II.2.3  Display plots

Simply click any sample name in the left-hand *text area*. The data will then plot in the right-hand *panel*. In the Edit menu, there are several options that can be checked

on or off. These options provide various plots that will be displayed by checking on or hidden by checking off. Options for different cross-plots of NRM/IRM, NRM/ARM, ARM/IRM, and plots after data normalization are illustrated in Figure A.II.3a.
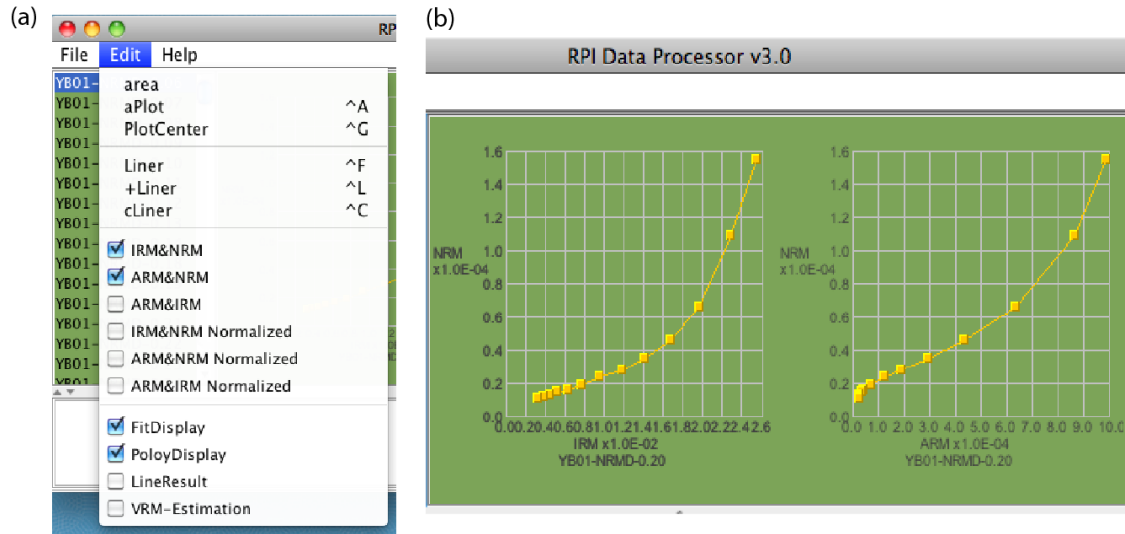


**Figure A.II.3**   Display plots. (a) The plot options in the Edit menu, where IRM&NRM represents the cross-plot of NRM/IRM. (b) Plots of NRM/IRM and NRM/ARM, which are the default plots.


## II.2.4  Show the data

Sometimes it is useful to visually check the data used in the plot. In this case, simply right-click on the plot that needs to be checked, select *Properties* in the pop-up menu, select the *data* tab, then check the data displayed in the *text area* (Figure A.II.4).
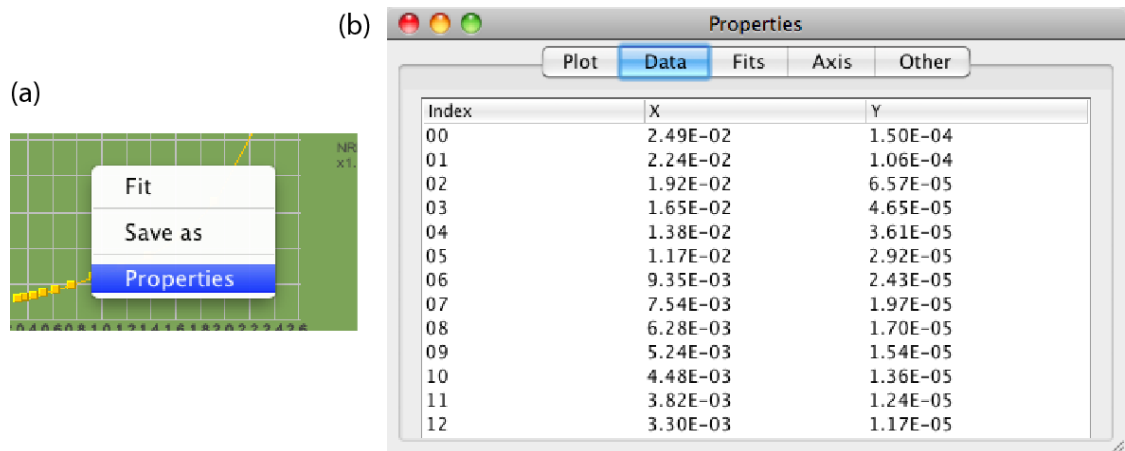


**Figure A.II.4**   Display of the data used in the plot. (a) The pop-up menu is obtained by right-clicking on the plot, and (b) the data will be displayed when the *Data* tab is checked.

## II.2.5  Line fitting

Based on inspection of data on plots, it is possible to decide which data are suitable for remanence normalization. In the *Properties* window, click the *Fits* tab, input the start and end index value of the data points desired for line fitting, and then click *Add* button. The line is fitted using the least-squares method and will be displayed on the plot (Figure A.II.5). Each plot can have fitted lines added using the same procedure as described above.
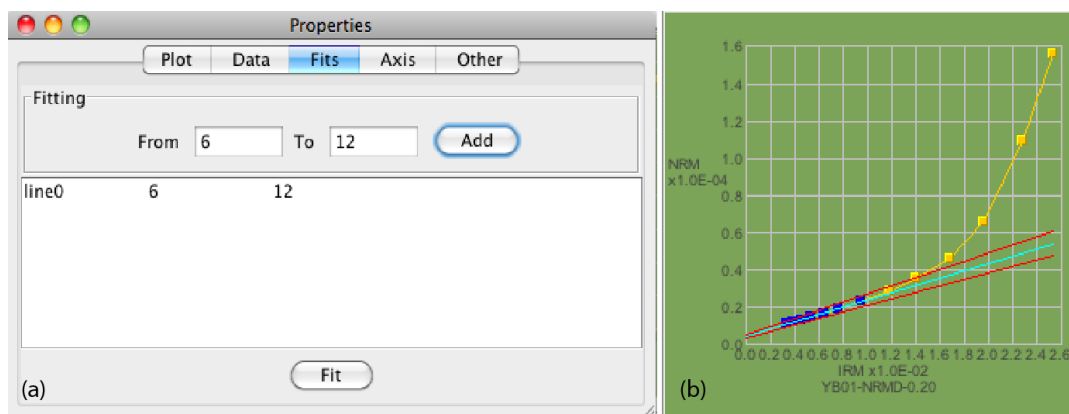


**Figure A.II.5**   Line fit in a remanence cross-plot. (a) Add a line fit by inputting the start and end index value of the desired data points, and (b) the fitted line displayed on the plot. Yellow dots represent the data, and dark blue dots represent the data used for the fit. The green line represents the best-fit line using the least-squares method, while the red lines represent the maximum error estimations.

## II.2.6  Draw the VRM area
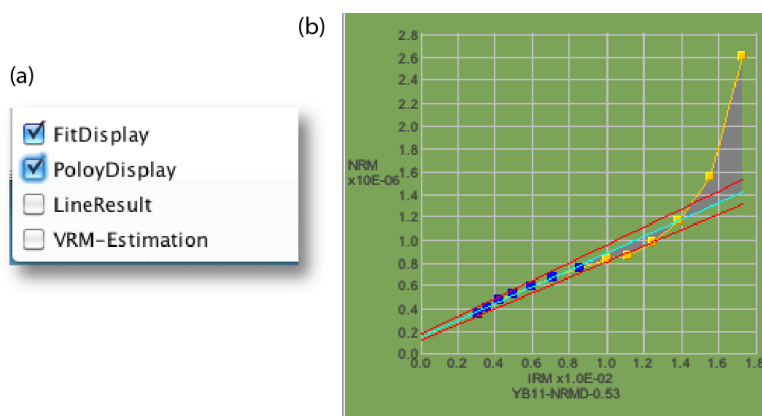


**Figure A.II.6**   Draw the VRM area. (a) Check on the option *Poloydisplay*, and (b) the VRM area (semi-transparent purple) will be displayed in the plot.

As described in Chapter 6, the VRM area is required to estimate the influence of VRM. By checking the *Poloydisplay* option in the Edit menu, the VRM area will be displayed on the plot (Figure A.II.6). The VRM area will display both above and

below the best-fit line in some cases, therefore we calculated these areas separately. We define the area above the best-fit line as positive; the area below the line is negative. The discussion in Chapter 5 provides more information on interpretation of VRM results.

## II.2.7 Calculation and results

Once the desired lines have been fitted, pressing *Ctrl+S* will activate the calculation function. The parameters for the best-fit line and the VRM area will appear in the bottom *text area* (Figure A.II.7).
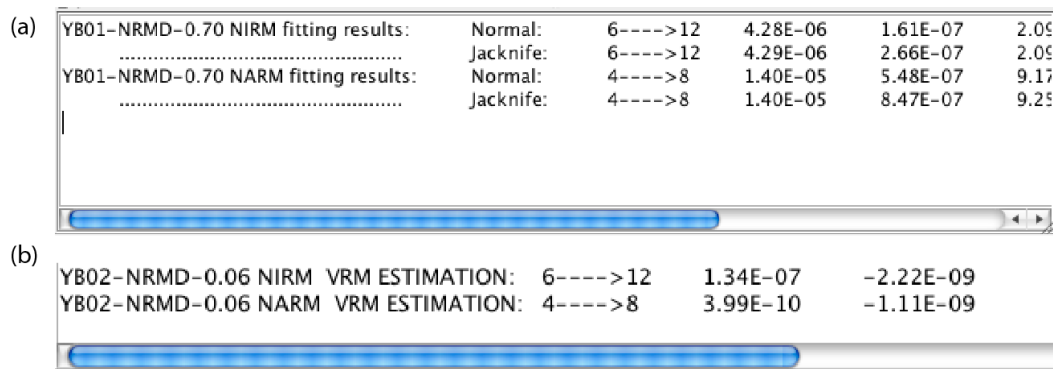


**Figure A.II.7** Results of calculations. (a) The fitting results determined using normal least-squares and jackknife methods. (b) VRM area estimation results.

## II.2.8 Save plot

By clicking the right-hand mouse button, and then clicking *Save as* in the pop-up menu, the plot will be saved as a PDF version, which allows modification of the plot for future use.

## II.2.9 A full screen

A full screen presentation of the RPI data processor program, in which all plots are displayed, with some plots having added line fits and the VRM area shown is provided in Figure A.II.8. The bottom *text area* includes some results.
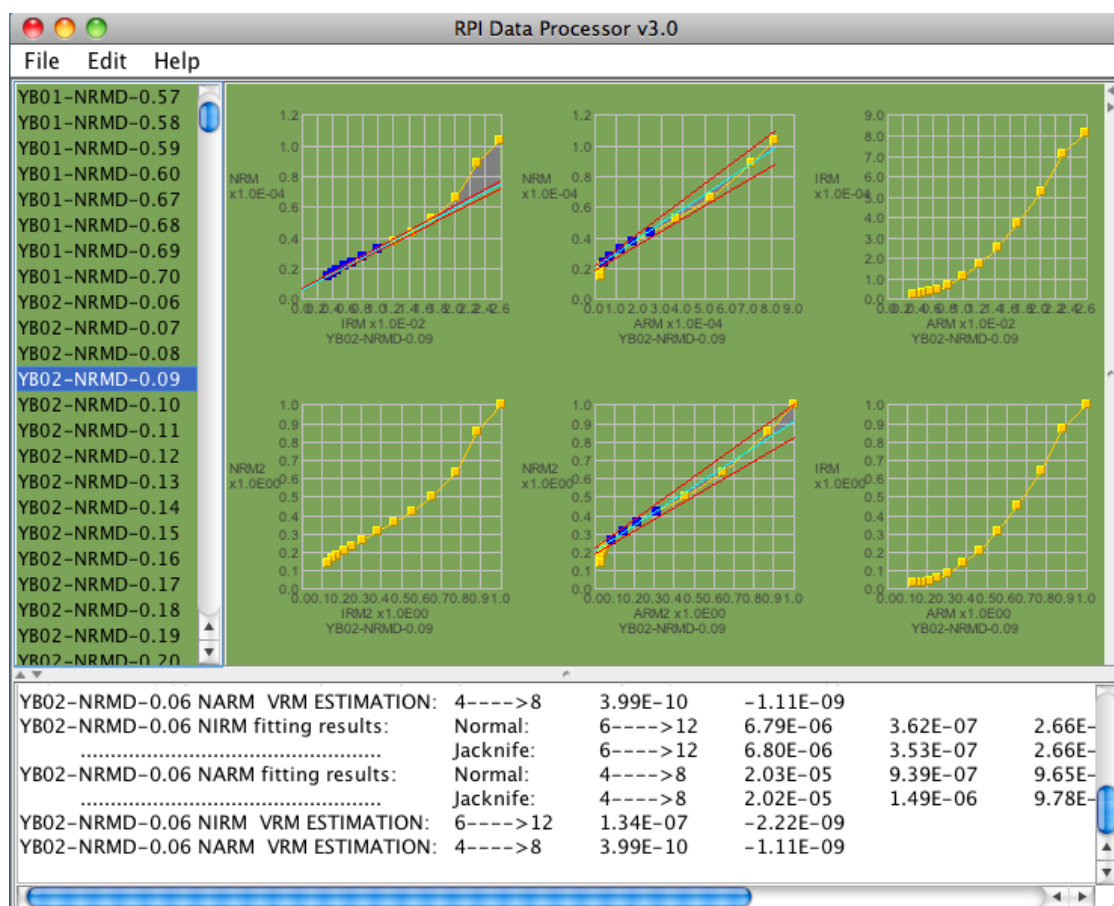
**Figure A.II.8** Full screen of the RPI data processor program.

## II.3  Summary

The software described above was used to process the normalized remanence data analyzed for this study, as presented in Chapter 5.

# References

An, Z. S. (2000). The history and variability of the East Asian paleomonsoon climate. *Quaternary Science Reviews*, *19*, 171–187.

An, Z. S. and J. L. Xiao (1990). Study on the eolian dust flux over the Loess Plateau: an example. *Chinese Science Bulletin*, *35*, 1627–1631.

An, Z. S., G. J. Kukla, S. C. Porter and J. Xiao (1991). Magnetic susceptibility evidence of monsoon variation on the loess plateau of central China during the last 130,000 years. *Quaternary Research*, *36*, 29–36.

An, Z. S., J. D. Wu and H. M. Li (1977). Paleomagnetic research of the Luochuan loess section. *Geochimica et Cosmochimica Acta*, *4*, 239–249.

Anson, G. L. and K. P. Kodama (1987). Compaction induced inclination shallowing of the post-depositional remanent magnetization in a synthetic sediment. *Geophysical Journal of the Royal Astronomical Society*, *88*, 673–692.

Arason, P. and S. Levi (1990). Compaction and inclination shallowing in deep-sea sediments from the Pacific Ocean. *Journal of Geophysical Research*, *95*, 4501–4510.

Balsam, W., J. F. Ji and J. Chen (2004). Climatic interpretation of the Luochuan and Lingtai loess sections, China, based on changing iron oxide mineralogy and magnetic susceptibility. *Earth and Planetary Science Letters*, *223*, 335–348.

Banerjee, S. K., C. P. Hunt and X. M. Liu (1993). Separation of local signals from the regional paleomonsoon record of the Chinese loess plateau: a rock-magnetic approach. *Geophysical Research Letters*, *20*, 843–846.

Barrón, V. and J. Torrent (2002). Evidence for a simple pathway to maghemite in Earth and Mars soils. *Geochimica et Cosmochimica Acta*, *66*, 2801–2806.

Barrón, V., J. Torrent and E. de Grave (2003). Hydromaghemite, an intermediate in the hydrothermal transformation of 2-line ferrihydrite into hematite. *American Mineralogist*, *88*, 1679–1688.

Barton, C. E., M. W. McElhinny and D. J. Edwards (1980). Laboratory studies of

depositional DRM. *Geophysical Journal of the Royal Astronomical Society*, *61*, 355–377.

Bloemendal, J., J. W. King, F. R. Hall and S. J. Doh (1992). Rock magnetism of Late Neogene and Pleistocene deep-sea sediments: relationship to sediment source, diagenetic processes and sediment lithology. *Journal of Geophysical Research*, *75*, 4361-4375.

Bloemendal, J. and X. M. Liu (2005). Rock magnetism and geochemistry of two Plio-Pleistocene Chinese loess/palaeosol sequences: implications for quantitative palaeoprecipitation reconstruction. *Palaeogeography Palaeoclimatology Palaeoecology*, *226*, 149–166.

Blow, R. A. and N. Hamilton (1978). Effect of compaction on the acquisition of a detrital remanent magnetization in fine-grained sediments. *Geophysical Journal of the Royal Astronomical Society*, *52*, 13–23.

Brachfeld, S. A. and S. K. Banerjee (2000). A new high-resolution geomagnetic paleointensity record for the North American Holocene: a comparison of sedimentary and absolute intensity data. *Journal of Geophysical Research*, *105*, 821–834.

Burbank, D. W. and J. Li (1985). Age and palaeoclimatic significance of the loess of Lanzhou, north China. *Nature*, *316*, 429–431.

Butler, R. F. (1992). *Paleomagnetism*, Oxford, Blackwell Scientific Publications.

Cande, S. C. and D. V. Kent (1995). Revised calibration of the geomagnetic polarity timescale for the Late Cretaceous and Cenozoic. *Journal of Geophysical Research*, *100*, 6093–6095.

Channell, J. E. T. (1999). Geomagnetic paleointensity and directional secular variation at Ocean Drilling Program (ODP) Site 984 (Bjorn Drift) since 500 ka: comparisons with ODP Site 983 (Gardar Drift). *Journal of Geophysical Research*, 104, 22937–22951.

Chang, L. (2009) Fundamental magnetic properties of Greigite ($Fe_3S_4$). University of Southampton, School of Ocean and Earth Science, PhD Thesis.

Channell, J. E. T., A. Mazaud, P. Sullivan, S. Turner and M. E. Raymo (2002). Geomagnetic excursions and paleointensities in the Matuyama Chron at Ocean Drilling Program Sites 983 and 984 (Iceland Basin). *Journal of Geophysical Research*, *107*, 2114, doi:10.1029/2001JB000491.

Chen, F. H., J. Bloemendal, J. M. Wang, J. J. Li and F. Oldfield (1997). High-resolution multi-proxy climate records from Chinese loess, evidence for rapid climatic changes over the last 75 kyr. *Palaeogeography Palaeoclimatology Palaeoecology*, *130*, 323–335.

Chen, F. H., J. Bloemendal, Z. D. Feng, J. M. Wang, E. Parker and Z. T. Guo (1999). East Asian monsoon variations during Oxygen Isotope Stage 5: evidence from the northwestern margin of the Chinese loess plateau. *Quaternary Science Reviews*, *18*, 1127–1135.

Chen, J., J. F. Ji, W. Balsam, Y. Chen, L. W. Liu and Z. S. An (2002). Characterization of the Chinese loess-paleosol stratigraphy by whiteness measurement. *Palaeogeography Palaeoclimatology Palaeoecology*, *183*, 287–297.

Chen, T. H., H. F. Xu, Q. Q. Xie, J. Chen, J. F. Ji and H. Y. Lu (2005). Characteristics and genesis of maghemite in Chinese loess and paleosols: mechanism for magnetic susceptibility enhancement in paleosols. *Earth and Planetary Science Letters*, *240*, 790–802.

Clement, B. M. (2004). Dependence of the duration of geomagnetic polarity reversals on site latitude. *Nature*, *428*, 637–640.

Cornell, R. M. and U. Schwertmann (2000). The Iron Oxides. Structure, Properties, Reactions, Occurrences and Uses. Weinheim, Germany, VCH.

Constable, C. (1992). Link between geomagnetic reversal paths and secular variation of the field over the past 5 Myr. *Nature*, *358*, 230–233.

Cox, A., J. Hillhouse and M. Fuller (1975). Paleomagnetic records of polarity transitions, excursions, and secular variation. *Reviews of Geophysics*, *13*, 185–189.

Cui, Y., K. L. Verosub and A. P. Roberts (1994). The effect of low-temperature oxidation on large multi-domain magnetite. *Geophysical Research Letters*, *21*, 757–760.

Dansgaard, W., S. J. Johnsen, H. B. Clausen, D. Dahl-Johnsen, N. Gunderstrup, C. U. Hammer, C. Hvidberg, J. Steffensen, A. Sveinbjörnsobttir, J. Jouzel and G. Bond (1993). Evidence for general instability of past climate from a 250 kyr ice core record. *Nature*, *364*, 218–220.

Day, R., M. Fuller and V. A. Schmidt (1977). Hysteresis properties of titanomagnetites: grain-size and compositional dependence. *Physics of the Earth and Planetary Interiors*, *13*, 260–266.

deMenocal, P., W. F. Ruddiman and D. V. Kent (1990). Depth of post-depositional remanence acquisition in deep-sea sediments: a case study of the Brunhes/Matuyama reversal and oxygen isotope stage 19.1. *Earth and Planetary Science Letters*, *99*, 1–13.

Deng, C. L. (2008). Paleomagnetic and mineral magnetic investigation of the Baicaoyuan loess-paleosol sequence of the western Chinese Loess Plateau over the last glacial-interglacial cycle and its geological implications. *Geochemistry Geophysics Geosystems*, *9*, Q04034, doi:10.1029/2007GC001928.

Deng, C. L., R. X. Zhu, M. J. Jackson, K. L. Verosub and M. J. Singer (2001). Variability of the temperature-dependent susceptibility of the Holocene eolian deposits in the Chinese loess plateau: a pedogenesis indicator. *Physics and Chemistry of the Earth*, *26*, 873–878.

Deng, C. L., R. Zhu, K. L. Verosub, M. J. Singer and N. J. Vidic (2004). Mineral magnetic properties of loess/paleosol couplets of the central loess plateau of China over the last 1.2 Myr. *Journal of Geophysical Research*, *109*, 1–13.

Deng, C. L., N. J. Vidic, K. L. Verosub, M. J. Singer, Q. S. Liu, J. Shaw and R. X. Zhu (2005). Mineral magnetic variation of the Jiaodao Chinese loess/paleosol sequence and its bearing on long-term climatic variability. *Journal of Geophysical Research*, *110*, 148–227.

Deng, C. L., R. X. Zhu, K. L. Verosub, M. J. Singer and B. Yuan (2000). Paleoclimatic significance of the temperature-dependent susceptibility of Holocene

loess along a NW-SE transect in the Chinese loess plateau. *Geophysical Research Letters*, *27*, 3715-3718.

Deng, C. L., J. Shaw, Q. S. Liu, Y. X. Pan and R. X. Zhu (2006). Mineral magnetic variation of the Jingbian loess/paleosol sequence in the northern Loess Plateau of China: implications for Quaternary development of Asian aridification and cooling. *Earth and Planetary Science Letters*, *241*, 248–259.

Ding, Z. L. and D. S. Liu (1992). Climatic correlation between Chinese Loess and deep-sea cores in the last 1.8 Ma. *Chinese Science Bulletin*, *37*, 217–220.

Ding, Z. L., J. M. Sun, T. S. Liu, R. X. Zhu, S. L. Yang and B. Guo (1998a). Wind-blown origin of the Pliocene red clay formation in the central Loess Plateau, China. *Earth and Planetary Science Letters*, *161*, 135–143.

Ding, Z. L., J. M. Sun, S. L. Yang and T. S. Liu (1998b). Preliminary magnetostratigraphy of a thick eolian red clay-loess sequence at Lingtai, the Chinese Loess Plateau. *Geophysical Research Letters*, *25*, 1225–1228.

Ding, Z. L., S. L. Yang, S. S. Hou, X. Wang, Z. Chen and T. S. Liu (2001). Magnetostratigraphy and sedimentology of the Jingchuan red clay section and correlation of the Tertiary eolian red clay sediments of the Chinese Loess Plateau. *Journal of Geophysical Research*, *106*, 6399–6407.

Ding, Z. L., E. Derbyshire, S. L. Yang, Z. W. Yu, S. F. Xiong and T. S. Liu (2002). Stacked 2.6-Ma grain size record from the Chinese loess based on five sections and correlation with the deep-sea $\delta^{18}O$ record. *Paleoceanography*, *17*, 1033, doi:10.1029/2001PA000725.

Dunlop, D. J. (2002a). Theory and application of the Day plot ($M_{rs}/M_s$ versus $H_{cr}/H_c$). 1. Theoretical curves and tests using titanomagnetite data. *Journal of Geophysical Research*, *107*, 2057, doi:10.1029/2001JB000487.

Dunlop, D. J. (2002b). Theory and application of the Day plot ($M_{rs}/M_s$ versus $H_{cr}/H_c$). 2. Application to data for rocks, sediments, and soils. *Journal of Geophysical Research*, *107*, 2056, doi:10.1029/2001JB000486.

Dunlop, D. J. and Ö. Özdemir (1997). *Rock Magnetism: Fundamentals and Frontiers*. Cambridge, Cambridge University Press.

Egli, R. (2003). Analysis of the field dependence of remanent magnetization curves. *Journal of Geophysical Research*, *108*, 2081, doi:10.1029/2002JB002023.

Evans, M. E. and F. Heller (1994). Magnetic enhancement and palaeoclimate: study of a loess/palaeosol couplet across the loess plateau of China. *Geophysical Journal International*, *117*, 257–264.

Evans, M. E. and F. Heller (2001). Magnetism of loess/palaeosol sequences: recent developments. *Earth-Science Reviews*, *54*, 129–144.

Eyre, J. K. (1996). The application of high resolution IRM acquisition to the discrimination of remanence carriers in Chinese loess. *Studia Geophysica et Geodaetica*, *40*, 234–242.

Eyre, J. K. and J. Shaw (1994). Magnetic enhancement of Chinese loess: the role of $\alpha$-$Fe_2O_3$? *Geophysical Journal International*, *117*, 265–271.

Fang, X. M., J. J. Li, R. van der Voo, C. M. Niocaill, X. R. Dai, R. A. Kemp, E. Derbyshire, J. X. Cao, J. M. Wang and G. Wang (1997). A record of the Blake Event during the last interglacial paleosol in the western Loess Plateau of China. *Earth and Planetary Science Letters*, *146*, 73–82.

Fang, X. M., J. J. Li and R. Van der Voo (1999). Rock magnetic and grain size evidence for intensified Asian atmospheric circulation since 800,000 years B.P. related to Tibetan uplift. *Earth and Planetary Science Letters*, *165*, 129–144.

Florindo, F., R. X. Zhu, B. Guo, L. P. Yue, Y. X. Pan and F. Speranza (1999). Magnetic proxy climate results from the Duanjiapo loess section, southernmost extremity of the Chinese loess plateau. *Journal of Geophysical Research*, *104*, 645–659.

Guillou, H., B. S. Singer, C. Laj, C. Kissel, S. Scaillet and B. R. Jicha (2004). On the age of the Laschamp geomagnetic excursion. *Earth and Planetary Science Letters*, *227*, 331–343.

Guo, B., R. X. Zhu, L. X. Bai and F. Florindo (2001a). Rock magnetic properties of a loess-paleosol couple along an N-S transect in the Chinese Loess Plateau. *Science in China* D, *44*, 1099–1109.

Guo, B., R. X. Zhu, A. P. Roberts and F. Florindo (2001b). Lack of correlation between paleoprecipitation and magnetic susceptibility of Chinese loess/paleosol sequences. *Geophysical Research Letters*, *28*, 4259–4262.

Guo, Z. T., T. Liu, J. Guiot, N. Wu, H. Lu, J. Han, J. Liu and Z. Gu (1996). High frequency pulses of East Asian monsoon climate in the last two glaciations: link with the North Atlantic. *Climate Dynamics*, *12*, 701–709.

Guo, Z. T., W. F. Ruddiman, Q. Z. Hao, H. B. Wu, Y. S. Qiao, R. X. Zhu, S. Z. Peng, J. J. Wei, B. Y. Yuan and T. S. Liu (2002). Onset of Asian desertification by 22 Myr ago inferred from loess deposits in China. *Nature*, *416*, 159–163.

Guyodo, Y., P. Gaillot and J. E. T. Channell (2000). Wavelet analysis of relative geomagnetic paleointensity at ODP Site 983, *Earth and Planetary Science Letters*, *184*, 109-123.

Grinsted, A., J. C. Moore, S. Jevrejeva (2004). Application of the cross wavelet transform and wavelet coherence to geophysical time series, *Nonlinear Processes Geophysics*, *11*, 561566, doi:10.5194/npg-11-561-2004.

Guyodo, Y. and J.-P. Valet (1996). Relative variations in geomagnetic intensity from sedimentary records: the past 200,000 years. *Earth and Planetary Science Letters*, *143*, 23–36.

Han, J. M., H. Y. Lu, N. Q. Wu and Z. T. Guo (1996). The magnetic susceptibility of modern soils in China and its use for paleoclimate reconstruction. *Studia Geophysica et Geodaetica*, *40*, 262–275.

Heller, F. and M. E. Evans (1995). Loess magnetism. *Reviews of Geophysics*, *33*, 211–240.

Heller, F. and T. S. Liu (1982). Magnetostratigraphical dating of loess deposits in China. *Nature*, *300*, 431–433.

Heller, F. and T. S. Liu (1984). Magnetism of Chinese loess deposits. *Geophysical Journal of the Royal Astronomical Society*, *77*, 125–141.

Heller, F. and T. S. Liu (1986). Palaeoclimatic and sedimentary history from magnetic susceptibility of loess in China. *Geophysical Research Letters*, *13*, 1169–1172.

Heller, F., X. M. Liu, T. S. Liu and T. C. Xu (1991). Magnetic susceptibility of loess in China. *Earth and Planetary Science Letters*, *103*, 301–310.

Heller, F., C. D. Shen, J. Beer, X. M. Liu, T. S. Liu, A. Bronger, M. Suter and G. Bonani (1993). Quantitative estimates of pedogenic ferromagnetic mineral formation in Chinese loess and palaeoclimatic implications. *Earth and Planetary Science Letters*, *114*, 385–390.

Heslop, D. and M. Dillon (2007). Unmixing magnetic remanence curves without *a priori* knowledge. *Geophysical Journal International*, *170*, 556–566.

Heslop, D., C. G. Langereis and M. J. Dekkers (2000). A new astronomical timescale for the loess deposits of Northern China. *Earth and Planetary Science Letters*, 184, 125–139.

Heslop, D., J. Shaw, J. Bloemendal, F. Chen, J. Wang and E. Parker (1999). Sub-millennial scale variations in East Asian monsoon systems recorded by dust deposits from the north-western Chinese Loess Plateau. *Physics and Chemistry of the Earth*, *24*, 785–792.

Heslop, D., M. J. Dekkers, P. P. Kruiver and I. H. M. van Oorschot (2002). Analysis of isothermal remanent magnetization acquisition curves using the expectation-maximization algorithm. *Geophysical Journal International*, *148*, 58–64.

Hill, M. J. and J. Shaw (2000). Magnetic field intensity study of the 1960 Kilauea lava flow, Hawaii, using the microwave palaeointensity technique. *Geophysical Journal International*, *142*, 487–504.

Horng, C. S., A. P. Roberts and W. T. Liang (2003). A 2.14 Myr astronomically tuned record of relative geomagnetic paleointensity from the western Philippine Sea. *Journal of Geophysical Research*, *108*, 2059, doi:10.1029/2001JB001698.

Hovan, S. A., D. K. Rea, N. G. Pisias and N. J. Shackleton (1989). A direct link between the China loess and marine $\delta^{18}O$ records: eolian flux to the north Pacific. *Nature*, *340*, 296–298.

Hus, J. J. and R. Geeraerts (1986). Paleomagnetic and rock magnetic investigation of late Pleistocene loess deposits in Belgium. *Physics of the Earth and Planetary Interiors*, *44*, 21–40.

Hus, J. J. and J. M. Han (1992). The contribution of loess magnetism in China to the retrieval of past global changes: some problems. *Physics of the Earth and Planetary Interiors*, *70*, 154–168.

Irving, E. and A. Major (1964). Post-depositional detrital remanent magnetization in a synthetic sediment. *Sedimentology*, *3*, 135–143.

Imbrie, J. D., A. Mclntyre and A. C. Mix (1989). Oceanic response to orbital forcing in the late Quaternary: observational and experimental strategies. In: Berger, A. Schneider, and J. C. Duplessy (eds.), Climate and Geosciences, A Challenge for Science and Society in the 21th Century. Boston (Kluwer Academic), 121–164

Ji, J. F., J. Chen, W. Balsam, H. Y. Lu, Y. B. Sun and H. F. Xu (2004). High resolution hematite/goethite records from Chinese loess sequences for the last glacial-interglacial cycle: rapid climatic response of the East Asian Monsoon to the tropical Pacific. *Geophysical Research Letters*, *31*, L03207, doi:10.1029/2003GL018975.

Jin, C. S. and Q. S. Liu (2010). Reliability of the natural remanent magnetization recorded in Chinese loess. *Journal of Geophysical Research*, 115, B04103, doi:10.1029/2009JB006703.

Johnsen, S. J., D. Dahl-Jensen, N. Gundestrup, J. P. Steffensen, H. B. Clausen, H. Miller, V. Masson-Delmotte, A. E. Sveinbjörnsdottir and J. White (2001). Oxygen isotope and palaeotemperature records from six Greenland ice-core stations: Camp Century, Dye-3, GRIP, GISP2, Renland and NorthGRIP, *Journal of Quaternary Science*, *16*, 299–307. doi:10.1002/jqs.622.

Johnson, E. A., T. Murphy and O. W. Torreson (1948). Pre-history of the Earth's magnetic field. *Terrestrial Magnetism and Atmospheric Electricity*, *53*, 349–372.

Jouzel, J., C. Lorius, J. R. Petit, C. Genthon, N. I. Barkov, V. M. Kotlyankov and V. M. Petrov (1987). Vostok ice-core: a continuous isotope temperature record over the last climatic cycles (160,000 years). *Nature*, *329*, 403–408.

Kent, D. V. (1973). Post depositional remanent magnetization in deep sea sediments. *Nature*, *246*, 32–34.

King, J. W. and J. E. T. Channell (1991). Sedimentary magnetism, environmental magnetism, and magnetostratigraphy. *Reviews of Geophysics*, *29*, 358–370.

King, R. F. (1955). The remanent magnetism of artificially deposited sediments. *Monthly Notices of the Royal Astronomical Society, Geophysical Supplement*, *7*, 115–134.

Kirschvink, J. L. (1980). The least-squares line and plane and the analysis of palaeomagnetic data. *Geophysical Journal of the Royal Astronomical Society*, *62*, 699–718.

Kittl, P. (1984). Analysis of the Weibull distribution function. *Journal of Applied Mechanics Transactions of the ASME*, *51*, 221–222.

Kletetschka, G. and S. K. Banerjee (1995). Magnetic stratigraphy of Chinese loess as a record of natural fires. *Geophysical Research Letters*, *22*, 1341–1343.

Kok, Y. S. and L. Tauxe (1999). Long-$\tau$ VRM and relative paleointensity estimates in sediments. *Earth and Planetary Science Letters*, *168*, 145–158.

Kruiver, P. P., M. J. Dekkers and D. Heslop (2001). Quantification of magnetic coercivity components by the analysis of acquisition curves of isothermal remanent magnetisation. *Earth and Planetary Science Letters*, *189*, 269–276.

Kukla, G. J., F. Heller, X. M. Liu, T. C. Xu, T. S. Liu and Z. S. An (1988). Pleistocene climates in China dated by magnetic susceptibility. *Geology*, *16*, 811–814.

Kukla, G. J., Z. S. An, J. L. Melice, J. Gavin and J. L. Xiao (1990). Magnetic susceptibility record of Chinese loess. *Transactions of the Royal Society of Edinburgh*, *81*, 263–288.

Landau, L. D. and E. M. Lifshitz (1935). On the theory of the dispersion of magnetic permeability in ferromagnetic bodies. *Physikalische Zeitschrift der Sowjetunion*, *8*, 153–167.

Langereis, C. G., M. J. Dekkers, G. J. de Lange, M. Paterne and P. J. M. van Santvoort (1997). Magnetostratigraphy and astronomical calibration of the last 1.1 Myr from an eastern Mediterranean piston core and dating of short events in the Brunhes. *Geophysical Journal International*, *129*, 75–94.

Li, H. M., Z. S. An and J. D. Wang (1974). Primary paleomagnetic study of loess from Wucheng section, Northern China. *Geochimica et Cosmochimica Acta*, *2*, 93–104.

Ling, D., H. Z. Huang and Y. Liu (2009). A method for parameter estimation of mixed Weibull distribution. *Annual Reliability and Maintainability Symposium, 2009 Proceedings*, 129–133.

Liu, C. C., C. L. Deng, Q. S. Liu, L. T. Zheng, W. Wang, X. M. Xu, S. Huang and B. Y. Yuan (2010). Mineral magnetism to probe into the nature of palaeomagnetic signals of subtropical red soil sequences in southern China. *Geophysical Journal International*, *181*, 1395–1410.

Liu, H. F., J. Z. An and J. Wang (1993). Preliminary-study of the Olduvai termination recorded in the red loam in southeast Shanxi Province, China. *Journal of Geomagnetism and Geoelectricity*, *45*, 331–338.

Liu, Q. S., M. Jackson and S. Banerjee (2003). Determination of magnetic carriers of the characteristic remanent magnetization of Chinese loess by low-temperature demagnetization. *Earth and Planetary Science Letters*, *216*, 175–186.

Liu, Q. S., S. K. Banerjee, M. J. Jackson, F. H. Chen, Y. X. Pan and R. X. Zhu (2004a). Determining the climatic boundary between the Chinese loess and palaeosol: evidence from eolian coarse-grained magnetite. *Geophysical Journal International*, *156*, 267–274.

Liu, Q. S., S. K. Banerjee, M. J. Jackson, B. A. Maher, Y. X. Pan, R. X. Zhu, C. L. Deng and F. H. Chen (2004b). Grain sizes of susceptibility and anhysteretic remanent

magnetization carriers in Chinese loess/paleosol sequences. *Journal of Geophysical Research*, *109*, B03101, doi:10.1029/2003JB002747.

Liu, Q. S., M. J. Jackson, S. K. Banerjee, B. A. Maher, C. L. Deng, Y. X. Pan and R. X. Zhu (2004c). Mechanism of the magnetic susceptibility enhancements of the Chinese loess. *Journal of Geophysical Research*, *109*, B12107, doi:10.1029/2004JB003249.

Liu, Q. S., S. K. Banerjee, M. J. Jackson, C. L. Deng, Y. X. Pan and R. X. Zhu (2005a). Inter-profile correlation of the Chinese loess/paleosol sequences during Marine Oxygen Isotope Stage 5 and indications of pedogenesis. *Quaternary Science Reviews*, *24*, 195–210.

Liu, Q. S., C. L. Deng, Y. J. Yu, J. Torrent, M. J. Jackson, S. K. Banerjee and R. X. Zhu (2005b). Temperature dependence of magnetic susceptibility in an argon environment: implications for pedogenesis of Chinese loess/palaeosols. *Geophysical Journal International*, *161*, 102–112.

Liu, Q. S., J. Torrent, B. A. Maher, Y. J. Yu, C. L. Deng, R. X. Zhu and X. X. Zhao (2005c). Quantifying grain size distribution of pedogenic magnetic particles in Chinese loess and its significance for pedogenesis. *Journal of Geophysical Research*, *110*, B11102, doi:10.1029/2005JB003726.

Liu, Q. S., J. Bloemendal, J. Torrent and C. L. Deng (2006a). Contrasting behavior of hematite and goethite within paleosol S5 of the Luochuan profile, Chinese Loess Plateau. *Geophysical Research Letters*, *33*, L20301, doi:10.1029/2006GL027172.

Liu, Q. S., Y. J. Yu, J. Torrent, A. P. Roberts, Y. X. Pan and R. X. Zhu (2006b). Characteristic low-temperature magnetic properties of aluminous goethite [$\alpha$-(Fe, Al)OOH] explained. *Journal of Geophysical Research*, *111*, B12S34, doi:10.1029/2006JB004560.

Liu, Q. S., A. P. Roberts, J. Torrent, C. S. Horng and J. C. Larrasoaña (2007a). What do the HIRM and S-ratio really measure in environmental magnetism? *Geochemistry Geophysics Geosystems*, *8*, Q09011, doi:10.1029/2007GC001717.

Liu, Q. S., C. L. Deng, J. Torrent and R. X. Zhu (2007b). Review of recent developments in mineral magnetism of the Chinese loess. *Quaternary Science Reviews*, *26*, 368–385.

Liu, Q. S., A. P. Roberts, E. J. Rohling, R. X. Zhu and Y. B. Sun (2008). Post-depositional remanent magnetization lock-in and the location of the Matuyama/Brunhes geomagnetic reversal boundary in marine and Chinese loess sequences. *Earth and Planetary Science Letters*, *275*, 102–110.

Liu, T. S. (1985). *Loess and the Environment*. Beijing, China Ocean Press.

Liu, W. M., L. Y. Zhang and J. M. Sun (2010). High resolution magnetostratigraphy of the Luochuan loess-paleosol sequence in the central Chinese Loess Plateau. *Chinese Journal of Geophysics*, *53*, 888–894.

Liu, X. M., T. S. Liu, C. Liu, T. C. Xu and M. Y. Cheng (1988a). The Chinese loess in Xifeng. I. The primary study on magnetostratigraphy of a loess profile in Xifeng area, Gansu Province. *Geophysical Journal*, *92*, 345–348.

Liu, X. M., T. C. Xu and T. S. Liu (1988b). The Chinese loess in Xifeng. II. A study of anisotropy of magnetic susceptibility of loess from Xifeng. *Geophysical Journal*, *92*, 349–353.

Liu, X. M., T. S. Liu, F. Heller and T. C. Xu (1990). Frequency-dependent susceptibility of loess and Quaternary paleoclimate. *Quaternary Sciences*, *3*, 42–50.

Lu, H. Y. and Z. S. An (1998). Paleoclimatic significance of grain size of loess-palaeosol deposit in Chinese Loess Plateau. *Science in China D*, *41*, 626–631.

Lu, H. Y., X. D. Liu, F. Q. Zhang, Z. S. An and J. Dodson (1999). Astronomical calibration of loess-paleosol deposits at Luochuan, central Chinese Loess Plateau. *Palaeogeography Palaeoclimatology Palaeoecology*, *154*, 237–246.

Lund, S., J. S. Stoner, J. E. T. Channell and G. Acton (2006). A summary of Brunhes paleomagnetic field variability recorded in Ocean Drilling Program cores. *Physics of the Earth and Planetary Interiors*, *156*, 194–204.

Maher, B. A. (1986). Characterisation of soils by mineral magentic measurements. *Physics of the Earth and Planetary Interiors*, *42*, 76–92.

Maher, B. A. (1988). Magnetic properties of some synthetic sub-micron magnetites. *Geophysical Journal of the Royal Astronomical Society*, *94*, 83–96.

Maher, B. A. (1998). Magnetic properties of modern soils and Quaternary loessic paleosols: paleoclimatic implications. *Palaeogeography Palaeoclimatology Palaeoecology*, *137*, 25–54.

Maher, B. A. and R. Thompson (1991). Mineral magnetic record of the Chinese loess and paleosols. *Geology*, *19*, 3–6.

Maher, B. A. and R. Thompson (1992). Paleoclimatic significance of the mineral magnetic record of the Chinese loess and paleosols: reply. *Quaternary Research*, *38*, 268–268.

Maher, B. A., R. Thompson and L. P. Zhou (1994). Spatial and temporal reconstructions of changes in the Asian palaeomonsoon: a new mineral magnetic approach. *Earth and Planetary Science Letters*, *125*, 461–471.

Markey, B. G., L. Botter Jensen and G. A. T. Duller (1997). A new flexible system for measuring thermally and optically stimulated luminescence. *Radiation Measurements*, *27*, 83–89.

McIntosh, G. (1993). Post-depositional detrital remanent magnetization in Chinese loess: preliminairy results of laboratory experiments. *Geologica Carpathica*, *44*, 335–338.

Mehra, O. P. and M. L. Jackson (1960). Iron oxide removal from soils and clays by a dithionite-citrate system buffered with sodium bicarbonate. *Clays and Clay Minerals*, *7*, 317–327.

Meynadier, L., J. P. Valet, R. Weeks, N. J. Shackleton and V. L. Hagee (1992). Relative geomagnetic intensity of the field during the last 140 ka. *Earth and Planetary Science Letters*, *114*, 39–57.

Moskowitz, B. M. and T. S. Moon (1991). Experimental and theoretical fine particle magnetism. *Reviews of Geophysics*, *29*, 349–357.

Mullins, C. E. (1977). Magnetic susceptibility of the soil and its significance in soil science: a review. *Journal of Soil Science*, *28*, 223–246.

Muxworthy, A., W. Williams and D. Virdee (2003). Effect of magnetostatic interactions on the hysteresis parameters of single-domain and pseudo-single-domain grains. *Journal of Geophysical Research*, *108*, 2517, doi:10.1029/2003JB002588.

Néel, L. (1949). Théorie du traînage magnétique des ferromagnétiques en grains fins avec applications aux terres cuites. *Annales de Géophysique*, *5*, 99–136.

Néel, L. (1955). Some theoretical aspects of rock magnetism. *Advances in Physics*, *4*, 191–243.

Oda, H. (2005). Recurrent geomagnetic excursions: a review for the Brunhes normal polarity chron. *Journal of Geography*, *114*, 174–192.

Otofuji, Y. I., I. Katsura and S. Sasajima (1982). Decay of a post-depositional remanent magnetization in wet sediments due to the effect of drying. *Geophysical* Journal of the Royal Astronomical Society, 70, 191–203.

O'Reilly, W., V. Hoffmann, A. C. Chouker, H. C. Soffel and A. Menyeh (2000). Magnetic properties of synthetic analogues of pyrrhotite ore in the grain size range 1– 24 μm, *Geophysical Journal International*, *142*, 669–683.

Özdemir, Ö. and D. J. Dunlop (1996). Thermoremanence and Néel temperature of goethite. *Geophysical Research Letters*, *23*, 921–924.

Pan, Y. X., R. X. Zhu, J. Shaw, Q. S. Liu and B. Guo (2001). Can relative paleointensities be determined from the normalized magnetization of the wind-blown loess of China? *Journal of Geophysical Research*, *106*, 19221–19232.

Pan, Y. X., R. X. Zhu, Q. S. Liu, B. Guo, L. P. Yue and H. N. Wu (2002). Geomagnetic episodes of the last 1.2 Myr recorded in Chinese loess. *Geophysical Research Letters*, *29*, 1282, doi:10.1029/2001GL014024.

Park, Y. H., S. J. Doh, W. Kim and D. Suk (2005). Magnetic fabric and rock magnetic studies of metasedimentary rocks in the central Okcheon Metamorphic Belt, Korea. *Earth Planets and Space*, *57*, 855–869.

Parry, J. H. (1967). Helmholtz coils and coil design. *Methods in Palaeomagnetism*. Amsterdam, Elsevier, 551–567.

Payne, M. A. and K. L. Verosub (1982). The acquisition of post-depositional detrital remanent magnetization in a variety of natural sediments. *Geophysical Journal of the Royal Astronomical Society*, *68*, 625–642.

Porter, S. C. and Z. S. An (1995). Correlation between climate events in the North-Atlantic and China during last glaciation. *Nature*, *375*, 305–308.

Pye, K. (1987). *Aeolian Dust and Dust Deposits*. London, Academic Press.

Qiang, X. K., Z. X. Li, C. M. Powell and H. B. Zheng (2001). Magnetostratigraphic record of the Late Miocene onset of the East Asian monsoon, and Pliocene uplift of northern Tibet. *Earth and Planetary Science Letters*, *187*, 83–93.

Richthofen, F. von (1882). On the mode of origin of the loess. *Geological Magazine*, *9*, 293–305.

Roberts, A. P. (2006). High-resolution magnetic analysis of sediment cores: strengths, limitations and strategies for maximizing the value of long-core magnetic data. *Physics of the Earth and Planetary Interiors*, *156*, 162–178.

Roberts, A. P. (2008). Geomagnetic excursions: knowns and unknowns. *Geophysical Research Letters*, *35*, L17307, doi:10.1029/2008GL034719.

Roberts, A. P. and M. Winklhofer (2004). Why are geomagnetic excursions not always recorded in sediments? Constraints from post-depositional remanent magnetization lock-in modelling. *Earth and Planetary Science Letters*, *227*, 345–359.

Roberts, A. P., Y. L. Cui and K. L. Verosub (1995). Wasp-waisted hysteresis loops: mineral magnetic characteristics and discrimination of components in mixed magnetic systems. *Journal of Geophysical Research*, *100*, 17909–17924.

Roberts, A. P., C. R. Pike and K. L. Verosub (2000). First-order reversal curve diagrams: a new tool for characterizing the magnetic properties of natural samples. *Journal of Geophysical Research*, *105*, 28461–28475.

Roberts, A. P., B. Lehman, R. J. Weeks, K. L. Verosub and C. Laj (1997). Relative paleointensity of the geomagnetic field over the last 200000 years from ODP Sites 883 and 884, North Pacific Ocean. *Earth and Planetary Science Letters*, *152*, 11–23.

Roberts, A. P., W. T. Jiang, F. Florindo, C. S. Horng and C. Laj (2005). Assessing the timing of greigite formation and the reliability of the Upper Olduvai polarity transition record from the Crostolo River, Italy. *Geophysical Research Letters*, *32*, L05307, doi:10.1029/2004GL022137.

Robertson, D. J. and D. E. France (1994). Discrimination of remanence-carrying minerals in mixtures, using isothermal remanent magnetization acquisition curves. *Physics of the Earth and Planetary Interiors*, *82*, 223–234.

Roe, G. (2009). On the interpretation of Chinese loess as a paleoclimate indicator. *Quaternary Research*, *71*, 150–161.

Rolph, T. C., J. Shaw, E. Derbyshire and J. Wang (1989). A detailed geomagnetic record from Chinese loess. *Physics of the Earth and Planetary Interiors*, *56*, 151–164.

Rolph, T. C., J. Shaw, E. Derbyshire and J. T. Wang (1993). The magnetic mineralogy of a loess section near Lanzhou, China. *Geological Society of London. Special Publication*, *72***,** 311–323.

Rutter, N., Z. L. Ding and T. S. Liu (1991b). Comparison of isotope stages 1-61 with the Baoji-type pedostratigraphic section of North-Central China. *Canadian Journal of Earth Sciences*, *28*, 985–990.

Rutter, N., Z. Ding, M. E. Evans and Y. Wang (1990). Magnetostratigraphy of the Baoji loess/paleosol section in the north-central China Loess Plateau. *Quaternary International*, 7/8, 97–102.

Rutter, N., Z. L. Ding, M. E. Evans and T. S. Liu (1991a). Baoji-type pedostratigraphic section, Loess Plateau, North-Central China. *Quaternary Science Reviews*, *10*, 1–22.

Scheinost, A. C., A. Chavernas, V. Barron and J. Torrent (1998). Use and limitations of second-derivative diffuse reflectance spectroscopy in the visible to near-infrared range to identify and quantify Fe oxide minerals in soils. *Clays and Clay Minerals*, *46*, 528–536.

Schwertmann, U. (1988). Occurrence and formation of iron oxides in various pedoenvironments. *Iron in Soils and Clay Minerals*. Dordrecht, Reidel Publishing**,** 267–308.

Schwertmann, U. and N. Kampf (1985). Properties of goethite and hematite in kaolinitic soils of southern and central Brazil. *Soil Science*, *139*, 344–350.

Schwertmann, U., H. Stanjek and H. H. Becher (2004). Long-term *in vitro* transformation of 2-line ferrihydrite to goethite/hematite at 4, 10, 15 and 25°C. *Clay Minerals*, *39*, 433–438.

Shaw, J. (1974). A new method of determining the magnitude of the palaeomagnetic field: application to five historic lavas and five archaeological samples. *Geophysical Journal of the Royal Astronomical Society*, *39*, 133–141.

Singer, B. S., H. Guillou, B. R. Jicha, C. Laj, C. Kissel, B. L. Beard and C. M. Johnson (2009). $^{40}Ar/^{39}Ar$, K–Ar and $^{230}Th–^{238}U$ dating of the Laschamp excursion: a radioisotopic tie-point for ice core and climate chronologies. *Earth and Planetary Science Letters*, *286*, 80–88.

Smalley, I. J., I. F. Jefferson, T. A. Dijkstra and E. Derbyshire (2001). Some major events in the development of the scientific study of loess. *Earth-Science Reviews*, *54*, 5–18.

Snowball, I. F. (1991). Magnetic hysteresis propeties of greigite ($Fe_3S_4$) and a new occurrence in Holocene sediments from Swedish Lappland. *Physics of the Earth and Planetary Interiors*, *68*, 32–40.

Spassov, S., F. Heller, M. E. Evans, L. P. Yue and T. von Dobeneck (2003a). A lock-in model for the complex Matuyama-Brunhes boundary record of the loess/palaeosol sequence at Lingtai (Central Chinese Loess Plateau). *Geophysical Journal International*, *155*, 350–366.

Spassov, S., F. Heller, R. Kretzschmar, M. E. Evans, L. P. Yue and D. K. Nourgaliev (2003b). Detrital and pedogenic magnetic mineral phases in the loess/palaeosol sequence at Lingtai (Central Chinese Loess Plateau). *Physics of the Earth and Planetary Interiors*, *140*, 255–275.

Stephenson, A. (1971a). Single domain grain distributions I. A method for the determination of single domain grain distributions. *Physics of the Earth and Planetary Interiors*, *4*, 353–360.

Stephenson, A. (1971b). Single domain grain distributions II. The distribution of single domain iron grains in Apollo 11 lunar dust. *Physics of the Earth and Planetary Interiors*, *4*, 361–369.

Stevens, T., S. J. Armitage, H. Y. Lu and D. S. G. Thomas (2006). Sedimentation and diagenesis of Chinese loess: implications for the preservation of continuous, high-resolution climate records. *Geology*, *34*, 849–852.

Stevens, T., D. S. G. Thomas, S. J. Armitage, H. R. Lunn and H. Y. Lu (2007). Reinterpreting climate proxy records from late Quaternary Chinese loess: a detailed OSL investigation. *Earth-Science Reviews*, *80*, 111–136.

Stober, J. C. and R. Thompson (1979). Magnetic remanence acquisition in Finnish lake sediments. *Geophysical Journal of the Royal Astronomical Society*, *57*, 727–739.

Stockhausen, H. (1998). Some new aspects for the modelling of isothermal remanent magnetization acquisition curves by cumulative log Gaussian functions. *Geophysical Research Letters*, *25*, 2217–2220.

Stokking, L. B. and L. Tauxe (1990). Multicomponent magnetization in synthetic hematite. *Physics of the Earth and Planetary Interiors*, *65*, 109–124.

Suganuma, Y., T. Yamazaki, T. Kanamatsu and N. Hokanishi (2008). Relative paleointensity record during the last 800 ka from the equatorial Indian Ocean: implication for relationship between inclination and intensity variations. *Geochemistry Geophysics Geosystems*, *9*, Q02011, doi:10.1029/2007GC001723.

Sun, D., J. Shaw, Z. An, M. Cheng and L. Yue (1998). Magnetostratigraphy and paleoclimatic interpretation of continuous 7.2 Ma Late Cenozoic eolian sediments from the Chinese Loess Plateau. *Geophysical Research Letters*, *25*, 85–88.

Sun, D. H., J. Shaw, Z. S. An and T. Rolph (1993). Matuyama/Brunhes (M/B) transition recorded in Chinese loess. *Journal of Geomagnetism and Geoelectricity*, *45*, 319–330.

Sun, D. H., D. S. Liu, T. S. Liu, M. Y. Chen, Z. S. An and J. Shaw (1997). Magnetostratigraphy and palaeoclimate of Red Clay sequences from Chinese Loess Plateau. *Science in China D*, *40*, 337–343.

Sun, J. and T. Liu (2000). Multiple origins and interpretations of the magnetic susceptibility signal on Chinese wind-blown sediments. *Earth and Planetary Science Letters*, *180*, 287–296.

Sun, Y. B. and Z. S. An (2002). History and variability of Asian interior aridity recorded by eolian flux in the Chinese Loess Plateau during the past 7 Ma. *Science in China D*, *45*, 420–429.

Sun, Y. B., H. Y. Lu and Z. S. An (2006). Grain size of loess, palaeosol and Red Clay deposits on the Chinese Loess Plateau: significance for understanding pedogenic alteration and palaeomonsoon evolution. *Palaeogeography Palaeoclimatology Palaeoecology*, *241*, 129–138.

Tauxe, L. (1993). Sedimentary records of relative paleointensity: theory and practice. *Reviews of Geophysics*, *31*, 319–354.

Tauxe, L. (2005). Inclination flattening and the geocentric axial dipole hypothesis. *Earth and Planetary Science Letters*, *233*, 247–261.

Tauxe, L. and Y. Gallet (1991). A jackknife for magnetostratigraphy. *Geophysical Research Letters*, *18*, 1783–1786.

Tauxe, L. and J. P. Valet (1989). Relative paleointensity of the Earth's magnetic field from marine sedimentary records: a global perspective. *Physics of the Earth and Planetary Interiors*, *56*, 59–68.

Tauxe, L., T. Pick and Y. S. Kok (1995). Relative paleointensity in sediments: a pseudo Thellier approach. *Geophysical Research Letters*, *22*, 2885–2888.

Tauxe, L., H. N. Bertram and C. Seberino (2002). Physical interpretation of hysteresis loops: micromagnetic modeling of fine particle magnetite. *Geochemistry Geophysics Geosystem*, *3*, 1055, doi:10.1029/2001GC000241.

Tauxe, L., J. L. Steindorf and A. Harris (2006). Depositional remanent magnetization: toward an improved theoretical and experimental foundation. *Earth and Planetary Science Letters*, *244*, 515–529.

Tauxe, L., T. Herbert, N. J. Shackleton and Y. S. Kok (1996). Astronomical calibration of the Matuyama-Brunhes boundary: consequences for magnetic remanence acquisition in marine carbonates and the Asian loess sequences. *Earth and Planetary Science Letters*, *140*, 133–146.

Thellier, E. (1938). Sur l'aimantation des terres cuites et ses applications géophysiques. *Annales de l'Institut de Physique du Globe, Université de Paris, et Bureau Central de Magnetisme Terrestre*, *16*, 157–302.

Thellier, E. (1981). Sur la direction du champ magnétique terrestre en France durant les deux derniers millénaires. *Physics of the Earth and Planetary Interiors*, *24*, 89–132.

Thellier, E. and O. Thellier (1959). Sur l'intensité du champ magnétique terrestre dans le passé historique et géologique. *Annales de Géophysique*, *15*, 285–376.

Thompson, R., G. M. Turner, M. Stiller and A. Kaufman (1985). Near East Paleomagnetic Secular Variation Recorded in Sediments from the Sea of Galilee (Lake Kinneret). *Quaternary Research*, *23*, 175–188.

Thompson, R. and B. A. Maher (1995). Age models, sediment fluxes and palaeoclimatic reconstructions for the Chinese loess and palaeosol sequences. *Geophysical Journal International*, *123*, 611–622.

Thouveny, N., J. Carcaillet, E. Moreno, G. Leduc and D. Nerini (2004). Geomagnetic moment variation and paleomagnetic excursions since 400 kyr BP: a stacked record from sedimentary sequences of the Portuguese margin. *Earth and Planetary Science Letters*, *219*, 377-396.

Torrent, J., V. Barrón, and Q. S. Liu (2006). Magnetic enhancement is linked to and precedes hematite formation in aerobic soil. *Geophysical Research Letter*, *33*, L02401, doi:10.1029/2005GL024818.

Torrent, J., Q. S. Liu, J. Bloemendal and V. Barron (2007). Magnetic enhancement and iron oxides in the upper Luochuan loess-paleosol sequence, Chinese loess plateau. *Soil Science Society of America Journal*, *71*, 1570–1578.

Tric, E., J. P. Valet, P. Tucholka, M. Paterne, L. Labeyrie, F. Guichard, L. Tauxe and M. Fontugne (1992). Paleointensity of the geomagnetic field during the last 80,000 years. *Journal of Geophysical Research*, *97*, 9337–9351.

Tucker, P. (1980). Stirred remanent magnetization: a laboratory analogue of redepositional remanent magnetization. *Journal of Geophysics*, *48*, 153–157.

Tutkovskii, P. A. (1899). The question of the method of loess formation. *Zemlevedeie*, *1-2*, 213–311.

Valet, J. P. and L. Meynadier (1993). Geomagnetic field intensity and reversals during the past four million years. *Nature*, *366*, 234–238.

Valet, J. P. and L. Meynadier (1998). A comparison of different techniques for relative paleointensity. *Geophysical Research Letters*, *25*, 89–92.

Valet, J. P., L. Meynadier, F. C. Bassinot and F. Garnier (1994). Relative paleointensity across the last geomagnetic reversal from sediments of the Atlantic, Indian, and Pacific Oceans. *Geophysical Research Letters*, *21*, 485–488.

van Velzen, A. J. and M. J. Dekkers (1999). Low-temperature oxidation of magnetite in loess-paleosol sequences: a correction of rock magnetic parameters. *Studia Geophysica et Geodaetica*, *43*, 357–375.

Vandenberghe, R. E., E. de Grave, J. J. Hus and J. M. Han (1992). Characterization of Chinese loess and associated palaeosol by Mössbauer spectroscopy. *Hyperfine Interactions*, *70*, 977–980.

Verosub, K. L., R. A. Ensley and J. S. Ulrick (1979). The role of water content in the magnetization of sediments. *Geophysical Research Letters*, *6*, 226–228.

Verosub, K. L., P. Fine, M. J. Singer and J. TenPas (1993). Pedogenesis and paleoclimate: interpretation of the magnetic susceptibility record of Chinese loess-paleosol sequences. *Geology*, *21*, 1011–1014.

Wang, R. H. and R. Løvlie (2010). Subaerial and subaqueous deposition of loess: experimental assessment of detrital remanent magnetization in Chinese loess. *Earth and Planetary Science Letters*, *298*, 394–404.

Wang, X. S., R. Løvlie, Z. Y. Yang, J. L. Pei, Z. Z. Zhao and Z. M. Sun (2005). Remagnetization of Quaternary eolian deposits: a case study from SE Chinese Loess Plateau. *Geochemistry Geophysics Geosystems*, *6*, Q06H18, doi:10.1029/2004GC000901.

Wang, X. S., Z. Y. Yang, R. Løvlie, Z. M. Sun and J. L. Pei (2006). A magnetostratigraphic reassessment of correlation between Chinese loess and marine oxygen isotope records over the last 1.1 Ma. *Physics of the Earth and Planetary Interiors*, *159*, 109–117.

Wang, Y., M. E. Evans, N. Rutter and Z. Ding (1990). Magnetic susceptibility of Chinese loess and its bearing on paleoclimate. *Geophysical Research Letters*, *17*, 2449–2451.

Weltje, G. J. and M. A. Prins (2003). Muddled or mixed? Inferring paleoclimate from size distributions of deep-sea clastics. *Sedimentary Geology*, *162*, 39–62.

Williams, W. and D. J. Dunlop (1989). Three-dimensional micromagnetic modelling of ferromagnetic domain structure. *Nature*, *337*, 634–637.

Xiao, J. L., S. C. Porter, Z. S. An, H. Kumai and S. Yoshikawa (1995). Grain size of quartz as an indicator of winter monsoon strength on the loess plateau of central China during the last 130,000 yr. *Quaternary Research*, *43*, 22–29.

Yang, T. S., M. Hyodo, Z. Y. Yang and Z. M. Sun (2005). A first paleomagnetic and rock magnetic investigation of calcareous nodules from the Chinese Loess Plateau. *Earth Planets and Space*, *57*, 29–34.

Yang, T. S., M. Hyodo, Z. Y. Yang, L. Ding, J. L. Fu and T. Mishima (2007a). Early and middle Matuyama geomagnetic excursions recorded in the Chinese loess-paleosol sediments. *Earth Planets and Space*, *59*, 825–840.

Yang, T. S., M. Hyodo, Z. Y. Yang and J. L. Fu (2007b). Two geomagnetic excursions during the Brunhes chron recorded in Chinese loess-palaeosol sediments. *Geophysical Journal International*, *171*, 104–114.

Zhao, H., Y. C. Lu, C. M. Wang, J. Chen, J. F. Liu and H. L. Mao (2010). ReOSL dating of aeolian and fluvial sediments from Nihewan Basin, northern China and its environmental application. *Quaternary Geochronology*, *5*, 159–163.

Zheng, H., T. Rolph and J. Shaw (1995). A detailed paleomagnetic record for the last interglacial period. *Earth and Planetary Science Letters*, *133*, 399–351.

Zhou, L. P. and N. J. Shackleton (1999). Misleading positions of geomagnetic reversal boundaries in Eurasian loess and implications for correlation between continental and marine sedimentary sequences. *Earth and Planetary Science Letters*, *168*, 117–130.

Zhou, L. P., F. Oldfield, A. G. Wintle, S. G. Robinson and J. T. Wang (1990). Partly pedogenic origin of magnetic variations in Chinese loess. *Nature*, *346*, 737–739.

Zhu, R. X., C. Deng and M. J. Jackson (2001). A magnetic investigation along a NW-SE transect of the Chinese loess plateau and its implications. *Physics and Chemistry of the Earth*, *26*, 867–872.

Zhu, R. X., C. Laj and A. Mazaud (1994a). The Matuyama-Brunhes and Upper Jaramillo transitions recorded in a loess section at Weinan, north-central China. *Earth and Planetary Science Letters*, *125*, 143–158.

Zhu, R. X., R. S. Coe, B. Guo, R. Anderson and X. Zhao (1998a), Inconsistent palaeomagnetic recording of the Blake event in Chinese loess related to sedimentary environment. *Geophysical Journal International*, *134*, 867–875.

Zhu, R. X., C. Laj and A. Mazaud (1998b). A recording phase lag between ocean and continent climate changes constrained by the Matuyama/Brunhes polarity boundary. *Chinese Science Bulletin*, *43*, 1593–1598.

Zhu, R. X., Q. S. Liu and M. J. Jackson (2004). Paleoenvironmental significance of the magnetic fabrics in Chinese loess-paleosols since the last interglacial (<130 ka). *Earth and Planetary Science Letters*, *221*, 55–69.

Zhu, R. X., Y. X. Pan and Q. S. Liu (1999). Geomagnetic excursions recorded in Chinese loess in the last 70,000 years. *Geophysical Research Letters*, *26*, 505–508.

Zhu, R. X., L. P. Zhou, C. Laj, A. Mazaud and Z. L. Ding (1994b). The Blake geomagnetic polarity episode recorded in Chinese loess. *Geophysical Research Letters*, *21*, 697–700.

Zhu, R. X., X. Y. Zhu, Z. L. Ding, Z. T. Guo, J. Q. Liu, C. J. Li, B. C. Huang and D. S. Liu (1996). Paleomagnetic secular variation and its influences on environment through the last 150 000 a. *Science in China D*, *39*, 26–34.

Zhu, R. X., B. Guo, Y. X. Pan, Q. S. Liu, Z. Zeman and V. Suchy (2000). Reliability of geomagnetic secular variations recorded in a loess section at Lingtai, north-central China. *Science in China*, *43*, 1–9.

Zhu, R. X., R. Zhang, C. L. Deng, Y. X. Pan, Q. S. Liu and Y. B. Sun (2007). Are Chinese loess deposits essentially continuous? *Geophysical Research Letters*, *34*, L17306, doi:10.1029/2007GL030591.